Tree biomechanics:

A study of the mechanical stability of broadleaf trees



Submitted for the degree of Doctor of Philosophy in the School of Geography and the Environment, University of Oxford.

Candidate: Tobias Jackson, Linacre College

Supervisors: Dr Alexander Shenkin and Professor Yadvinder Malhi

Acknowledgments

Firstly, I'd like to thank Allie Shenkin and Yadvinder Malhi for their friendly guidance throughout this project. Also, everyone in Oxford Ecosystems Lab for helping create a work environment that is both inspiring and relaxing, I really enjoyed my time working with you all.

I'd like to thank Axel Wellpott for hours of detailed advice on electronics. Also Barry Gardiner for general guidance and for introducing me to a great crowd of wind and tree researchers. I'm grateful to the UCL team – Mat Disney, Andy Burt, Kim Calders, Phil Wilkes and Matheus Bon Vicari – as well as Pasi Raumonen and Alvaro Lau for help with TLS data, which can be infuriating! I'd also like to thank everyone in Danum Valley field station, especially Azlin, Unding and Julian, for helping with my field work.

As ever, I'm extremely grateful to Joana and my family for supporting me. And finally, all my Oxford squash friends for the simple pleasure of chasing a ball around a room for a few hours – it really helps take your mind off things!



Image: A branch sketching out its path in the wind, by Pat Pickett (http://patpickett.com/)

Contents

Abstract 12

Introduction 13

Thesis aims and outline 15

Literature review 17

The effects of wind on trees and forests 17

What limits tree height? 19

Wind flow over forests: theory 21

Wind flow over forests: data 24

Tree response: statics 25

Tree response: dynamics 27

Breakage conditions 30

Material properties 32

Review of methodology 35

Field data collection 35

Field data processing 39

Terrestrial laser scanning data collection and processing 42

Extracting architectural indices 45

Finite element analysis 46

Paper 1 - Finite element analysis of trees in the wind based on terrestrial laser scanning data 51

Paper 2 - A new architectural perspective on wind damage in a natural forest 71

Paper 3 - An architectural model of resonant frequencies in trees 90

Paper 4 - The mechanical stability of the world's tallest hardwood trees 111

Discussion 134

Comparing Wytham Woods and Danum Valley 134

Tree architecture and mechanical stability 136

Limitations 137

Further research 139

Conclusion 141

Data availability and online resources 143

References 144

Appendix 1 – Pull and release data 1544

Appendix 2 – Example Abaqus input file 1555

List of figures

Literature review

Figure 1 – Left: Windswept tree leaning away from the prevailing wind. Right: Cross-section of a tree trunk showing asymmetric growth and reaction wood. Images from http://planete.gaia.free.fr/vegetal/dendro/equilibre.html 18

Figure 2 – Similar effects of wind damage to the interior of a stand in a conifer plantation (left) and a rice field (right). Images from Greame Prest and Kana Kamimura. 18

Figure 3 – Tallest trees in the world (image from Hemp et al., 2017). 20

Figure 4 – Aerodynamic drag factor (CD) on a cylinder with increasing Reynolds number. Image from Sunden (2016). 22

Figure 5 – Patterns of wind flow over forests (Finnigan & Brunet 1995). 23

Figure 6 – A: Single Tree experiment in Roskilde, Denmark. B: Small-scale representation of a forest canopy in a wind tunnel. C: WinDEEE dome, the largest wind tunnel in the world, exposing a small tree to a highly controlled wind loading. 24

Figure 7 – Theoretical diagram of the gust factor and dynamical amplification factor. 28

Figure 8 – Sway motion of *E. teretecornus* showing (a) complex sway motion of tree trunk and (b) spectrum showing sway frequency with broad, single peak at 0.32 Hz. From James et al. (2006). 29

Figure 9 – Left – Large conifer snapped by a wind storm in Fort Smallwood (from By the Bay Photos on Flickr, creative commons). Right – *Liriodendron tulipifera* tree uprooted by wind on the campus of Shinshu university, Japan (photo by Kana Kamimura). 30

Figure 10 – Overview of mode of death studies. Percentage of dead trees that snapped divided by region (top left) and forest type (top right). Bottom: number of studies that mention mode of death from 1955 -2015, where each date represents the previous 5 years. 31

Figure 11 – Relationship between dry wood density and green wood density (left) green wood elasticity (middle) and green wood modulus of rupture(right). 34

Methodology

Figure 12 – Diagram of strain gauge monitoring system 1. 36

Figure 13 – Top left: printed circuit board containing 12 wheatstone bridge circuits. Top right – single wheatstone bridge circuit. Bottom left – CR23X. Bottom right – strain gauge calliper with red rectangles showing the location of the two strain gauges. 37

Figure 14 – Diagram of strain gauge monitoring system 2. 38

Figure 15 – Example Welch's power spectrum for strain data collected in Wytham Woods. Left – unsmoothed spectrum. Right – smoothed spectrum used to automatically detect peaks. 40

Figure 16 – Strain data showing characteristic drift over time with running modes overlaid. ..40

Figure 17 – Top two panels – Strain data from North and East facing side of the trunk. Bottom – Maximum strain calculated by combining the two strain channels. ……41

Figure 18 – Mean wind against maximum strain at different time resolutions for a single tree in Wytham Woods. ……42

Figure 19 – Left: Comparison of the TLS data for a 51 m *Parashorea malaanonan* from Danum and a 24 m *Fraxinus excelsior* from Wytham Woods. The trees are to scale. Right: TLS data processing workflow diagram. ……43

Figure 20 – Example of a typical problem with a QSM ……43

Figure 21 – TLS data processing steps for a *Shorea parvifolia* from Danum Valley. A – single tree point cloud. B – point cloud with noise and leaves manually deleted. C – selected QSM. D – simplified QSM. ……44

Figure 22 – Diagram showing two key architectural measures derived from TLS data. ……45

Figure 23 – Diagram of the TLS to finite element analysis workflow. ……47

Figure 24 – Abaqus output. Top left: strain against time for a step-wise increasing wind speed. Top right: wind-strain relationship interpolated from the step-wise means. Bottom: frequency analysis output showing a dominant, low frequency paired mode as well as higher order modes.……48

Paper 1

Figure 1 – Workflow diagram showing the main analysis and validation steps. ……53

Figure 2 – Left – QSM directly from the fitting process. Right – simplified QSM with longer cylinders and fewer small branches - this is our input for finite element analysis. ……55

Figure 3 – Above – TLS data showing trees near the canopy walkway. The coloured trees are the ones used in this analysis. The black arrow shows the prevailing wind direction and is located at the point of the wind measurement. Left - simulated strain (coloured lines) against field data (black lines, inverted for clarity). The time-lag (field strain – simulated strain) as well as the cross correlation co-efficient are given for each signal. ……60

Figure 4 – Strain produced by wind speeds of 5 ms^{-1} (A) and 15 ms^{-1} (B) from field data and finite element analysis. C – critical wind speed estimates from field data and finite element analysis. ……61

Figure 5 – Field measured fundamental frequency against modelled fundamental frequency for 20 trees (one tree was excluded due to errors in the simulation). ……62

Figure SI-2 – A - Mean wind speed against maximum strain at varying temporal resolution. B – Vertical wind speed profiles in summer and winter, as measured from anemometers at 5, 10 and 15m on the canopy walkway. The dashed lines represent the power law function used to model the vertical variation in wind speed, only the winter data was used in this study. C –

Mean hourly wind speed against maximum wind speed, measured at 5s resolution at the ECN weather station. D – Hourly mean wind speed inside and outside the canopy, in summer and winter. ……68

Paper 2

Graphical abstract – Critical wind speed for 397 broadleaf trees. ……71

Figure 1 – Left – Raw strain output from simulation showing steps of increasing strain, corresponding to the stepwise wind ramp used to force each tree. Right – Strain against squared wind speed. ……76

Figure 2 – Left: Critical wind speed estimates from field data in summer and winter using mean hourly wind speeds. Right: Histograms of CWS estimates from field data in winter (above) and in summer (below). ……78

Figure 3 –Simulated critical wind speeds for the three species in our 1ha plot. ……79

Figure 4 – Left – Tree height against dbh for 397 model trees from the 1ha plot and the 17 trees for which I have field data. The points are scaled by dbh and coloured by species. Right – Tree height against dbh for the same trees, but coloured by simulated CWS (with species-specific material properties). ……80

Figure 5 – A: Critical wind speed against radial growth rate for the 397 trees modelled in the 1ha plot with the trees measured in the field overlaid. The marker size represents the tree dbh. B: subset of A, with modelled trees over 40cm dbh only and a best fit line overlaid. C: subset of A, with field data trees only and a best fit line overlaid. All plots have the same axes. …….82

Figure 6 – Wind speed, measured as the maximum occurring in each hour from 2008-2017 at the ECN weather station at Wytham Woods. Overlaid box and whisker plots represent leaf-in / leaf-out timings for the same period. ……83

Figure SI-1 – Wytham Woods and surrounding area, showing the ECN weather station, the 18ha permanent Smithsonian plot and the two areas within it in where data were collected for this study. ……86

Figure SI-4 – Left: Magnitudes of the effect sizes of height, dbh and the architectural terms in a linear model for CWS. Right: Interaction between tree height and dbh in the linear model for CWS……..88

Figure SI-5 – Change in coefficient of determination and Akaike's information criterion as predictor variables are added to the generalized linear model. ……88

Paper 3

Figure 1 – Simulated fundamental sway frequency of a tree. ……93

Figure 2 – Workflow diagram. ……94

Figure 3 – Fundamental frequencies from field data. ……98

Figure 4 – Tree architectural indices. ……99

Figure 5 – Simulated fundamental frequencies. ……100

Figure 6 – The effect of leaves on tree sway. ……103

Figure S1 – Summary of linear models for f_0. ……107

Figure S2 – Effect sizes in selected multiplicative models for simulated f_0. ……107

Figure S3 – Summary of linear models for D_0. ……108

Figure S4 – Summary of architectural models for D_0. ……109

Paper 4

Figure 1 – Left: H-D allometry for trees in this study, overlaid on manual measurements from the same plot (Sullivan et al., 2018) and a regional allometry (Feldpausch et al., 2011). Right: TLS scans of five trees to demonstrate the height range of our sample. From left to right: *Shorea faguetiana, Parashorea malaanonan, Eusidoxyleron zwageri, Shorea parvifolia and Pometia pinnata.* ……113

Figure 2 – A: Example five-minute time-series for strain and wind speed. B: Distributions of strain and squared wind speed. ……116

Figure 3 – A: point cloud of tree 1, showing the position of the anemometers and strain gauges. This image also gives an example of the manual leaf filtering, with points assumed to be leaves shown in green on part of the crown. B: Simplified QSM for tree A1n, showing manual definition of the crown and the centre of volume for the whole tree (lower) and the crown (upper). C: Vertical profiles of sail area and volume derived from the QSM and used for the analytical wind model and the mass taper calculation respectively……118

Figure 4 – Measured height of trees against maximum height, estimated using three models. The filled and hollow markers represent plot-level-mean and species-specific material properties respectively. ……122

Figure 5 – 10-minute maximum bending strain against maximum squared wind speed measured with the sonic anemometer for (A) 51 m tall *Parashorea malaanonan* logged with a CR1000 and (B) 17 m tall *Orophea myriantha* logged with a CR23X. Note the difference in scales and data availability. C: Gradients of the wind-strain relationship against tree height using data from the sonic anemometer, the random effects model and a 10-minute aggregation period. ……..124

Figure 6 – Left: gravitational risk factors for the trees in this study (points) and general allometry (lines) under two assumptions. Right: wind damage risk factors for a maximum wind speed of 20 and 25 m/s, point indicating specific trees derived from field data and the lines being best fit lines. ……..125

Figure 7 – Left: QSM of the tallest tree in the tropics (a 100 m *Shorea faguetiana*) in its rest position. Middle: Finite element simulation of same tree under gravity and 12 ms-1 wind loading. Right: Strain produced at the base of the stem of the same tree under simulated wind loading with and without gravity. ……..126

Figure S1 – Field data against QSM measurements for (A) dbh (B) height and (C) crown dimensions. Note that the two crown dimensions variables are not identical and this plot is presented on a log-log scale……130

Figure S2 – All of the graphs show wind-strain gradients with units $\mu m^{-2} s^2$. The first R^2 and rmse values refer to all of the trees in the graph while the second refers to only those trees logged with the CR1000s, there is some difference in data availability. All of the graphs have identical x-axes, the estimated wind-strain gradient derived from field data by for each tree separately using the sonic anemometer wind speed data and a ten-minute aggregation period. The y-axes are other estimates of the wind speed gradient. The top row are estimates from field data using (A) wind speed data from a cup anemometer 63 m away from the sonic anemometer (B) a one-minute aggregation period and (C) by pooling the data and fitting a random slope model. The second row are analytical models of the wind-strain gradient (D) with mean material properties (E) with species-specific material properties and (F) with total width of the tree as the sail area, instead of just the branches. The third row are finite element model estimates of the wind-strain gradient with (G) mean material properties (H) species-specific material properties and (I) the effects of gravity included. ……131

Figure S3 – A: vertical profile of wind speed measurements with possible power law fits overlaid. B: wind rose for 10-minute maximum wind speeds from the sonic anemometer. C and D: 10-minute maximum wind speeds measured at two heights in the tree 1 and 6, respectively. E: Correlation between 10-minute maximum wind speeds measured at tree 6 and that at tree 1, 63 m away, coloured by wind direction. ……132

Discussion

Figure 26 – Left: Wytham Woods in Autumn from above, showing the canopy walkway (photo from Yadvinder Malhi). Right: Danum Valley from above (photo from Alexander Shenkin)……134

Figure 27 – Forest research vehicle being crushed by a tree (photo courtesy of Barry Gardiner)……137

Glossary

General

- **Abaqus** – a commercial finite element software package used for all finite element analysis in this thesis.
- **AQUA** – a module within Abaqus which simulates fluid loading.
- **Cantilever beam** – an engineering approximation describing a straight beam with uniform material properties.
- **Coherent structures** – turbulent structures in wind flow over forests, often divided into sweeps and ejections.
- **Critical wind speed (CWS)** – the wind speed at which a windthrow is predicted to occur.
- **FLUXNET** – a global carbon flux monitoring network, which measures wind speed over forests worldwide.
- **ForestGALES** – a popular forest wind risk model used mainly for conifer plantations in the temperate zones.
- **Input file** – a file written in the Abaqus scripting language that defines, in this case, the tree geometry and loadings to be applied during the simulation.
- **Mode of death** – the specific cause of tree mortality, e.g. uprooted, snapped, disease.
- **Quantitative structure model (QSM)** – a 3D cylinder-based reconstruction of a tree from TLS data.
- **Reynolds number** – a central concept in fluid dynamics that describes the fluid flow regime. Low numbers denote viscous and high numbers denote turbulent fluid flow.
- **Strain gauge** – properly this is a small electrical component whose resistance changes as it deforms. However, in the literature the strain gauge and the strain transducer, which holds the strain gauges, have become synonymous. In this these I use it in the more general sense, except where I explicitly state otherwise.
- **Terrestrial laser scanning (TLS)** – a laser-based method of mapping environments in 3D.
- **Thigmomorphogenesis** – the process by which a tree adapts to its wind environment.
- **Windthrow** – the action of a tree being uprooted or snapped by wind.

Spectral analysis

- **Dominance of the fundamental mode** (D_0) - the proportion of a structure's motion that can be described by the fundamental mode alone.
- **Dynamic amplification factor** – the extent to which the tree motion is amplified by its dynamics.
- **Gust factor** – there are two slightly different definitions of this, see literature review for a full discussion
    - The ratio between maximum and mean strain in a given time period.
    - The ratio between maximum and mean wind speed in a given time period.
- **Fundamental frequency** (f_0) – the frequency of the fundamental mode.

- **Fundamental mode** – the lowest frequency, and generally the most significant, sway mode of a structure.
- **Multiple resonance damping** – the process of transferring sway energy from low frequency modes, where it is dangerous to the trunk of a tree, to high sway modes localized in small branches where it can be damped efficiently.
- **Resonant frequency** – the frequency at which a structure resonates (motion is significantly amplified) by the convergence of a loading frequency with a natural frequency.

Variables

- A_{sail} – the area upon which the drag force acts.
- C_d – the drag coefficient, which determines the magnitude of the fluid force on an object for a given Reynold's number.
- ε – the bending strain. Extension divided by original length (dimensionless).
- ε_{break} – the strain at which the wood will snap.
- E_{gw} – the Young's modulus of elasticity of green wood (often just 'elasticity').
- σ – the stress, defined as the force per unit area, in a material.
- F_D – the drag force on an object due to wind.
- H_{max} – the maximum height a beam or tree can reach before it collapses under its own weight.
- M_{wind} – the moment at the base of the tree produced by wind loading.
- M_{tree} – the resistive moment created by stresses and strains in the wood.
- MOR – the stress at which the wood will snap.
- ρ_{gw} – the density of green wood.
- v – wind speed.

Tree architecture

- **Crown area** – the maximum ground area covered by the crown viewed from above.
- **Crown aspect ratio** – the ratio of maximum crown width to crown height.
- **Crown asymmetry** – the ratio of mean to maximum area in segments of crown, which are defined by splitting the crown into eight azimuthal segments, centred on the stem.
- **Crown volume ratio (CVR)** – the ratio of total woody volume of the tree to that in the crown.
- ***K* –** the ratio of woody volume in the crown to that in the stem. This is similar to the CVR but was re-defined for paper 4 following (D. King & Loucks, 1978).
- **Mean branching angle** – the mean angle between two cylinders at each branching point
- **Path fraction** – the ratio of mean to maximum base-to-twig path length, this is considered a proxy for water use efficiency (Savage et al., 2010; Bentley et al., 2013).
- **Total volume** – total volume of all the cylinders that make up the tree.
- **Total sail area** – total area of the cylinders projected into the x-z plane.

Abstract

Wind is a key disturbance agent in forests worldwide, but the interaction between wind and trees is poorly understood in natural forests. Wind damage leads to the formation of canopy gaps, which drive structural and compositional changes in the forest. Trees also adapt to their local wind regime in the absence of any damage, a process known as *thigmomorphogenesis.* This process alters local height-diameter allometries and so influences forest carbon stocks. Previous work on the wind-tree interaction has focussed on conifer plantations due to their economic importance and the relative simplicity of these systems. In this thesis I use terrestrial laser scanning to map the 3D architecture of broadleaf trees and so simulate their response to wind loading using finite element analysis. I also use field techniques developed in the forestry industry to directly measure the response of broadleaf trees to the wind.

I found that the simulations performed well against field data for trees in Wytham Woods, UK, but that they failed to predict the field data from Danum Valley, Malaysia. This is likely due to the more complex topography and canopy structure in the tropical site. In Wytham Woods, I found that the critical wind speed, a measure of wind damage risk, was related to tree species, growth rate and architecture. I also found an interesting link between critical wind speed and the timing of autumn leaf phenology, although this requires further investigation. In Danum Valley I found that understory trees approach their gravitational limits to height in their struggle to reach the canopy but that gravitational risk factors decrease with tree height. In contrast, I found that wind risk factors increased with tree height meaning that tall trees are likely to be mechanically limited by wind. I also found that the natural frequencies of broadleaf trees do not follow the same simple pattern as those of conifers, a difference which is accounted for by tree architecture. Overall, this thesis emphasises the role of wind damage risk in forest ecology and the importance of tree architecture in determining the response to wind loading for broadleaf trees.

Introduction

Forests are home to globally essential stores of carbon (Malhi, Baldocchi, & Jarvis, 1999; Pan et al., 2011) and biodiversity (Klein, Randin, & Körner, 2015; Ricklefs & He, 2016). The terrestrial carbon cycle is strongly influenced by forest disturbance processes, and windthrow is a key agent of disturbance in many forests (Magnabosco Marra et al., 2018; Silvério et al., 2018). Windthrow events are spatially and temporally stochastic extreme events, making them a challenge to study. In the Amazon, small disturbance events (< 0.1 ha) have been estimated to cause 1.28 Pg carbon loss per year, compared to 0.2 Pg carbon per year lost due to logging in the 1990s (Espírito-Santo et al., 2014). It can take approximately 40 years for a forest patch to reach 90 % of its pre-disturbance biomass (Magnabosco Marra et al., 2018) and the changes in species composition endure far longer (Everham & Brokaw, 1996). Wind disturbance is thus a key driver of forest structure and functional composition, yet we do not understand the mechanisms of wind damage at the tree level (Seidl et al., 2011; J. Moore, Gardiner, & Sellier, 2018).

Tall trees dominate forest dynamics (Slik et al., 2013; Lutz et al., 2018) and post-damage surveys have shown them to be particularly vulnerable to wind damage (Rifai et al., 2016). Wind regimes are likely to change under future climate projections and the return times of extreme wind events may decrease (Dale et al., 2011). It is therefore essential that we understand the mechanisms involved in wind damage in order to predict how these changes may affect forests. If the return time of catastrophic wind storms exceeds the recovery time the forest may never fully recover and instead take on a new stable state (Everham & Brokaw, 1996). Even without damaging trees, wind sculpts forest structure since trees sense their wind environment and adapt their growth accordingly (Bonnesoeur, Constant, Moulia, & Fournier, 2016), altering local height-diameter allometries (Thomas, Martin, & Mycroft, 2015). Therefore wind exposure, as well as direct wind damage rate, is likely to be one of the limiting factors for tree height and forest carbon storage (Givnish *et al.* 2014; Coomes *et al.* 2018).

Most of the literature on wind-tree interactions focuses on conifer plantations, due to the economic importance of assessing the risk of wind damage in these forests (Schelhaas, Nabuurs, & Schuck, 2003). In general, the knowledge and tools gained through this research can be transferred to natural forests, although there are some key differences. Firstly, the structure of natural forests is more complex and assumptions such as uniform tree height, spacing and species do not hold. Secondly, broadleaf trees have a wider variety of architectures than plantation grown conifers, and this architecture has a strong effect on the

trees response to wind loading. One of the key aims of this thesis is to explore this relationship between tree architecture and response to wind loading.

Arborists have been visually assessing the likelihood of wind damage to broadleaf trees for centuries. The presence of large trees in cities and parks means that the risk of wind damage must be managed (Kheraj, 2007; Wessolly & Erb, 2016). An Arborist's assessment is often partially subjective, but it is also common for arborists to use scientific techniques to test for wood strength and the presence of weaknesses or disease (Roodbaraky, Baker, Dawson, & Wright, 1994; Brudi & Wassenaer, 2001; Wessolly & Erb, 2016). This experience provides us with phenomenological analyses of the effects of tree architecture on wind-tree interactions, but for a numerical treatment we must look to the finite element method (Sellier, Fourcaud, & Lac, 2006).

The finite element method (FEM) is a numerical technique for solving a complex calculation by splitting it up into a large number of smaller, simpler calculations. FEM is widely used in structural engineering to calculate how stresses and strains distribute over complex geometries, which are split up into finite elements or finite volumes. FEM has become the de-facto method for modelling the dynamics of trees in the wind (J. Moore et al., 2018), since it can explicitly model the distribution of wind induced forces across a complex tree structure by splitting the tree up into a number of cylinders, or beams. See the methodology section for a detailed treatment of the finite element analysis used in this thesis. However, due to the difficulty of manually mapping tree architecture, especially for large trees in forest environments (Lau et al., 2018), previous finite element studies have been limited to idealized fractal trees (Mathieu Rodriguez, De Langre, & Moulia, 2008) or a small number real trees (J. R. Moore & Maguire, 2008).

Terrestrial laser scanning (TLS) has revolutionised the 3D mapping of tree architecture allowing hundreds of trees to be digitized in a short time (Raumonen et al., 2015; Kim Calders et al., 2018; Malhi et al., 2018). 3D cylinder models, or quantitative structure models (QSMs), derived from TLS data are an efficient way to represent tree architecture and have been used to non-destructively estimate tree biomass across the tropics (K Calders et al., 2015; Gonzalez de Tanago Menaca et al., 2017; Disney et al., 2018). The availability of TLS data from both tropical and temperate sites provides a new lens on long-standing questions which have been hampered by a lack of detailed information on tree structure. Combining TLS data with finite element analysis overcomes previous barriers and allows us to model the detailed dynamics of real trees in the wind.

Thesis aims and outline

In this thesis I used field techniques developed in the forestry industry to monitor the interaction between trees and wind. I also used newly available data on 3D tree architecture as the basis for finite element simulations of tree dynamics. Together, the field data and simulations allowed me to explore the ecological role of wind in natural forests.

My key aims were:

1. To monitor and characterize the response of broadleaf trees to wind loading.
2. To build and test a finite element simulation of the response of broadleaf trees to wind loading based on TLS data in both temperate and tropical forests.
3. To explore the relationship between tree architecture and tree response to wind loading. In this context the tree's response to wind loading can be quantified by a number of variables representing both the quasi-static response and the dynamic response.
4. To explore whether tree height may be mechanically limited by either by gravity or wind damage risk.

In order to achieve these aims I measured the strain (extension / original length) in the trunks of trees in Wytham Woods, UK, and Danum Valley, Malaysia. I also collected wind speed data and participated in TLS data collection for both sites. Individual trees were then extracted from the TLS data and finite element analysis used to simulate their response to wind loading.

The first section of this thesis reviews the literature on the ecological importance of wind damage and outlines previous studies on wind damage mechanisms. The second section gives a detailed description of the methodology. This is followed by four papers:

- Paper 1 focusses on testing the accuracy of the simulated tree response using the field data. This paper describes the field data collection and processing for Wytham Woods, as well as the workflow from TLS data to finite element analysis.
    - *Published in Agriculture and Forest Meteorology*

- Paper 2 uses both field data and finite element analysis to explore the ecological role of wind damage risk in Wytham Woods. The key variable is the critical wind speed and I show how it varies with species, growth rates and the presence or absence of leaves.
    - *Published in Frontiers in Forests and Global Change*

- Paper 3 explores the relationship between tree architecture and natural frequencies in broadleaf trees. This paper brings together all available field data on the natural frequencies of broadleaf trees as well as all TLS data from broadleaf forests.
    - *Published in the Royal Society Interface*

- Paper 4 re-visits the theory that tree height is limited by mechanics, either by gravity or wind. This paper uses strain data collected in Danum Valley to quantify the response of tall trees to wind loading. It also compares models of gravitational maximum height using realistic tree architecture from TLS data.
    - *In review*

These papers are followed by a discussion section which puts the key results of each paper in context and outlines the limitations of this study and potential future research. The pull and release data and an example Abaqus input file can be found in Appendix 1 and 2, respectively.

Literature review

This literature review is arranged in eight sections. The first section gives an overview of the ecological role of wind in forests. One key aspect of this discussion is tree height limitation, which is discussed in detail in the second section. The third and fourth sections outline the current state of knowledge on wind flow in and around forests. Next, I focus on the tree's response to wind loading using a simplistic statics approach (section five) and the more realistic dynamics approach (section six). The seventh section outlines the parameterizations used to estimate when and how a tree will break as the wind speed increases, this includes a review of the literature on tree mode of death. Finally, I discuss the material properties of wood, how they relate to wood microstructure, their importance in tree mechanics and I give an overview of the material properties data sets used in this thesis.

The effects of wind on trees and forests

Wind has a profound effect on trees and forests through direct disturbance (Espírito-Santo et al., 2014), changes in growth patterns (Thomas et al., 2015; Bonnesoeur et al., 2016) and gap dynamics which drive species turnover (Everham & Brokaw, 1996; Magnabosco Marra et al., 2018). In some cases wind can uproot trees in large swathes or topple valuable veteran trees in cities. Figure 2 shows that the effect of wind on uniform forests can be very similar to that on crop plantations. The trees on the edge are not snapped or uprooted, since they have adapted to survive higher wind speeds than the more sheltered trees within the stand. However, once one tree within the stand is snapped or uprooted the wind penetrates into the gap and causes widespread damage (Dupont, Pivato, & Brunet, 2015). In natural forests this process is complicated by forest structure and tree architecture.

Wind also affects trees in the absence of any damage. Trees exposed to wind damage risk will adapt to strengthen themselves by increasing their diameter growth at the expense of growth in height (Bonnesoeur et al., 2016). These responses, the increased diameter growth, reduced growth in height, asymmetric growth and additional reaction wood, are cumulatively known as thigmomorphogenesis (Telewski, 2006). The signal to which the trees respond is the strain (extension / original length) which is 'felt' at both the whole tree and the cellular level (Telewski, 2006). At a much larger scale, therefore, the canopy height of forests exposed to occasional high wind speeds will be shorter than those in calmer climates (Coomes et al.,

2018), with knock on effects for carbon storage and species composition. Trees in hurricane regions often display clear adaptations to their wind environment, either through increased elasticity (Asner & Goldstein, 1997) or re-sprouting after catastrophic stem damage (Van Bloem et al., 2005). Wind also affects open-grown trees, sculpting their crowns into highly irregular shapes and inducing strong reaction wood growth (Fig 1).



Figure 1 – Left: Windswept tree leaning away from the prevailing wind. Right: Cross-section of a tree trunk showing asymmetric growth and reaction wood. Images from http://planete.gaia.free.fr/vegetal/dendro/equilibre.html



Figure 2 – Similar effects of wind damage to the interior of a stand in a conifer plantation (left) and a rice field (right). Images from Greame Prest and Kana Kamimura.

To date, most of the tree-level data on wind-response relates to conifer plantations, due to the timber industry where wind damage is a major source of financial risk and where research has been ongoing for many years (Mayhead, 1973). European forests have experienced an increased rate of wind disturbance events in recent decades (Schelhaas et al., 2003; Neumann et al., 2018) which often interact with other types of disturbance. For example, a large scale wind disturbance provides the perfect conditions for a subsequent forest fire, or a bark beetle outbreak (Seidl et al., 2011).

In stark contrast to conifer plantations, the wind-tree interaction in natural forests (and especially tropical broadleaf forests) is poorly understood. This is partly due to the complexity of mixed-age and mixed-species natural forests, since they contain trees of multiple species and sizes with no fixed spacing, whereas wind damage models often rely on assumptions of single-species and uniform spacing. This is also partly due to the architectural complexity of broadleaf trees. Recent work in the Amazon, using a combination of permanent monitoring plots and Landsat data, has shown that, following a windthrow event, recovery to 90% of the pre-disturbance biomass takes approximately 40 years (Magnabosco Marra et al., 2018). Increased tree mortality can continue long after the initial disturbance event, initially through changes in the local environment and then through self-thinning as a result of the intense competition for light in the gaps left by the disturbance (Everham & Brokaw, 1996). Wind damage can also lead to changes in functional composition through selective mortality (Rifai et al., 2016) and changes in the light environment favouring fast growing, low wood density, early successional species (Everham & Brokaw, 1996; Magnabosco Marra et al., 2018). If the return time of catastrophic wind events approaches the recovery time of the forest, or if this return time changes with climate change (Dale et al., 2011), forests may enter an alternative stable state. This could see tall old growth rain forests begin to resemble the shorter forests of the hurricane belts, with all the reduced biomass stocks and changes in plant and animal species that entails.

What limits tree height?

Tall trees store the majority of forest vegetation carbon (Slik et al., 2013; Lutz et al., 2018) although their yearly carbon accumulation is limited (Ligot et al., 2018). More generally, canopy height is closely related to carbon storage (Asner & Mascaro, 2014; Bastin et al., 2015) species diversity (Marks, Muller-Landau, & Tilman, 2017) and forest respiration (McDowell et al., 2002; Larjavaara, 2014). Therefore, the question '*what limits tree height?*' has been hotly debated in the literature. The primary theories are:

(1) Mechanical limitation i.e. that above a given height
    a. tree can no longer support their own weight (McMahon, 1975; D. A. King, Davies, Tan, & Nur Supardi, 2009) or
    b. the risk of wind damage will be too high (Givnish *et al.* 2014; Coomes *et al.* 2018) or

c. the support costs will exceed the available energy. This is known known as the allometric allocation hypothesis (Givnish *et al.* 2014).

(2) Hydraulic limitation of photosynthesis - above a certain height turgor pressure will no longer be able to support the weight of the water column and the risk of cavitation and embolism will grow too large (K. J. Niklas & Spatz, 2004; K. J. Niklas, 2007).

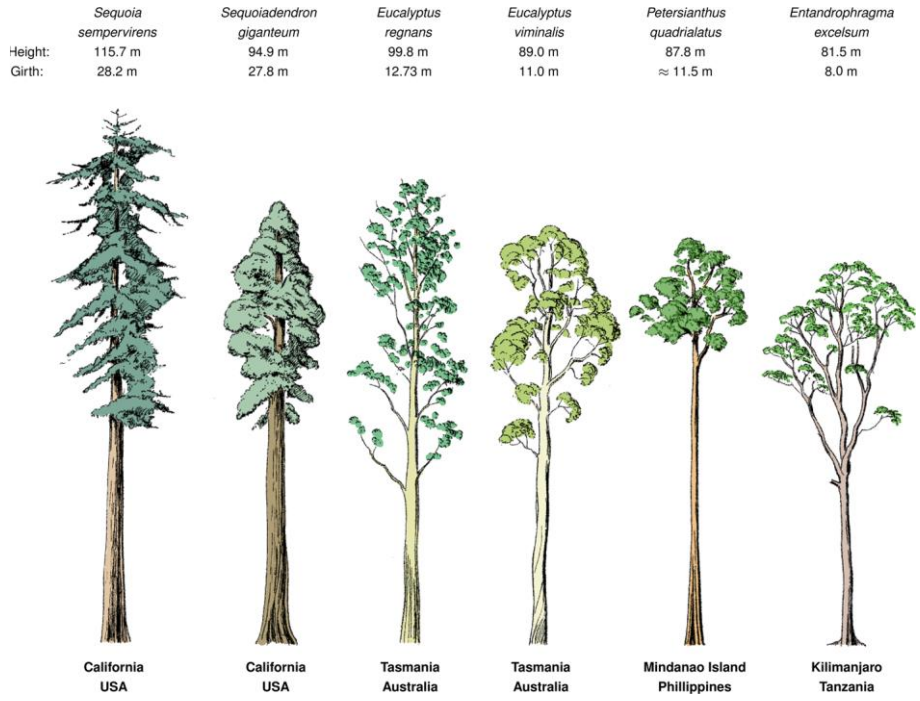


Figure 3 – Tallest trees in the world (image from Hemp et al., 2017).

Neither hydraulic nor wind-induced limitation provide an absolute limit on tree height from first principles. Rather, they each demonstrate the increasing difficulties associated with continued height growth. Furthermore, the risk of wind disturbance and drought is probabilistic, so only trees which survive hundreds of years without experiencing extreme events have the potential to reach record heights.

Givnish *et al.* (2014) utilized a strong precipitation gradient with tree heights ranging from 3 – 90 m, to show that both allometric allocation and hydraulic limitation determine maximum tree height for *Eucalyptus* trees in Victoria, Australia. These tall eucalypts are characterised by a very high slenderness and low wood density. At a global scale, Moles *et al.* (2009) found that precipitation in the wettest month of the year was the strongest predictor tested for mean plant height (R^2=0.256). Furthermore, Klein, Randin & Körner (2015) showed that global forest canopy height can be predicted by water availability. Both of these global analyses support the

hydraulic limitation hypothesis, although neither tested the correlation of canopy height with wind speeds.

Perhaps the simplest measure of a tree's mechanical stability, since it does not take into account any environmental factors, is the resistance to buckling under its own weight. Greenhill (1881) demonstrated that the maximum height a beam can reach before it buckles under its own weight, the height at which gravitational forces cause collapse, is given by Euler's equation:

$$H_{max} = C\left(E_{gw}/\rho_{gw}g\right)^{\frac{1}{3}}D^{\frac{2}{3}} \quad \textit{Equation 1}$$

Where E_{gw} and ρ_{gw} are the green wood modulus of elasticity and density, respectively, g is the acceleration due to gravity and D is the diameter of the base of the beam. The coefficient, C, is dependent on the geometry of the beam. For a cylindrical column $C = 1.26$, but C increases for tapered beams. For trees with an idealized crown or top-weight King & Loucks (1978) showed that C is proportional to the ratio between crown weight and stem weight, *K*. McMahon (1975) found that record sized trees do indeed follow the $H{\sim}D^{2/3}$ pattern, also known as elastic self-similarity, although they are much smaller than the maximum height. King *et al.* (2009) found that understory trees can approach this theoretical maximum height in the tall, dense, lowland forests of Malaysia. Dean & Long (1986) and Niklas (1995) showed that the height-diameter allometry changes for trees of different sizes, with short trees following elastic self-similarity while taller trees tended towards the constant stress model $H{\sim}D^{1/2}$, which equalizes wind-induced stress throughout the tree.

Wind flow over forests: theory

'I am an old man now, and when I die and go to heaven, there are two matters on which I hope for enlightenment. One is quantum electrodynamics and the other is the turbulent motion of fluids. About the former, I am really rather optimistic.' – Sir Horace Lamb.[1]

[1] In an address to the British Society for the Advancement of Science 1932. Cited by Tom Mullin in 'Turbulent Times for Fluids' New Scientist (11 Nov 1989).

The Reynolds number is a central concept in fluid dynamics. It can be defined as:

$$Re = \rho v L/\mu \quad \textit{Equation 2}$$

Where ρ (kgm^{-3}) is the density of the fluid, v (ms^{-1}) is the velocity of the fluid, L (m) is a characteristic length scale, and μ (kgm^{-1}s^{-1}) is the dynamic viscosity of the fluid. Flow at low Reynolds numbers is dominated by viscous forces while high Reynolds number flow is dominated by inertial processes. In this thesis, I assume a high Reynolds number regime. This is accurate for flow around branches due to the low density of air and the focus on high wind speeds. However, flow around the leaves will almost certainly have a viscous component, due to the small length scales. The drag force exerted by a fluid is related to the Reynolds number (Figure 4) and the complex shape of this relationship demonstrates the non-linear nature of fluid-structure interaction (de Langre, 2008).

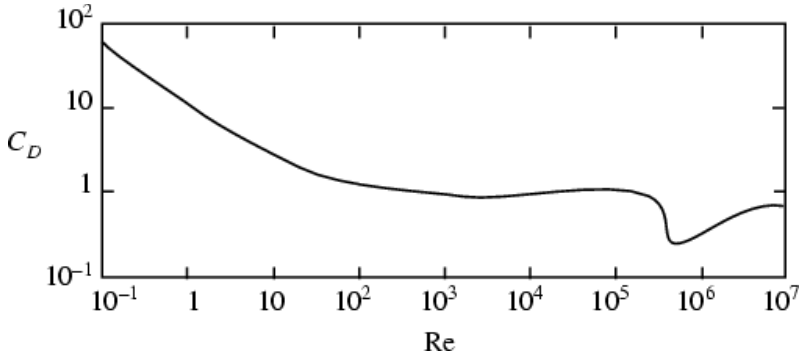


Figure 4 – Aerodynamic drag factor (C_D) on a cylinder with increasing Reynolds number. Image from Sunden (2016)

On a global-scale, extreme winds are driven by different weather systems depending on the region. In the temperate zones, extra-tropical storm systems dominate leading to large-scale pressure gradients and rapid wind flow from a consistent direction. In the tropics, convective storm systems dominate, which are much smaller and more stochastic, leading to chaotic wind flow including strong vertical components. An exception to this rule is the tropical cyclone belt, where wind damage is dominated by the return time of cyclones / hurricanes (Van Bloem et al., 2005; Ibanez et al., 2018). The wind regimes caused by these storm systems have been quantified by global monitoring networks. However, the meteorological stations are generally placed away from complex topography or forests and wind flow through and over forests is less well understood. Furthermore, mean wind speeds are much easier to measure and to measure and model than the extreme events and maximum wind speeds, which are more relevant to wind damage.

It is helpful to address the literature on wind flow over forests chronologically, based on three papers in the *Annual Reviews of Fluid Mechanics*. Prior to Raupach & Thom (1981), it was assumed that wind flow in forest canopies was a superposition of standard surface-layer turbulence and small-scale eddies produced by interaction with leaves and branches. Raupach & Thom (1981) measured wind flow over forests and showed that it is actually dominated by large (whole canopy scale) coherent structures, known as sweeps and ejections. Finnigan (2000) described the processes which give rise to these coherent structures, but only for forests of uniform height on flat ground and at a large distance from an edge. Importantly, the mean vertical velocity profile inside the canopy is inflected (Figure 5) and the dominant eddies in the flow are the result of an instability in this velocity profile. Belcher, Harman & Finnigan (2012) lifted the assumption of homogenous forest canopies and flat terrain and tackled realistic wind flow. They quantified the distance from a forest edge required for the flow to adjust to the canopy and the effect of unstable atmospheric stratification. They also show that hills can have a profound effect on the flow, since there is often a region of flow reversal on the downwind side of the hill and this can lead to an ejection of canopy air into the boundary layer above.

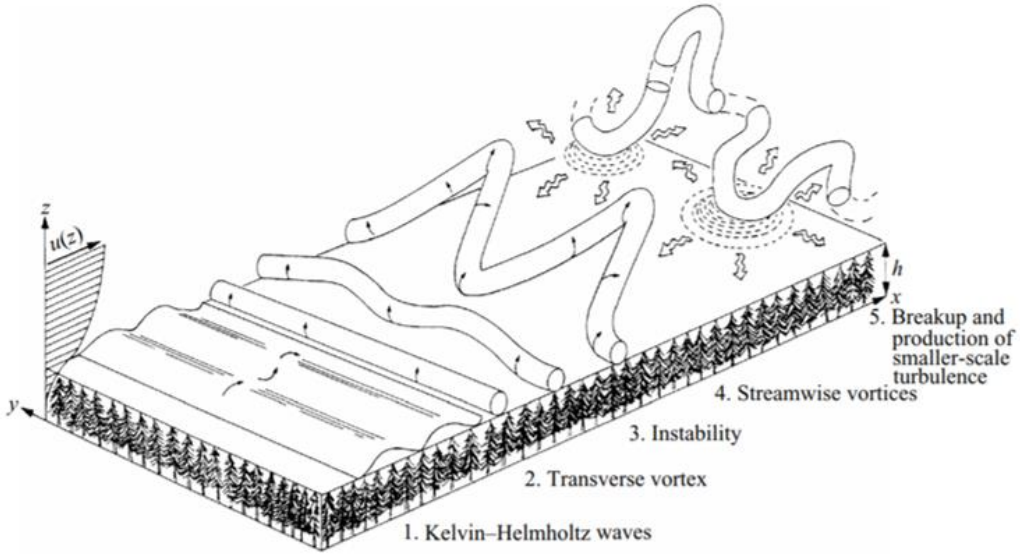


Figure 5 – Patterns of wind flow over forests (J. J. Finnigan & Brunet, 1995)

Wind flow over forests: data and simulations

Experimental measurements of wind flow in and over forests are complex, since wind speeds are highly variable in both time and space. The global FLUXNET project (Baldocchi et al., 2001) measures high resolution 3D wind flow at numerous forest sites across the world, but the interpretation of these measurements still relies on assumptions of isotropy. Belcher, Harman & Finnigan (2012) demonstrated that a single tower is not sufficient to accurately characterize wind flow. Therefore, recent field campaigns comprised of arrays of 3D sonic anemometers arranged in and around the forest canopy (Patton et al., 2011). However, the results from these expensive experiments are often highly site specific since they depend on the density of the surrounding canopy.

Information can more easily be interpreted if the wind incident on the tree or forest is controlled, and a number of wind tunnel experiments have been performed. Some of these wind tunnel experiments used 'tombstone' model trees (Figure 6B), arranged to represent the different possible planting strategies in conifer plantations (Poëtte et al., 2017). Others focussed on a single tree, aiming to characterise the streamlining behaviour and the effect of the canopy on the wind regime.

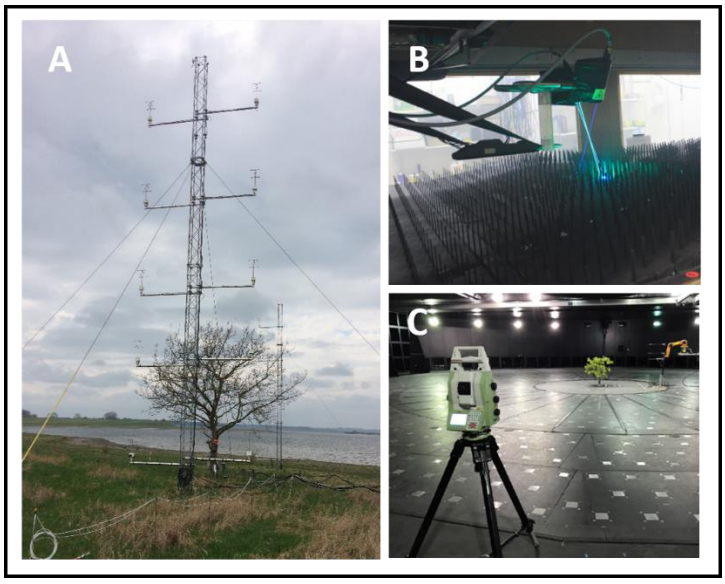


Figure 6 – A: Single Tree experiment in Roskilde, Denmark. B: Small-scale representation of a forest canopy in a wind tunnel. C: WinDEEE dome, the largest wind tunnel in the world, exposing a small tree to a highly controlled wind loading.

Simulations of wind flow can be broadly split into Reynolds Averaged Navier Stokes (RANS) simulations and large eddy simulations (LES). RANS models represent turbulence from large

scales right down to the dissipation scales, but only calculate the mean properties of the flow. LES methods represent only part of the turbulent scales, but explicitly models flow at different Reynolds numbers. Both methods are computationally intensive and neither has yet been applied to model wind flow through forest canopies with a realistic representation of the trees.

At a larger scale, there is increasing interest in the use of simple models (e.g. WAsP) combined with accurate information about the canopy and the terrain derived from airborne laser scanning (Boudreault et al., 2015). The WAsP model translates wind speeds across a forested landscape using information on topography and canopy roughness (Mortensen et al. 2001; Agafonova *et al.* 2014). It does not attempt to simulate the flow, instead it calculates 'speed-up factors' at each location, based on topography and canopy roughness, and multiplies the incoming wind speed by these factors. Initial results suggest that the accuracy of these methods is sufficient to extract mean wind speeds at 30 m resolution in temperate zones where large-scale pressure gradients drive strong winds, and efforts are ongoing to scale these analyses up to the entire globe (http://globalwindatlas.net/).

Tree response: statics

Since the forces due to wind and gravity are additive, it follows that wind is usually the limiting factor in the mechanical stability of trees (K. K. J. Niklas & Spatz, 2012). As previously explained, the full treatment of wind loading involves fluid mechanics, structural dynamics and fluid-structure interactions (de Langre, 2008). Therefore, studies on wind damage generally parameterize its effects. The instantaneous force on an object due to wind loading is given by:

$$F_D = \frac{1}{2}\rho_{air}\int_0^z A(z)\cdot C_d(Re)\cdot v(z)^2 dz \qquad \textit{Equation 3}$$

where A is the area and C_d is the drag factor, an experimentally determined parameter that depends on the Reynolds number of the flow. If we assume a constant drag factor and a vertically uniform wind profile then

$$F_D = \frac{1}{2}\rho_{air}A_{sail}C_d v^2 \qquad \textit{Equation 4}$$

where $\mathrm{A_{sail}}$ is the total sail area of the tree. The moment produced by this force at the bottom of the tree is given by

$$M_{wind} = F_D H \cos\theta \qquad \textit{Equation 5}$$

where θ is the bending angle of the tree. In order to maintain equilibrium, there must exist an equal moment in the tree, i.e. $M_{tree} = M_{wind}$. This moment is produced by the stress, σ, in the wood

$$M_{tree} = \sigma \frac{I}{r} = \sigma \frac{\pi}{4} r^3 \qquad \textit{Equation 6}$$

where I is the second moment of area, which describes the mechanical properties of a specific geometer, in this case the circular cross section of a tree trunk. Re-arranging this to solve for strain, and substituting $\sigma = \varepsilon E$, we find

$$\varepsilon = (4\pi / E_{gw} r^3)\ M_{tree} = (4\pi / E_{gw} r^3)\, F_D H \cos\theta \qquad \textit{Equation 7}$$

If we assume small deflections ($\cos\theta \approx 1$) then

$$\varepsilon = 2\pi\, (H A_{sail} / E_{gw} r^3) \rho_{air} C_d v^2 \qquad \textit{Equation 8}$$

This is the strain produced at the base of the tree for a given wind speed. In this thesis, I measure and model the strains produced in the trunks of trees. For some species, data on the modulus of rupture is available, from which the breaking strain can be obtained. If the wind speed is so high that the strain reaches the breaking strain, then the tree will snap – this is referred to as the critical wind speed (CWS).

$$CWS = \left[\frac{1}{2\pi \rho_{air} C_d} \frac{E_{gw} r^3}{H A_{sail}} \varepsilon_{break} \right]^{\frac{1}{2}} \qquad \textit{Equation 9}$$

In practice, the uniform vertical profile of wind speed is often replaced by a more realistic logarithmic profile (B. Gardiner, Peltola, & Kellomäki, 2000). Also, a number of factors are added to account for the presence of knots, the weight of the crown and the fact that wind loading is not static, but dynamic. This final point is discussed in the next section.

Possibly the most widely used wind damage model is ForestGALES (B. Gardiner et al., 2008), which assumes that the wind can be approximated by a static loading and that all trees respond in a similar and linear manner. For a given set of input parameters, ForestGALES calculates the critical wind speed for tree breakage, and the critical wind speed for uprooting

$$u(h_{break}) = \frac{1}{k D_{spacing}} \left[\frac{\pi \cdot MOR \cdot dbh^3}{32 \rho_{air} G (d - 1.3)} \right]^{\frac{1}{2}} \left[\frac{f_{knot}}{f_{CW}} \right]^{\frac{1}{2}} ln\left(\frac{h-d}{z_0} \right) \qquad \textit{Equation 10}$$

$$u(h_{over}) = \frac{1}{k D_{spacing}} \left[\frac{C_{reg} \cdot SW}{\rho_{air} G d} \right]^{\frac{1}{2}} \left[\frac{1}{f_{CW}} \right]^{\frac{1}{2}} ln\left(\frac{h-d}{z_0} \right) \qquad \textit{Equation 11}$$

where h is the average tree height, dbh is the tree diameter at breast height, $D_{spacing}$ is the average spacing between trees, z_0 is the aerodynamic roughness, ρ is the density of air, d is the zero-plan displacement, MOR is the modulus of rupture for the species, SW is the stem weight and $k = 0.4$ (the von Karman constant). The factor f_{CW} accounts for the overhanging crown weight, f_{knot} accounts for the presence of knots (usually 0.8-1), C_{reg} is a coefficient from tree pulling tests that accounts for the effects of species, soil type and rooting depth and G is the gust factor.

Other mechanistic models of wind damage include crown competition, sheltering effects and the possibility of a direct collision by a falling neighbour (Schelhaas et al., 2007). Acclimation to the local wind environment has been parameterized using the detailed aspect method of scoring (DAMS) as a scaling factor for wind loading (Nicoll et al., 2008).

For broadleaf trees, the architecture of a tree has a significant effect on the turning moment produced by a given wind loading (Pluciński et al., 2008) and so on its critical wind speed. In general, branches will snap under wind stress before the trunk, thus reducing the drag and the danger of uprooting or snapping of the whole tree. The preference for branch breakage has been shown to be general even in the most simple tree models (Lopez et al., 2011). I discuss the importance of tree architecture in the next section.

Tree response: dynamics

In the above, it was assumed that the wind speed was constant and that the tree's response was static and linear. In reality, both the wind loading and the tree's response are dynamic. The simplest way to account for the dynamic nature of wind and tree sway is by introducing a multiplication factor. ForestGALES uses a single gust factor (GF), which is defined as the maximum strain in any given hour divided by the mean strain in that hour (Gardiner, Peltola & Kellomäki 2000). This is a convenient definition, since hourly mean wind speeds, which are related to hourly mean strain measurements, are routinely recorded at many sites. However, this definition integrates the dynamic nature of wind and the dynamic behaviour of the tree, which does not help us understand these separate processes. The dynamic nature of wind is well quantified whereas the dynamic behaviour of trees is an area of ongoing study. To account for this, a dynamic amplification factor (DAF) has been introduced (Sellier & Fourcaud, 2009; Ciftci, Brena, Kane, & Arwade, 2013). This changes the definitions so that the GF is now

the ratio of maximum wind speed to mean wind speed and the DAF is the extent to which the strain is amplified, or damped, due to the dynamic motion of the tree (see Figure 7). Importantly, the DAF can be either positive or negative, because the dynamic motion of the tree can either amplify or damp the stresses and strains produced in the trunk.

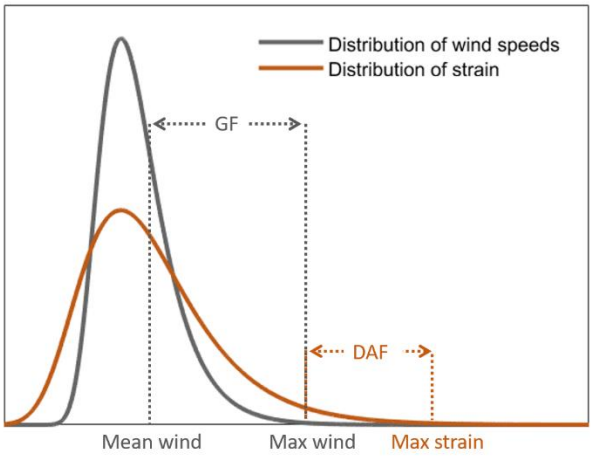


Figure 7 – Theoretical diagram of the gust factor and dynamical amplification factor.

There is ongoing debate around the value of the DAF and how it changes between trees. Schindler & Mohr (2018) use singular spectrum analysis to argue that there is no evidence for dynamical amplification (i.e. that DAF=1) for four Scots pine trees (*Pinus sylvestris*). Ciftci *et al.* (2013) use a modelling approach to argue that there is a large dynamic amplification factor and that it is dependent on tree architecture. In addition to positive amplification, the dynamic nature of tree sway can also act as a damping mechanism (Hanns Christof Spatz, Brüchert, & Pfisterer, 2007; H. Spatz & Theckes, 2013). This damping is termed either multiple resonance damping, damping by branching or structural damping. These terms are not wholly synonymous, but there is a large overlap between them and they are often used interchangeably. Théckès, Boutillon & De Langre (2015) showed that damping by branching is an efficient damping mechanism under laboratory conditions. The existence of this damping mechanism underlines the interaction between tree architecture and dynamics.

Moore and Maguire (2004a) gave a comprehensive review of the models and experiments investigating the fundamental frequencies of conifers. A meta-analysis including 602 conifers showed that the natural frequency of oscillation is proportional to dbh and tree height. This relationship can be derived from simple beam theory.

$$f_0 \propto (dbh/H^2)\sqrt{E_{gw}/\rho_{gw}} \qquad \textit{Equation 12}$$

Dupont, Pivato & Brunet (2015) used this simple relationship for conifers to model tree response to wind loading at the plot level, using a modal dynamics approach and coupling the tree motion model with an LES model. Unfortunately, natural forests are unlikely to follow the same simplifying assumptions as conifer plantations due to their complex architecture, so further work is needed before a similar model can be developed for natural forests. However, tall emergent trees may be susceptible to a simplistic description of this kind. This is discussed in papers 3 and 4.

If branching architecture plays a significant role in determining the dynamics of trees in the wind, models must therefore represent this architecture. This can be achieved using finite element analysis (J. R. Moore & Maguire, 2008; M Rodriguez, Ploquin, Moulia, & de Langre, 2012). James, Haritos & Ades (2006) developed a model of tree dynamics in which each branch is represented as an oscillating mass with a spring constant and damping coefficient. This model was used to describe three different trees that represent normal geometry, bushy trees and trees with steeply inclined main branches. Figure 8 gives the spectrum of frequencies experienced by a *Eucalyptus Teretecornus,* a 'bushy' tree, during an hour with 17 ms^{-1} average wind speed. However, these finite element analyses rely on architectural information about the trees in question, which is difficult to collect for anything but saplings.

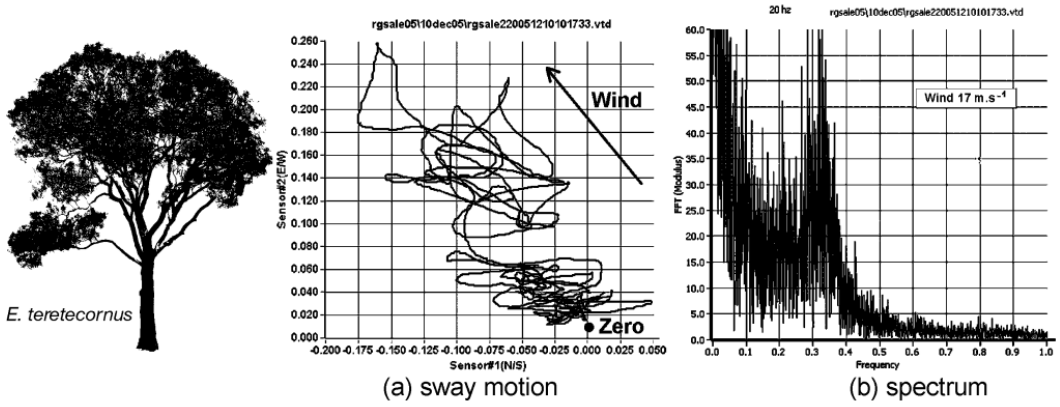


Figure 8 – Sway motion of E. teretecornus showing (a) complex sway motion of tree trunk and (b) spectrum showing sway frequency with broad, single peak at 0.32 Hz. From James et al. (2006).

Breakage conditions

Wind loading bends the branches and trunk of the tree, creating stresses and strains within the wood. If these stresses and strains reach the mechanical limits of the material, it will break. This may happen in the branches, which is not catastrophic and may even be a safety mechanism to reduce the risk of trunk breakage (Lopez, Michelin, & De Langre, 2011), the trunk or the roots. In addition, the bending force from wind loading may surpass the root-soil cohesive forces, causing the tree to uproot (Yang, Défossez, Danjon, & Fourcaud, 2014). Calculation of the force needed to uproot a tree is complex, since it depends on the details of the root architecture and material properties (Yang et al., 2014).



Figure 9 – Left – Large conifer snapped by a wind storm in Fort Smallwood (from By the Bay Photos on Flickr, creative commons). Right – Liriodendron tulipifera tree uprooted by wind on the campus of Shinshu university, Japan (photo by Kana Kamimura)

The breaking moment, above which the tree will snap, is given by:

$$M_{break} = \frac{\pi}{32} f_{knot} \cdot MOR \cdot dbh^3 \qquad \textit{Equation 13}$$

Where MOR is the modulus of rupture (see next section) and f_{knot} is an empirical factor between 0.8-1 that accounts for the weakening of the stem due to knots in the wood (Gardiner, Peltola & Kellomäki 2000). The moment at which the tree will overturn, or uproot, is generally parameterized as:

$$M_{over} = C_{reg} SW \qquad \textit{Equation 14}$$

where SW is the stem's fresh weight and C_{reg} is an empirical factor integrating the response of the root system and soil which must be estimated from tree pulling tests.

Data on the dominant type of failure for a given site is available from mode of death surveys. These surveys generally include categories for snapping, uprooting, standing dead, and unknown (de Toledo, Magnusson, Castilho, & Nascimento, 2012). These categories do not definitively tell us what caused the tree death, for example a large tree may snap numerous

surrounding trees when it falls, and trees uprooted by wind may first have been weakened by disease. Nevertheless, mode of death surveys represent the best estimate of the rates of snapping and uprooting. Everham & Brokaw (1996) provided a summary of all mode of death studies up to that date and I have collated a number of more recent studies (Figure 10, Table 1).

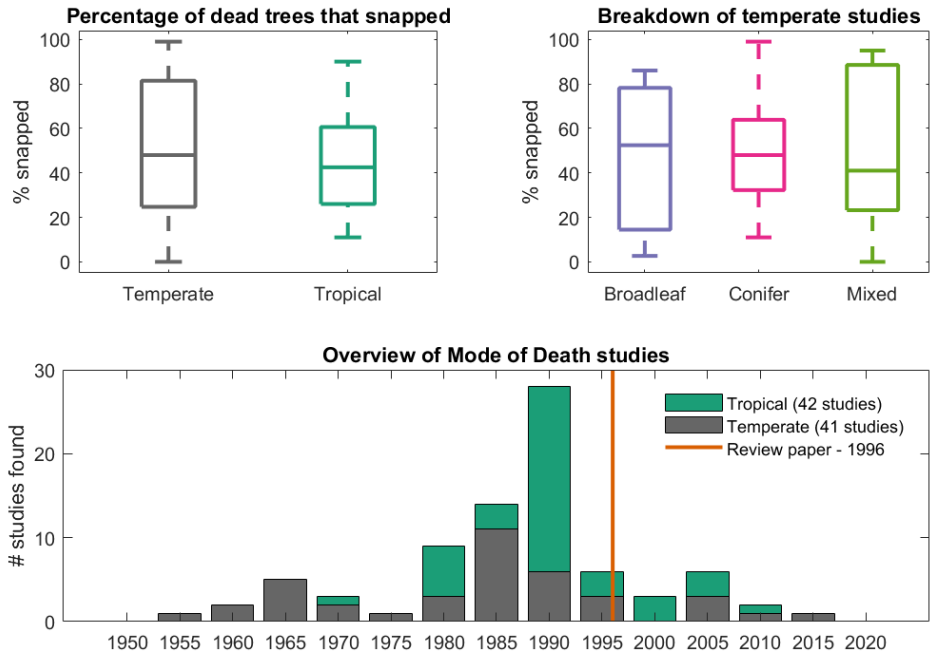


Figure 10 – Overview of mode of death studies. Percentage of dead trees that snapped divided by region (top left) and forest type (top right). Bottom: number of studies that mention mode of death from 1955 -2015, where each date represents the previous 5 years.

In general, I find that mean the ratio of snapped trees to uprooted trees is approximately 50-50, although there is massive variation across different sites. Differences in the methodology and data presented in the papers preclude a simple analysis to test whether environmental or topographic predictors explain part of this variation. However, Gale & Hall (2001) surveyed the mode of deaths in Danum Valley and found that, of 516 dead trees, 37% of trees died standing, 22% snapped, 24% either snapped or died standing, 14% uprooted and 3% were not determined. They also show that the proportion of snapped trees was greatest in the valleys, and that uprooting is more common on deeper soils.

From a modelling point of view, it is far easier to predict the wind speed at which a tree will snap, rather than uproot, since the latter requires a map of the root system and an understanding of the forces at the soil boundary (Yang et al., 2014). In this thesis I assume that, on average, trees will grow so as to maintain roughly equal likelihoods of snapping or

uprooting i.e. that they are not 'over-engineered' in either aspect. I therefore focus on snapping and neglect uprooting.

Author	Location	Year	Percentage		
			Snapped	Uprooted	Standing
van der Meer & Bongers (1996)	French Guiana	1996	62	38	0
Gale & Barfod (1999)	Ecuador	1999	35	34	15
Gale & Hall (2001)	Danum Valley, Malaysia	2001	22	14	37
	Belalong, Bruneii	2001	26	21	31
	Andalau, Bruneii	2001	11	14	46
Nishimura (2005)	Japan	2005	55	45	0
Jönsson *et al.* (2007)	Sweden	2007	49	41	22
	Sweden	2007	45	0	55
Martini *et al.* (2008)	Brazil	2008	27	33	26
Chao *et al.* (2009)	Lowland Peru	2009	51	19	14
	Venezuela	2009	14	25	48
de Toledo *et al.* (2012)	Central Amazonia	2012	26	16	51
Holzwarth *et al.* (2013)	Germany	2013	3	5	61
Guillemette, Gauthier & Ouimet (2017)	Quebec	2017	22	17	61

Table 1 – Mode of death studies since 1996 review

Material properties

In this thesis I assume uniform material properties throughout the tree. The three most important properties of wood, from the point of view of mechanics, are the green wood density, ρ_{gw}, modulus of elasticity (often referred to just as the 'elasticity'), E_{gw}, and the modulus of rupture, *MOR*. Elasticity is a measure of a materials resistance to bending and is defined as the ratio of the applied stress (or pressure, in units of MPa) to the strain (dimensionless). E_{gw} can be determined by a three-point bending test, where a beam is supported at both ends and a force is applied in the middle. It is important to distinguish elasticity from stiffness. The former is a material property (an intensive property), while the latter is a property of a beam or structure (an extensive property). The stiffness of a cylindrical beam is a product of its elasticity and its radius raised to the 4^{th} power, so a tree can achieve a high stiffness through changes in elasticity or by diameter growth. The modulus of rupture is the tensile stress at the point at which the material fractures, measured in bending. In the

example of the three-point bending test, if the force is increased until the sample breaks then the modulus of rupture has been reached.

Wood material properties vary within individual trees, both radially and with height, between trees of the same species, and between species. The variation in material properties of trees is associated with different life strategies. In general, shade-tolerant trees invest in dense wood and grow slowly while emergent trees grow quickly, leading to relatively light wood. The macroscale properties of wood are a consequence of its complex anatomy. In this thesis we focus on hardwoods, which are distinguished from softwoods by the presence of vessels and lack of conifer-type tracheids. The main structural element of the cell wall is cellulose (Barnett & Bonham, 2004). Cells with thick walls, usually fibres, contribute a large part of the mechanical strength of the wood. The angle at which cellulose microfibrils spiral within the cell walls contributes to the wood's resistance to bending and torsion. The nature and arrangement of vessels, parallel to the trunk of the tree, and rays, perpendicular to the trunk of the tree, also influences macroscale properties (Hepworth, Vincent, Stringer, & Jeronimidis, 2002; K. K. J. Niklas & Spatz, 2012). The complexity of wood anatomy and the wide variation between species means that calculating macrostructural properties as a superposition of microstructural properties is prohibitively complex (de Borst, Bader, & Wikete, 2012). However, it is clear that wood is a highly asymmetric material and that trees will respond differently to bending and torsional forces depending on the direction of force (Niklas & Spatz 2012). In addition, the material properties of wood change with moisture content. A striking example of this are baobab trees which, despite their large diameters, are not exceptionally stable since the their saturated wood has a very low elasticity (Chapotin, Razanameharizaka, & Holbrook, 2006).

Publication	Density	Elasticity	MOR	# Species
The strength properties of timbers (Lavers, 1983)	Yes, Yes	Yes*, Yes*	Yes*, Yes*	221
Worldwide correlation of mechanical properties (K. J. Niklas & Spatz, 2010)	Yes	Yes	Yes	177
Stuttgart table of tree strengths (Wessolly & Erb, 2016)		Yes	Yes	46
Global wood density data base (Chave et al., 2009)	Yes			8412

*Table 2 – Sources of data on the material properties of wood. Green text indicates that values were measured for green wood. * indicates that error estimates were provided.*

The main data sets for wood material properties are described in Table 1. Dry wood density data has been widely collected, but elasticity and green wood material properties are more rarely studied. We have data on the elasticity of dried timber, and in some cases green wood elasticity too. These measurements focus on the differences between species. They also give us some information about the variability within species, but about the variability within individual trees much less information exists.

Crucially, it is the ratio of elasticity to density that is relevant to Euler buckling (Equation 1), and the fundamental frequency of trees (Equation 12). Elasticity and density are strongly related, so their ratio is quite stable. However, the resistance to wind loading (neglecting the self-weight of the tree) depends only the elasticity equation (Equation 9). The properties of green wood and dry wood are also strongly related. Where no pertinent data exist I use equations 15-17, derived from Lavers (1983), to predict the unknown information. Where no material properties data at all exist for a species, I use a genus average. Where no data on a given genus exist, or we do not know the genus of the tree, I use plot-level averages. Each stage of abstraction brings increased uncertainty in addition to the variation at the tree and sub-tree levels.

$$\rho_{gw} = 1.2 \times \rho_{dw} + 27.3 \quad \textit{Equation 15}$$

$$E_{gw} = 14.6 \times \rho_{dw} + 157.6 \quad \textit{Equation 16}$$

$$MOR_{gw} = 0.12 \times \rho_{dw} - 7.14 \quad \textit{Equation 17}$$

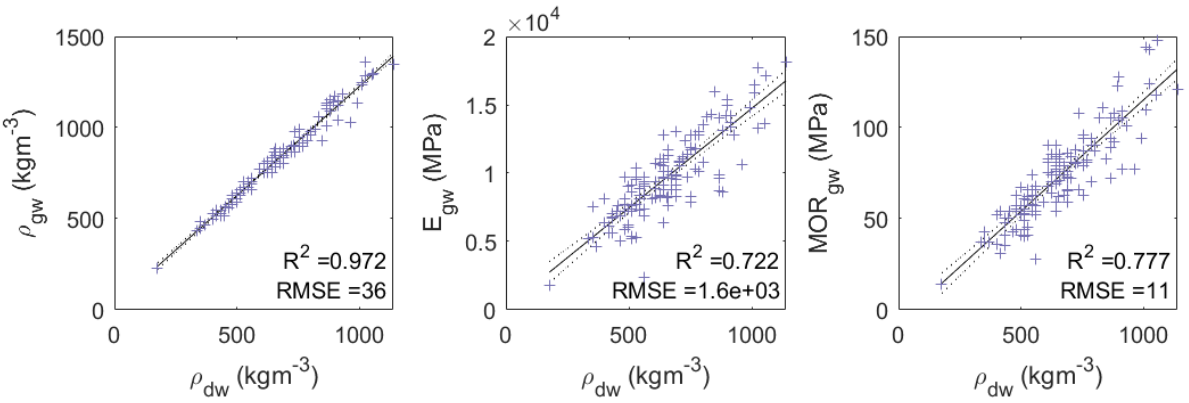


Figure 11 – Relationship between dry wood density and green wood density (left) green wood elasticity (middle) and green wood modulus of rupture(right).

Review of methodology

I used a combination of field data and modelling to achieve the aims of this thesis. The field experiment was small-scale, using strain gauges and anemometers to monitor wind speeds and tree responses for 21 trees in Wytham Woods, Oxford and for 19 trees in Danum Valley, Malaysia. Due to the high cost of sonic anemometers and data loggers I chose not to measure wind speeds in great detail, focussing my resources on the tree responses. The modelling work primarily involved finite element models of trees in the wind, where the 3D architecture of the trees was derived from TLS data. I use both the field data and modelling work separately to explore the response of trees to wind loading, and also combine the two in order to test the accuracy of the modelling approach. Each step of the data collection, processing and finite element analysis are discussed in detail below.

Field data collection

In this section I discuss the field data collection methods. The two most common sensors used to measure the motion of trees in response to wind loading are accelerometers and strain gauges (Table 1). I decided to use strain gauges in order to measure absolute values of strain and so estimate the critical wind speeds, although accelerometer data from co-authors is used in paper 3. In the following, I describe the circuits and data logging systems used in conjunction with the strain gauge.

	Accelerometer	*Strain gauge*
Measures	Acceleration (2D or 3D)	Strain (1D)
Data logger required?	No – internal storage	Yes – with excitation voltage
Absolute values?	Difficult, requiring double integration	Yes – with appropriate calibration
Cost	Cheap – used in smartphones	Medium – mainly due to data loggers
Common mounting position	Top of the trunk, to capture maximum acceleration	Near the bottom of the trunk, in perpendicular pairs.
Used for	Spectral analysis	Spectral analysis and critical wind speed estimates

Table 3 – Comparison of strain gauges and accelerometers for measuring tree sway.

Firstly, the usage of the term 'strain gauge' in this thesis, and in the literature more generally, is a slight misnomer. The 'T' shaped metal sensor attached to the tree (Fig 12, 13) is rightly called a strain gauge calliper (or transducer), and is used to amplify the extension so that it can be more accurately measured. The strain gauge is a small electrical component whose resistance changes as it is bent, and it is glued onto the strain gauge calliper. I distinguish between strain gauges and strain gauge callipers in this section, but in other parts of the thesis they are used interchangeably. Each tree requires two strain gauges attached approximately perpendicular, in order to capture the two independent axes of motion.

Due to equipment limitations, I used two separate systems to measure strain. I here describe the first system in detail and then point out the differences for the second system. Strain transducers were designed by Blackburn (1997) and Moore *et al.* (2005) and the Northern Research Station, Forest Research.

System 1

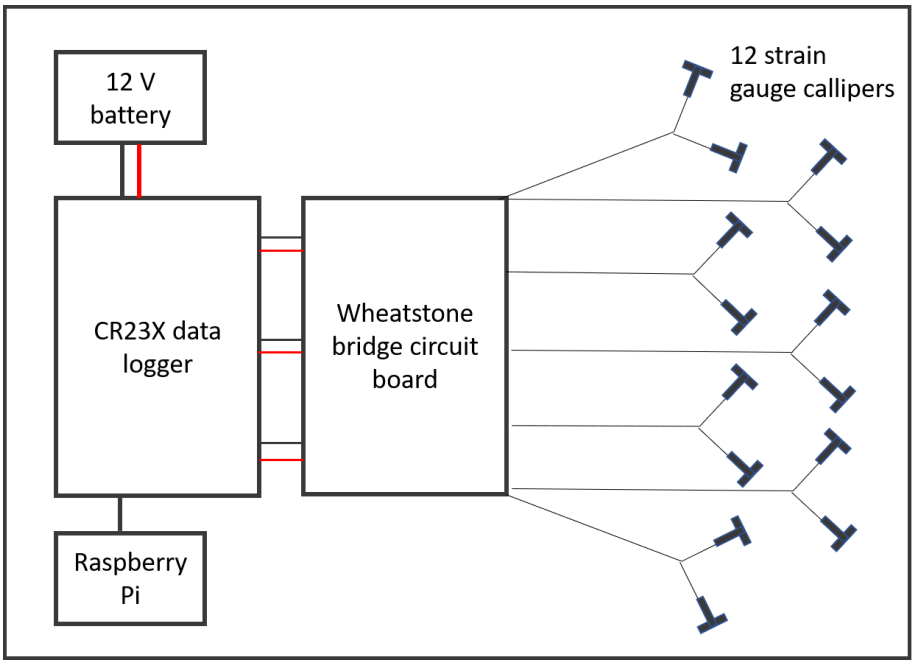


Figure 12 – Diagram of strain gauge monitoring system 1.

This system used a CR23X data logger to monitor 12 strain gauge callipers. The limited (4 Mb) storage of the CR23X was supplemented using a Raspberry Pi. The callipers were wired in pairs to reduce the total length and weight of wire. An excitation voltage was pulsed at 4 Hz from the data logger through a circuit containing the strain gauges. This circuit contains a wheatstone bridge, across which the voltage was measured, also at 4 Hz. As the tree bends,

the resistance of the strain gauges and so the voltage across the wheatstone bridge changes proportionally. In this system, each calliper had two strain gauges attached so that they both respond to the bending of the tree, thus doubling the signal (marked in red on Figure 13, R1 and R2 in the wheatstone bridge circuit diagram).

The wheatstone bridge circuit contains a variable resistor which can be adjusted with a screwdriver, so that the voltage signal can be adjusted in the field to keep it close to zero. The voltage signal must be kept between -10 and 10 mV for the data logger to store the values at sufficient resolution. Since the voltage drifts with environmental conditions I often found that the signal exceeded this range and so the resolution decreased, leading to an unreliable signal. This was more problematic in Malaysia than in the UK due to the climate, and system 1 was more susceptible than system 2. Unfortunately, this fault led to the loss of data from the Malaysian field campaign, the implications are discussed in detail in the fourth paper.

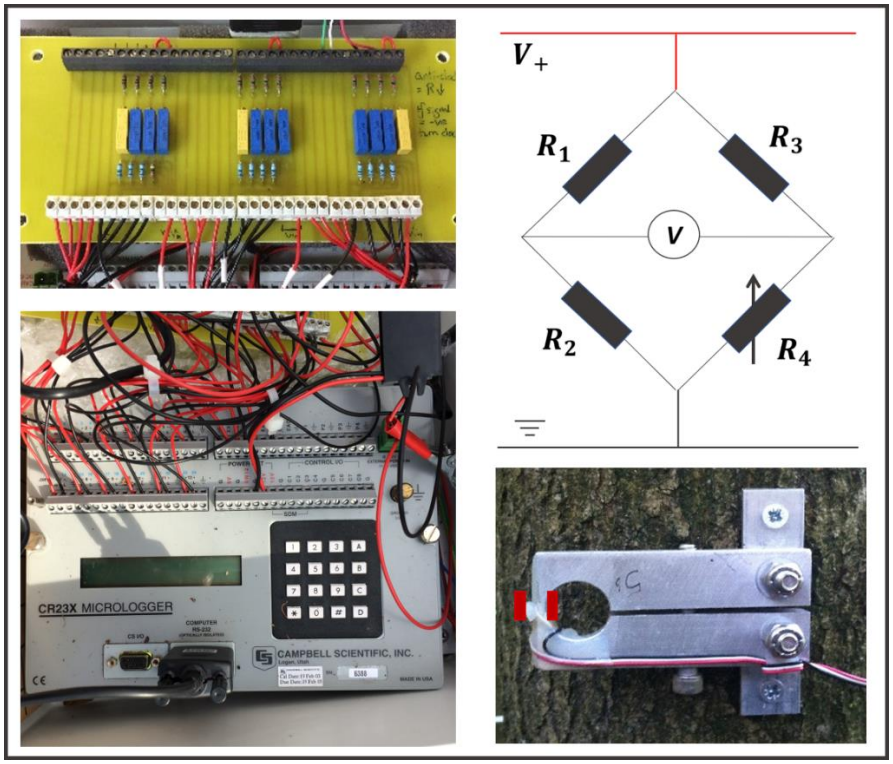


Figure 13 – Top left: printed circuit board containing 12 wheatstone bridge circuits. Top right – single wheatstone bridge circuit. Bottom left – CR23X. Bottom right – strain gauge calliper with red rectangles showing the location of the two strain gauges.

System 2

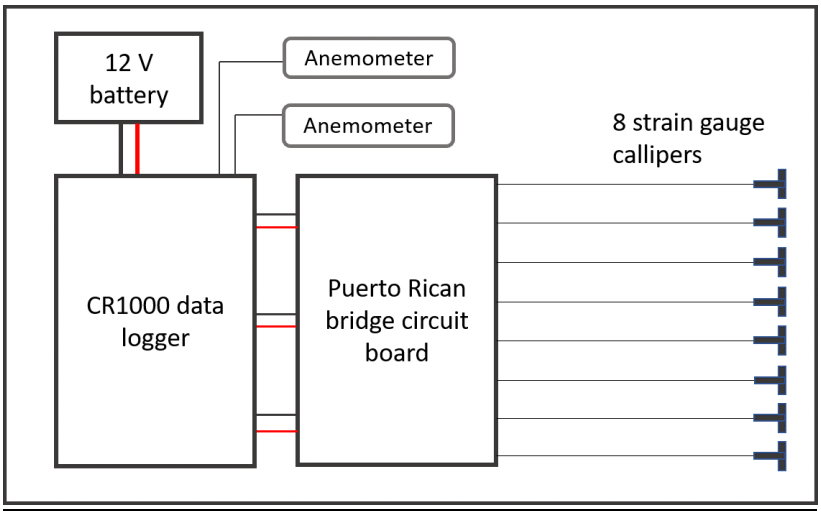


Figure 14 – Diagram of strain gauge monitoring system 2.

System 2 monitors 8 strain gauge callipers and 2 anemometers using a CR1000 data logger. The differences between system 2 and system 1 are:

- the callipers are wired individually, meaning that more wire is required;
- the wheatstone bridge is replaced with a Puerto Rican bridge (this is only a slight variant)
- only one of the strain gauges is active, the other is attached to the calliper in order to account for the thermal expansion of the material, thus reducing the signal drift. This final point proved very important since it meant that much of the data collected with system 2 in Malaysia is unreliable.

Data logger programming and power constraints

The CR1000 data loggers were programmed using CR basic scripting language, and the CR23X data loggers using EdLog. Strain gauges are active sensors, meaning that they require an excitation voltage to function. In order to save battery power, the excitation voltage was pulsed at 4 Hz and the response voltage monitored at the same frequency. For this reason, and due to the power supply to the raspberry pi in the case of the CR23Xs, the amount of battery power proved a limiting factor.

The CR1000s logged for approximately 2 weeks using a standard 12 v, 7.2 Ah motorcycle battery, whereas the CR23X with raspberry pi lasted only 2-3 days before running out of battery. Therefore, a trigger system was designed so that the Raspberry Pi would only be switched on during windy condition. This trigger was based on the fact that a high variance in

the strain data corresponds to windy conditions, since the CR23Xs cannot log wind speed sensors. Unfortunately, the strain offset increased dramatically over time due to environmental conditions and the growth of the trees. This led to a reduction in the resolution of the data logged by the CR23X and consistently low variances and the failure of the trigger system. For this reason, the Raspberry Pis failed to log significant amounts of data during the Malaysian field campaign.

Field data processing

I analysed the field data in both time and frequency domains. Spectral analysis (frequency domain) has the significant advantage of not requiring calibrations or other data treatment prior to analysis. I calculated the Welch's power spectrum (Krauss, Shure, & Little, 1994) for each section of strain data and so extracted the fundamental frequency as well as higher order natural frequencies. In order to do this efficiently and automatically I smoothed the power spectrum and used Matlabs *findPeaks* function (Figure 15).

Time-domain analysis (e.g. estimating critical wind speeds) relies on a number of data processing steps. In this analysis I followed the approach taken in multiple previous studies (Gardiner, Peltola & Kellomäki 2000; Wellpott 2008; Hale *et al.* 2012). Firstly, the mV data were multiplied by a calibration coefficient to give strain values. These calibration coefficients were derived prior to installation by stretching the callipers by a known amount and recording the change in voltage. Second, since the resistance of the strain gauges drifts with environmental factors, the resulting offset was removed by subtracting a running mode in papers 1 and 2 (Figure 16) or a Butterworth filter in paper 4. Thirdly, the data were re-projected into the northward and eastward directions, since irregularities in the bark meant the callipers were not always attached on these sides. Finally, the maximum strain at any point on the circumference of the trunk was calculated from the signals from each pair of callipers using Pythagoras' Theorem (Figure 17).

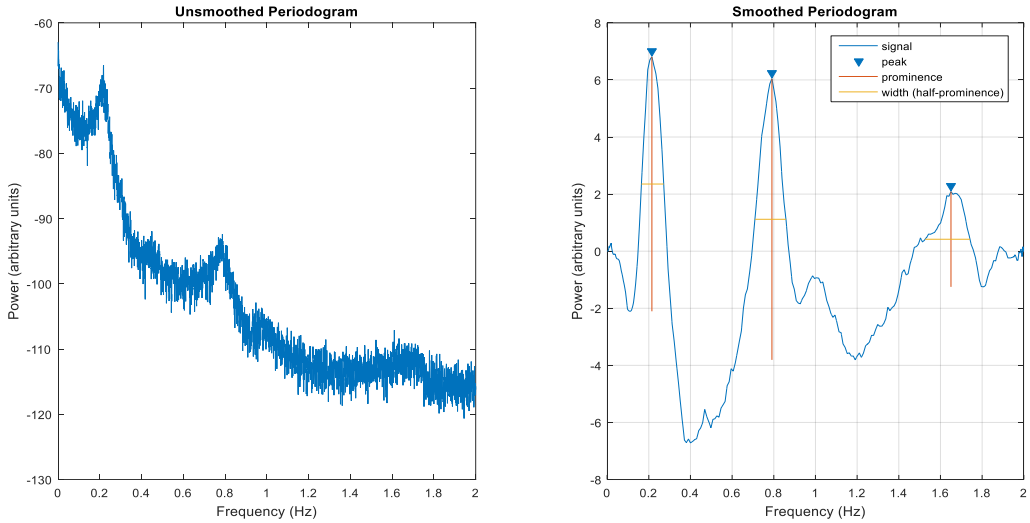


Figure 15 – Example Welch's power spectrum for strain data collected in Wytham Woods. Left – unsmoothed spectrum. Right – smoothed spectrum used to automatically detect peaks.

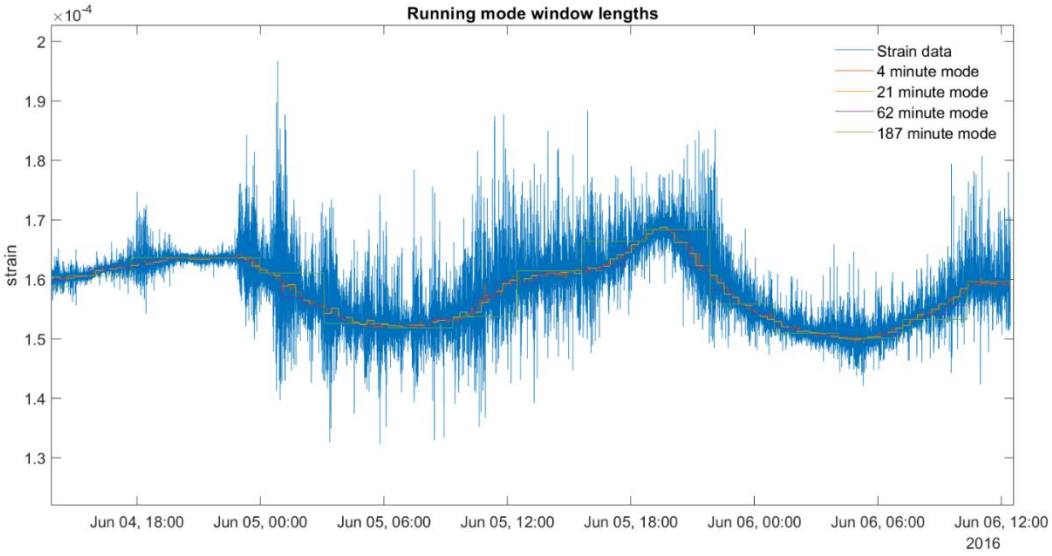


Figure 16 – Strain data showing characteristic drift over time with running modes overlaid.

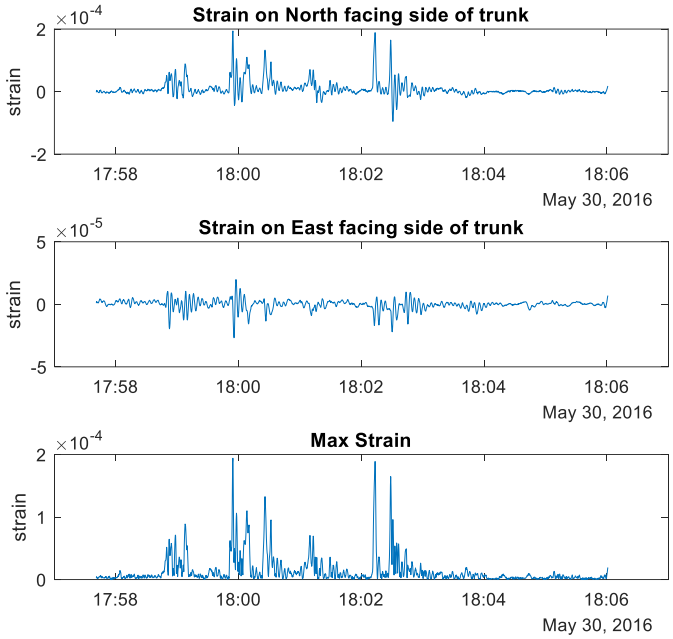


Figure 17 – Top two panels – Strain data from North and East facing side of the trunk. Bottom – Maximum strain calculated by combining the two strain channels.

There was a detailed discussion about the best method to remove the inevitable offset at the 2017 Wind and Trees conference in Boulder, Colorado, and the 2018 Wind and Tree Response Measurement Workshop in Roskilde, Denmark. The current method was presented in both the conference and the workshop and compared to other methods used to remove this offset. The use of the running mode is based on the assumption that the tree will regularly pass through its equilibrium position (Wellpott, 2008; S. E. Hale et al., 2012) and is relatively insensitive to the length of the running mode window (see paper SI-2). For the strain data from Danum Valley, a bandpass filter was applied to remove the offset. This technique gave very similar results to the running mode and was considered a simpler solution.

The result of the above data treatment process was a 4 Hz time-series of maximum strain for each tree. I used this high-resolution data to test the direct correlation between wind and strain (paper 1 Figure 3). In order to explore the more general properties of the wind-strain relationship I extracted the wind and strain maxima at one minute, ten minute and hourly resolutions (Figure 18). The appropriate time-resolution depends on the aims of the analysis and was constrained by the quality of the data. I generally used hourly data for Wytham Woods and ten-minute maxima for Danum Valley. Furthermore, since the data quality was lower in Danum Valley I used a robust maximum selection method (Wellpott, 2008; S. E. Hale et al., 2012). I then calculated the gradient of strain against squared wind speed for each tree

using an ordinary least squares technique. In the case of Wytham Woods, this gradient was used to extrapolate up to the critical wind speeds, as described in papers 1 and 2.

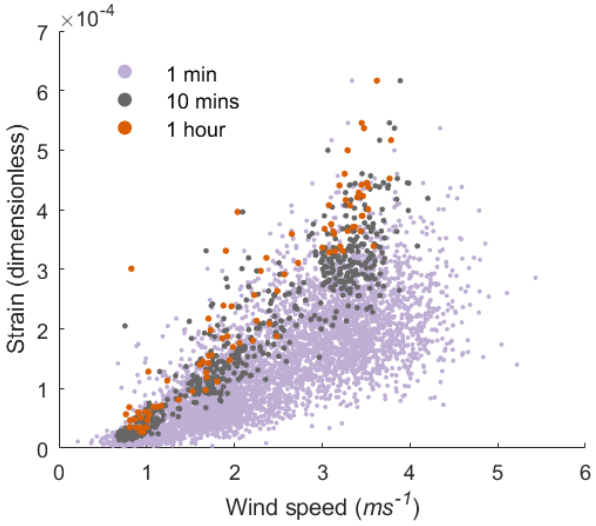


Figure 18 – Mean wind against maximum strain at different time resolutions for a single tree in Wytham Woods.

Terrestrial laser scanning data collection and processing

TLS data collection was carried out in collaboration with colleagues at University College London and the National Physical Laboratory. All TLS data used in this thesis was collected with a Riegl VZ-400. In Wytham Woods and Danum Valley the data were collected by marking out a 10 m grid, performing a horizontal and a vertical scan at each vertex on the grid at 0.04 degrees angular resolution, and then co-locating the resulting 242 scans using reflectors placed around the scanner at each location. Automatic tree segmentation algorithms were then used (mainly by UCL collaborators) to extract individual trees from the plot level point cloud (Burt, 2017; Kim Calders et al., 2018). The accuracy of this extraction depends on the resolution of the TLS scan which, as we used consistent scanning techniques, depends on the forest structure. Dense or tall forests result in a lower density point cloud, due to occlusion and beam divergence. The result was that the Wytham Woods TLS data are of very high quality and the Danum Valley TLS data are not. In fact, the automatic tree segmentation algorithms did not work as expected on the Danum Valley TLS data, so the focal trees were manually extracted as described in paper 4.



1. Collect data
Using a Riegl VZ-400, 0.04 degrees angular resolution on a 10 m grid.

2. Co-locate scans
Horizontal and vertical scans at each location (242 total). Co-locate using reflectors.

3. Find individual trees
Manually or automatically using *treeseg*.

4. Fit QSMs
Using *TreeQSM*, and select optimum parameters.

5. Simplify QSM
Delete small branches and combine neighbouring cylinders together.

Figure 19 – Left: Comparison of the TLS data for a 51 m Parashorea malaanonan from Danum and a 24 m Fraxinus excelsior from Wytham Woods. The trees are to scale. Right: TLS data processing workflow diagram.

Once the individual tree point cloud had been obtained I fitted a quantitative structure model (QSM) using the freely available package *TreeQSM*. I occasionally refer to the QSM as a 3D cylinder model, since the QSM comprises a number of cylinders which outline the geometry of the tree. This package was under development during the course of this work, so multiple versions were used at different points, but all published results, and the results in this thesis, use the most up to date version. QSM fitting is a stochastic process and produces slightly different results each time. Unless otherwise stated I always used the optimal QSM, which is selected automatically by minimizing the point-cylinder distances. A growing body of

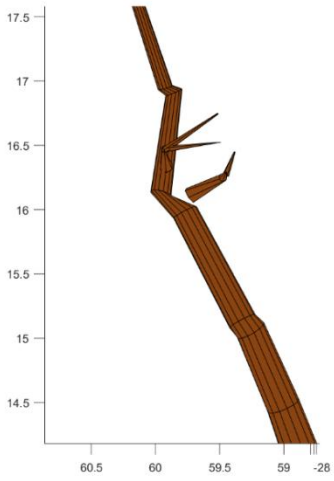


Figure 20 – Example of a typical problem with a QSM

literature deals with QSM optimization, primarily with the aim of accurate biomass estimation (K Calders et al., 2015; Burt, 2017; Disney et al., 2018).

I often found that the QSMs had unrealistic topology, such as multiple cylinders occupying the same space or two large cylinders connected by one small one. These idiosyncrasies are not a serious problem if the aim is to estimate total volume, but even one poor connection in the trunk radically alters the mechanical stability of the structure and is therefore important for the current study. For this reason I found that many of the finite element simulations failed to converge as soon as any force was applied. I therefore inserted a simplification step between QSM fitting and conversion to finite element analysis. This step consisted of combining neighbouring cylinders and deleting cylinders with a radius under a given threshold (usually 2 cm) and is described in paper 1. I made no attempt to use TLS data to retrieve information about the leaf distribution nor to validate that the tree reconstructions accurately represented the tree geometry.

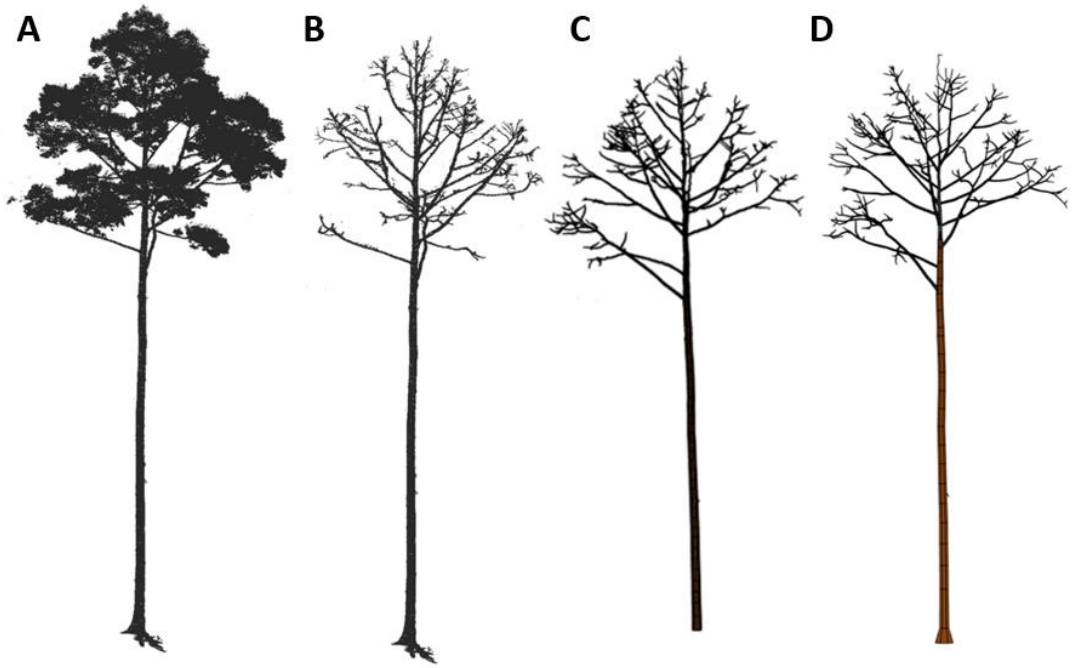


Figure 21 – TLS data processing steps for a Shorea parvifolia from Danum Valley. A – single tree point cloud. B – point cloud with noise and leaves manually deleted. C – selected QSM. D – simplified QSM.

Extracting architectural indices

Once the simplified QSMs were obtained, I extracted the following architectural indices from them:

- Crown area – maximum ground area covered by the crown viewed from above.
- Crown aspect ratio – ratio of maximum crown width to crown height.
- Crown volume ratio (CVR) – ratio of total woody volume of the tree to that in the stem. Note that in paper 4 I use a slightly different metric, *K*, instead.
- Crown asymmetry – the ratio of mean to maximum volume in segments of the crown, which are defined by splitting the crown into eight azimuthal segments, centred on the stem.
- Path fraction – ratio of mean to maximum base-to-twig path length, this is considered a proxy for water use efficiency (Savage et al., 2010; Bentley et al., 2013).
- Mean branching angle – the average angle between two cylinders at each branching point.
- Total volume – total volume of all the cylinders that make up the tree.
- Total sail area – total woody area projected into the x-z plane.

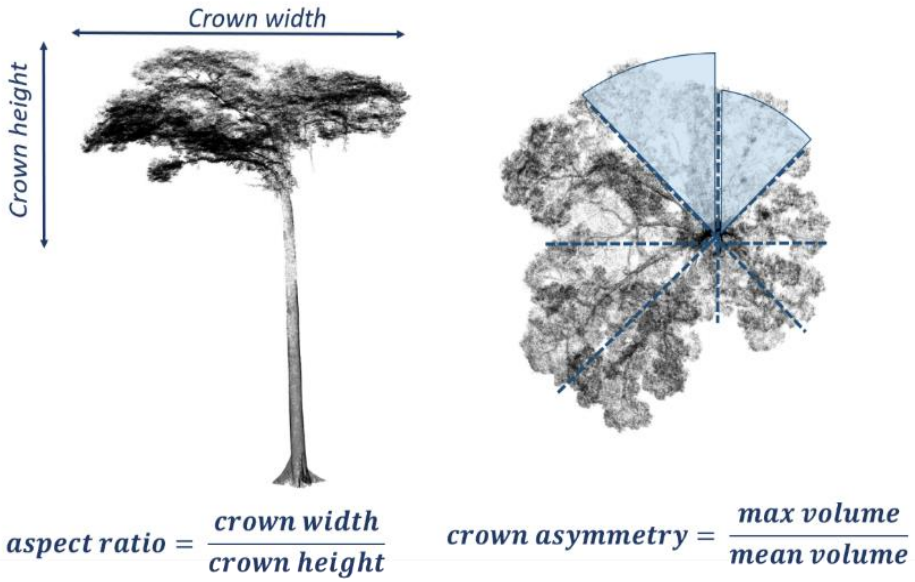


Figure 22 – Diagram showing two key architectural measures derived from TLS data.

Finite element analysis

Finite element analysis is a common engineering technique which involves breaking up a complex calculation into a large number of smaller, more tractable calculations (Pepper & Heinrich, 2017; Rao, 2017). In this case, the complexity arises from the tree geometry and the simplification is to compute the effect of the forces on each cylinder individually. I decided to use the finite element package Abaqus based on personal recommendations, because a license was readily available from the Oxford engineering department and because it includes an AQUA module, which parameterizes the effect of wind loading. Abaqus automatically solves the following equation of motion at each time-step in the simulation

$$M\ddot{q} + D\dot{q} + Kq = G + F_D \qquad \textit{Equation 18}$$

where q, $\dot{q}$ and $\ddot{q}$ are the nodal displacement, velocity and acceleration vectors. M, D and K are the mass, damping and stiffness matrices respectively, and G represent the force due to gravity. The wind drag force, $\mathrm{F_D}$, on each cylinder of the QSM is given by

$$F_D = Amp \cdot \rho_{air} C_D r \Delta V_{fn} \left\| \Delta V_{fn} \right\| \qquad \textit{Equation 19}$$

where Amp is a user defined amplitude that describes the horizontal variation in wind speed, ρ_{air} is the density of air, C_D is the drag factor, r is the radius of the cylinder, and ΔV_{fn} is velocity difference between the wind and the beam. As in previous work (Sellier et al., 2006; J. R. Moore & Maguire, 2008; Sellier & Fourcaud, 2009; Ciftci et al., 2013), I assumed a constant drag factor, although in fact the drag factor varies with the Reynolds number of the flow.

A number of previous studies have used the finite element method to simulate the dynamics of trees in the wind (Sellier et al., 2006; Sellier, Brunet, & Fourcaud, 2008; J. R. Moore & Maguire, 2008; Ciftci et al., 2013). However, these studies either focused on a small number of trees or used theoretical tree geometry derived from fractal branching models. The advantage of TLS is that tree geometry can now be mapped for hundreds of trees. I therefore developed a batch processing workflow (summarized in Figure 23) to convert a QSM into an Abaqus input file written in the Abaqus scripting language.

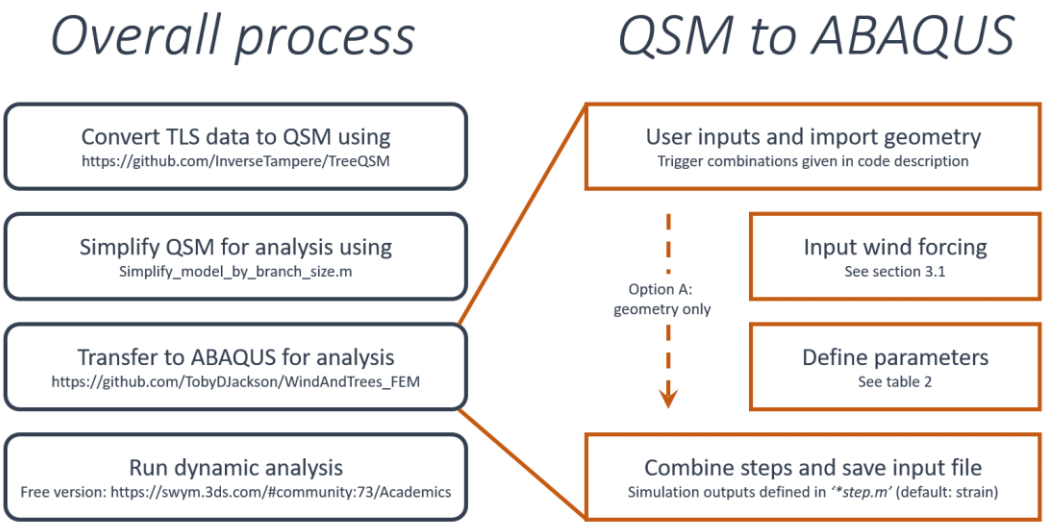


Figure 23 – Diagram of the TLS to finite element analysis workflow

The right-hand side of figure 23 describes the Matlab package written as part of this project (Tobias Jackson, 2017). The first step is to import the tree geometry. Each cylinder is imported as a two-node Euler-Bernoulli (B31) and assigned an individual coordinate system aligned along its main axis. No information on the roots was available so the lowest cylinder of the QSM was fixed, via a universal joint and dashpot system, to the ground. This is an attempt to model the root-soil boundary with the universal joint and dashpot modelling the flexing and damping respectively.

It is important to emphasise that this workflow simulates each tree individually and applies the same wind regime independent of the trees location within the forest. This is a fundamental limitation and is not attempted to be overcome in this thesis. Another limitation of the Abaqus AQUA module is that the vertical profile of wind speed is limited to a power law.

$$v = v_0 \left({}^{h}/_{h_{ref}} \right)^{\gamma} \qquad \textit{Equation 20}$$

where v is the wind speed at a given height h, v_0 is the reference wind speed at reference height h_{ref} and γ is a user defined parameter. I chose the γ value that best reflected my limited wind data.

In order to characterize a tree's response to wind loading I extracted three outputs from Abaqus simulations.

1. I extracted the natural frequencies of the tree based on the eigenvalues of the mass matrix using a subspace method (Viberg, 1995). This is used in papers 1 and 3.
2. I apply a stepwise wind ramp to estimate the gradient of the wind-strain relationship. This is comparable to the static loading described by equations 3-11, except that changes in the tree geometry and the weight of the overhanging crown are explicitly modelled. This is used in papers 1, 2 and 4.
3. I apply a time-series of wind loading derived from field measurements in order to compare the simulated trees response with the measured trees response. This allows us to investigate the spectral properties of the response, but its applicability is strongly limited by the location and resolution of the wind measurements.

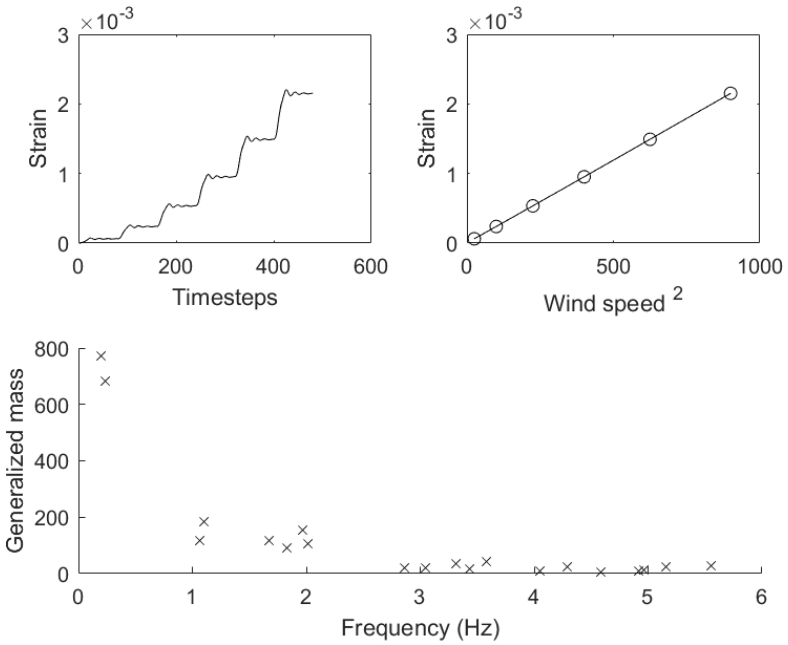


Figure 24 – Abaqus output. Top left: strain against time for a step-wise increasing wind speed. Top right: wind-strain relationship interpolated from the step-wise means. Bottom: frequency analysis output showing a dominant, low frequency paired mode as well as higher order modes.

Paper 1

My first paper is essentially a methods paper, giving a detailed description of the workflow involved in carrying out finite element analysis based on TLS data. This paper also describes the field data collection in Wytham Woods and the data processing pipeline. I then test the accuracy of finite element analysis using the field data and the sensitivity of the finite element analysis to changes in the input parameters. This paper serves as a baseline for papers 2 and 3, which use finite element analysis to study the response of trees to the wind in an ecological sense. This paper addresses thesis aim 1 by applying field techniques developed for plantation forests (strain gauges) to natural forests, this is extended in papers 3 and 4. This paper also addresses thesis aim 2 by using TLS data as the basis of a finite element analysis and then validating these simulations against the field data.

The ideas and structure of this paper were conceived and by me and my supervisors, and much improved by an anonymous reviewer. I assisted with the TLS data collection in summer 2015, this was led by co-authors from UCL and the National Physical Laboratory. I developed the TLS to finite element analysis workflow and created a batch processing script in Matlab which coverts multiple QSMs to Abaqus input files. Professor Thierry Fourcaud advised me on the implementation of the finite element analysis. I received strain gauges from Forest Research, Scotland, and from Scion Research, New Zealand. I then built the circuit boards and programmed the data loggers in order to deploy these strain gauges in the field, Dr Axel Wellpott's experience with data logging systems was invaluable here. I also led the fieldwork with the help of summer student Jess Zionts and the field data analysis with the help of Bavisha Kalyan. This paper was presented at the 2017 Wind and Trees conference in Boulder, Colorado, and is published in an associated special issue of Agriculture and Forest Meteorology.

Finite element analysis of trees in the wind based on terrestrial laser scanning data

T. Jackson[1], A. Shenkin[1], A. Wellpott[2], K. Calders[3], N. Origo[4,5], M. Disney[5,6], A. Burt[5], P. Raumonen[7], B. Gardiner[8], M. Herold[9], T. Fourcaud[10], Y. Malhi[1]

1 – Environmental Change Institute, School of Geography and the Environment, University of Oxford, OX1 3QY, UK

2 – Facility for Airborne Atmospheric Measurements, Wharley End, Bedford MK43 0AL, UK

3 – CAVElab - Computational & Applied Vegetation Ecology, Ghent University, Belgium

4 – Earth Observation, Climate and Optical Group, National Physical Laboratory, Hampton Road, Teddington, Middlesex, TW11 0LW, UK

5 – Department of Geography, University College London, WC1E 6BT, UK

6 – NERC National Centre for Earth Observation (NCEO), UK

7 – Tampere University of Technology, Korkeakoulunkatu 10, 33720 Tampere, Finland

8 – Institut national de la recherche agronomique, 33140 Villenave d'Ornon, Bordeaux, France

9 – Laboratory of Geo-Information Science and Remote Sensing, Wageningen University, Wageningen, the Netherlands

10 – AMAP, University of Montpellier, CIRAD, CNRS, INRA, IRD, Montpellier, France

Corresponding author – tobydjackson@gmail.com

Abstract

Wind damage is an important driver of forest structure and dynamics, but it is poorly understood in natural broadleaf forests. This paper presents a new approach in the study of wind damage: combining terrestrial laser scanning (TLS) data and finite element analysis. Recent advances in tree reconstruction from TLS data allowed us to accurately represent the 3D geometry of a tree in a mechanical simulation, without the need for arduous manual mapping or simplifying assumptions about tree shape. We used this simulation to predict the mechanical strains produced on the trunks of 21 trees in Wytham Woods, UK, and validated it using strain data measured on these same trees.

For a subset of five trees near the anemometer, the model predicted a five-minute time-series of strain with a mean cross-correlation coefficient of 0.71, when forced by the locally measured wind speed data. Additionally, the maximum strain associated with a $5ms^{-1}$ or $15ms^{-1}$ wind speed was well predicted by the model (N=17, R^2=0.81 and R^2=0.79, respectively). We also predicted the critical wind speed at which the trees will break from both the field data and models and find a good overall agreement (N=17, R^2=0.40). Finally, the model predicted the correct trend in the fundamental frequencies of the trees (N=20, R^2=0.38) although there was a systematic underprediction, possibly due to the simplified treatment of material properties in the model. The current approach relies on local wind data, so must be combined with wind

flow modelling to be applicable at the landscape-scale or over complex terrain. This approach is applicable at the plot level and could also be applied to open-grown trees, such as in cities or parks.

Keywords: TLS; terrestrial laser scanning; wind damage; finite element analysis; critical wind speed; resonant frequency

Introduction

Wind damage to forests is a significant but poorly understood driver of the terrestrial carbon cycle. Trees respond to strong winds by leaning and swaying in a dynamic manner. This response has been characterized using static models (S. A. Hale et al., 2015), dynamic models with simplistic tree geometry (Kerzenmacher & Gardiner, 1998) and dynamic models which represent the effect of branches (Kenneth R James, Dahle, Grabosky, Kane, & Detter, 2014). The literature has mostly focused on wind damage in conifer plantations due to their importance to the forestry industry (S. E. Hale et al., 2012; Dupont et al., 2015; S. A. Hale et al., 2015). In broadleaf forests the variety of tree sizes and shapes influence their response to wind forcing, meaning that finite element analysis is necessary to model the detailed effects of wind on trees (Mathieu Rodriguez et al., 2008; H. Spatz & Theckes, 2013; Kenneth R James et al., 2014). Previous finite element analysis studies have been limited to small numbers of trees due to the difficulty of manually mapping tree geometry (Sellier et al., 2006; J. R. Moore & Maguire, 2008). However, terrestrial laser scanning (TLS) data offers the potential for dramatic advances in this area. Recent developments in the extraction of accurate 3D tree models from TLS data can provide detailed geometrical information for a scanned tree in a matter of minutes (K Calders et al., 2015; Raumonen et al., 2015; Gonzalez de Tanago Menaca et al., 2017).

We used 3D tree models derived from TLS data as the basis of a finite element analysis, applied using the engineering software Abaqus (Simulia Software Company, 2017). This approach allowed us to simulate the dynamics of broadleaf trees without the need to manually map their geometry. In addition to its application in natural forests, this approach could be useful in testing proposed interventions on urban amenity trees, or valuable veteran trees, in a model environment before implementation (Reiland, Kane, Modarres-Sadeghi, & Ryan, 2015).

This paper tests the hypothesis that finite element models developed using TLS data can be successfully used to simulate the behaviour of broadleaved trees under applied wind loading. We describe the method and discuss the assumptions involved. We also provide software to implement this technique. We test the model against field data collected in Wytham Woods,

UK, for which we have both TLS data and field measurements of strain and wind speed. This validation takes three forms:

1. We predict the exact time-series of strain produced during a five-minute period based on high time-resolution wind data.
2. We calculate the maximum hourly strain produced on a tree given maximum hourly wind speeds of 5 ms^{-1} or 15 ms^{-1}. We also estimate the critical wind speeds (CWS) at which trees will break by extrapolating from long term field data (S. E. Hale et al., 2012).
3. We predict the fundamental frequencies of the trees and compare these to the frequencies extracted from the field data using Fourier analysis.

Finally, we discuss the results of this study in the context of other work in the field.

Materials and Methods

The workflow involved field data collection and analysis, TLS data collection and modelling work, followed by three separate tests of the model against the field data (Figure 1).

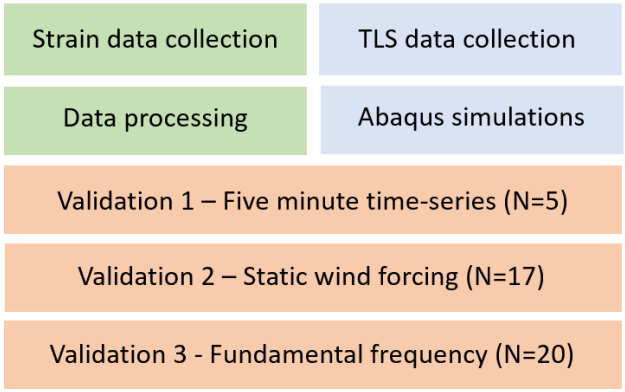


Figure 1 – Workflow diagram showing the main analysis and validation steps.

Study site and field data

Wytham Woods (51°46'27.2" N 1°20'20.1" W) is a mature temperate deciduous woodland near Oxford, UK. The woodland contains approximately 950 trees per hectare and the dominant species are sycamore (*Acer pseudoplatanus)*, ash (*Fraxinus excelsior*), beech (*Fagus sylvatica*) and English oak (*Quercus robur*). We measured the bending strains produced on 21 trees (eight ash, nine sycamore, four birch (*Betula spp.*) and one oak) ranging from 12 to 24 m tall. One of the sycamore trees had four main stems below 1.3 m, each of which are treated as separate trees in the forest census and were instrumented as such in this study, we therefore refer to them as separate trees in this paper. Seven of the trees were located near a canopy walkway structure, and the remaining 14 trees were located 230 m away. Average canopy height was 21-23 m in both locations.

Strain was measured using the method developed by Moore et al., (2005): pairs of strain transducers were fixed to the trees at approximately 1.3 m and perpendicular to each other.

These transducers were then connected to Campbell Scientific data loggers and measured at 4 Hz (two CR23xs and three CR1000s). The limited storage capacity of the CR23x data loggers was supplemented using a Raspberry Pi.

In the field, strain gauge resistances drift with environmental factors. We partially corrected these in situ using a variable resistor within a wheat-stone bridge circuit. We further accounted for this drift by subtracting a 5000 point (20 minute) running mode from the signal. This is based on the assumption that the tree will regularly pass through its equilibrium position. This same technique was used in Wellpott (2008) and Hale *et al.* (2012, 2015) and we found our results to be relatively insensitive to this window length (SI-1).

Wind speed was measured in winter using three cup anemometers (Vector Instruments A100LK/5M) mounted at 5 m, 10 m and 15 m heights above ground level on a canopy walkway next to the focal trees and supplemented, notably during the 5-minute high-resolution validation period, with a 3D sonic anemometer (Campbell Scientific CSAT3) mounted at 15 m. In summer, we used a Gill Sonic-1 anemometer recording at 1 Hz mounted at 15 m. Local climate data are available through a meteorological station approximately 1 km away, just outside the forest, operated by the Environmental Change Network (ECN). This station records mean hourly wind speed as well as the maximum 5 s mean within that hour (5 s maximum gust speed). The wind data taken from anemometers within the canopy were considered unreliable, especially in summer, because of localized sheltering effects. We therefore used the ECN meteorological station's hourly maximum wind speeds for all critical wind speed analysis and select the maximum strain on each tree within each hour. A comparison of the different measures of wind speed is given in SI-2.

Development of quantitative structure models

TLS data were collected in Wytham Woods, Oxford, as part of a separate project (K Calders et al., 2016; Kim Calders et al., 2018). Trees were manually extracted from the point cloud and cylinder fitting algorithms, developed primarily for biomass estimation, were used to extract the tree shapes (Burt, 2017; Åkerblom, 2017). This method represents each tree as a series of cylinders – a quantitative structure model (QSM).

We adapted these QSMs by removing cylinders under 2 cm diameter, which are generally the least accurate in the QSM reconstruction due to limitations of TLS scanning resolution (see Figure 2). We then longitudinally averaged neighbouring cylinders, replacing each pair of neighbouring cylinders with a single cylinder with the average length, radius and direction of the original pair (Åkerblom, 2017). This reduced the number of cylinders from approximately

4000 per tree to 500, without significantly affecting the total woody volume of the tree. This process resulted in a new set of QSMs comprised of cylinders with a higher length to radius ratio, allowing us to use beam theory to build a dynamic model of the tree without significantly altering the overall structure (Carrera, Giunta, & Petrolo, 2011). It is important to note that the Wytham Woods TLS data were collected in ideal conditions based on a 10 m grid using a Riegl VZ-400 with 0.04 degrees angular resolution (Wilkes *et al.* 2017). Most of the trees were scanned in winter, but those near the walkwaywere scanned in summer and the leaves removed through filtering (Vicari, 2017). Optimization of the QSM approach shows that there is very little variance between the QSMs in these conditions (Burt, 2017).

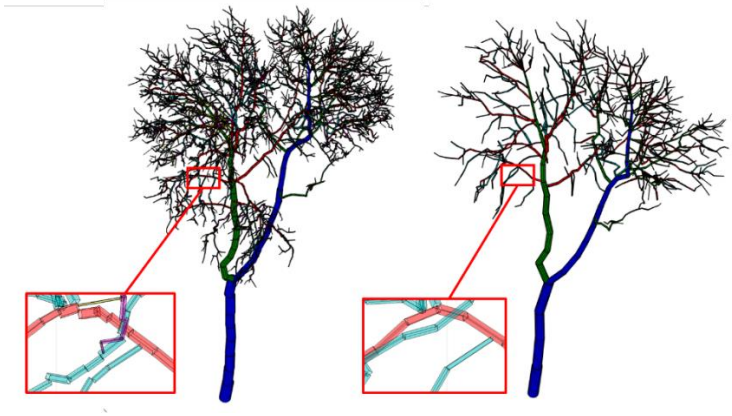


Figure 2 – Left – QSM directly from the fitting process. Right – simplified QSM with longer cylinders and fewer small branches - this is our input for finite element analysis.

Development of finite element models

To build a finite element model in Abaqus, each cylinder in the QSM was represented as a two node Euler-Bernoulli beam element (B31) and the orthotropic features of wood were neglected, as in (Sellier et al., 2006). Since we intend this approach to be scale-able, we did not measure the material properties of the trees individually. Values of green wood density, ρ_{gw}, elasticity, E_{gw}, and modulus of rupture, MOR_{gw}, were taken from the literature (Lavers, 1983; K. J. Niklas & Spatz, 2010) (Table 1). Breaking strain was defined as $\varepsilon_{break} = MOR_{gw}/E_{gw}$ (K. J. Niklas & Spatz, 2010). The intra-specific variation in elasticity is between 14 and 20% (defined as standard deviation divided by mean value) in sycamore, ash and oak. No estimates of variation in green wood density were given. The inter-specific variation in wood density is 20% and elasticity 25% in Wytham Woods (defined as the range divided by the minimum value). The values used in finite element analysis were:

Latin Name	Common Name	Density (kgm^{-3})	Elasticity (MNm^{-2})	MOR (MNm^{-2})
Acer pseudoplatanus	Sycamore	721	8400 (1340, 43)	66 (8.8, 43)
Fraxinus excelsior	Ash	801	9500 (1880, 204)	66 (10.9, 204)
Quercus robur	English Oak	865	10500 (1280, 40)	72 (7.9, 40)
Betula spp.	Birch	801	9900 (410, 6)	63 (5.1, 6)

Table 1 – Material properties of green wood used in finite element analysis. Values in brackets are standard deviation and number of samples tested. Quercus rubra was used as a substitute for Quercus robur, since data for the latter was not available from the same testing method. This affects only a single tree in the frequency analysis validation.

Root anchorage was modelled as a universal joint with two rotational degrees of freedom and symmetric elasticity $E_{root} = 5\text{x}10^6$ Pa in each direction. Energy dissipation at the root-soil boundary was modelled by a dashpot with coefficient $C_s = 10$. Previous authors used tree pulling data to tune these model parameters, which gives accurate results in the case of a few trees (Sellier et al., 2006; Sellier & Fourcaud, 2009). However, we are attempting to generalize to many trees without intensive field measurements, so the root parameter values were arbitrarily chosen because the model is insensitive to these parameters in this range (Table 2). Roots are therefore included in the model primarily so that future studies can tune these parameters if they possess the necessary data.

Applying gravity in a realistic way proved difficult, since the trees were scanned in their gravity deformed positions. Branches develop reaction wood and grow in irregular shapes to counteract the force of gravity (Scurfield, 1973), whereas our model assumes cylindrical branches with isotropic material properties. We tested three approaches to modelling the effect of gravity and found a small but interesting difference between them (see SI-3). For all analysis in the main text of this paper we first applied an inverse gravity force to the model tree, extracted the nodal displacements and then restarted the analysis applying a realistic gravitational force to the displaced geometry. This is the most physically realistic approach since branches are not displaced before the analysis begins and the additional load due to self-weight of the displaced crown is accounted for.

Dynamic simulation

The dynamic simulation of a tree's response to wind forcing was conducted using the Abaqus Aqua module (Simulia Software Company, 2017). Each tree was modelled individually, meaning that the dynamic response does not include crown clashing which is thought to be significant in some forest structures (Rudnicki, Silins, Lieffers, & Josi, 2001; Rudnicki, Lieffers, &

Silins, 2003). In all simulations, we used a non-linear solution method to account for large displacements in the tree structure. The equation of motion takes the form

$$M\ddot{q} + D\dot{q} + Kq = G + F_D \qquad \textit{Equation 1}$$

where q, $\dot{q}$ and $\ddot{q}$ are the nodal displacement, velocity and acceleration vectors. M, D and K are the mass, damping and stiffness matrices respectively, and G and F_D represent the gravitational and wind induced forces. The output variable, strain, is calculated internally by Abaqus and we use the strain at the approximate position of the strain gauges (1.3 m), so as to correspond with the field data.

While horizontal wind velocities were fully represented, the vertical profile of wind speed was limited to a power law fit (equation 2), using field data from three heights within the canopy (Figure SI-2).

$$v = v_0 \left({}^{h}/_{h_{ref}} \right)^{\gamma} \qquad \textit{Equation 2}$$

where v is the wind speed at a given height h, v_0 is the reference wind speed at reference height h_{ref} and γ is a variable parameter determined by the local wind profile (Figure SI-2). The wind drag force, $\mathrm{F_D}$, per unit length on each cylinder of the QSM is given by

$$F_D = Amp \cdot \rho_{air} C_D r \Delta V_{fn} \left\| \Delta V_{fn} \right\| \qquad \textit{Equation 3}$$

where Amp is a user defined amplitude that describes the horizontal variation in wind speed, ρ_{air} is the density of air, C_D is the drag factor, r is the radius of the beam, and ΔV_{fn} is velocity difference between the wind and the beam. As in previous work (Sellier et al., 2006; J. R. Moore & Maguire, 2008; Sellier & Fourcaud, 2009; Ciftci et al., 2013), we assumed a constant drag factor, although in fact the drag factor varies with wind speed and with the size of the branch.

The most significant source of damping, that due to aerodynamic drag, was modelled implicitly in the Aqua module. Material damping was modelled using Rayleigh's hypothesis (Rayleigh, 1877).

$$D = \alpha_W M + \beta K \qquad \textit{Equation 4}$$

where $\alpha_W M$ is the mass proportional damping and βK is the stiffness proportional damping. Following Sellier, Fourcaud & Lac (2006) we assumed stiffness proportional damping would be insignificant in the high Reynolds number regime in question, and so set $\beta = 1\text{x}10^{-3}$. Contact

between branches was allowed but no attempt was made to accurately model the energy transfer of these contacts.

Multiple simulations were carried out to test the sensitivity of the model. All continuous parameters were tested at ±20%. Non-continuous parameters, such as the simplification of the QSM, were tested at different levels.

Validation techniques

All the strain data used for validation were collected in winter, when the absence of leaves makes the modelling and interpretation simpler. Future work will parameterize the effects of leaves, but the change in Reynolds number and drag coefficient make the full treatment of wind flow over leaves highly complex (de Langre, 2008).

Time series validation

For the time-series validation, we use a five-minute subset of data from 14:00-14:05 on 28th March 2016, chosen for high wind speeds and high (10 Hz) wind measurement resolution. Two trees were removed due to problems with the field data, in the first case the balancing circuit failed and in the second the physical connection to the tree came undone, leaving five trees with reliable data. We therefore compared measured and modelled strain time-series for five trees close to the anemometers. We did not expect an exact correspondence for the 5-minute time-series, since the wind forcing applied to each model tree was identical and reflects the wind regime measured at the position of the canopy walkway. In the field, each individual tree experiences a slightly different wind forcing due to its position (Kerzenmacher & Gardiner, 1998). A previous finite element analysis study found a reduced correlation at 12 m from the wind measurements, although no correlation statistics were given (Sellier et al., 2008).

Hourly maximum strain validation

In this validation, we used the five trees from time series validation as well as twelve additional trees situated approximately 230 m away. Two of these additional trees were excluded due to a poor connection between the tree and the strain gauge. We used hourly maximum wind speed measurements taken from the ECN meteorological station. For each hour we extracted the maximum strain value for every tree. All but four trees had over 500 hours of data available, and for these four trees we had 165 hours of data. We tested a robust maximum selection technique, using the mode of the maxima of subsections of the hours data, but found no increase in accuracy. Details of the strain data processing and reference to the software and data repository to repeat this analysis are given in SI-1. We regressed the hourly maximum strain data against the squared hourly maximum wind speed and so predicted the strain at 5

and 15 ms^{-1} wind speeds. We used this regression line to extrapolate the relationship up to the breaking strain, giving an estimate of the critical wind speed from the field data. In the simulation, we artificially increased the wind forcing until the lowest beam in the trunk reached its breaking strain.

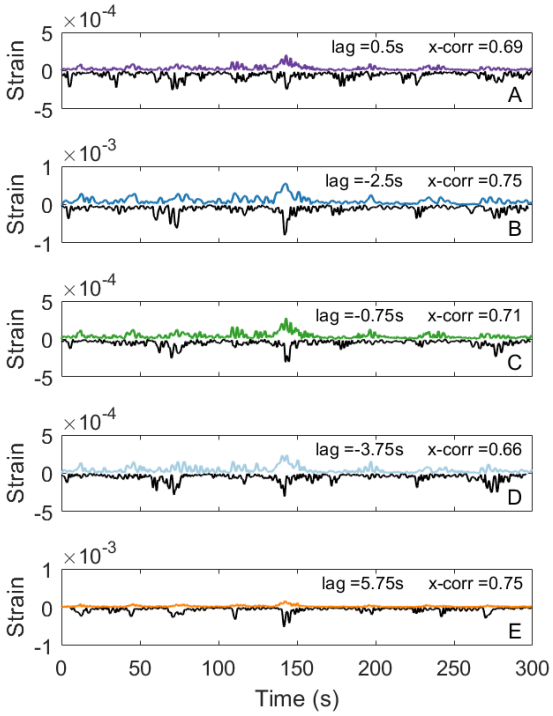
Fundamental frequency validation

We used a Welch's power spectral density function (Krauss et al., 1994) to extract the fundamental frequency for each hour of field data during winter and take the mean. This analysis only requires one strain gauge per tree, so three of the four strain gauge failures had no effect here, meaning that we can carry out this analysis for 20 trees. Using Abaqus, we predicted all the undamped sway modes from the QSMs using a subspace method (Viberg, 1995). This can be performed separately from the dynamic analysis and is much faster, it is also available in the free version of Abaqus.

Results

Time-series validation

The modelled five-minute time-series of strain was similar to that measured in the field (Figure 3, mean cross-correlation = 0.71). We found the lag between measured and simulated strain was partially explained by the position of the trees in relation to the wind measurements. However, all modelled trees displayed some peaks that were not evident in the field data, and vice-versa. This was presumably due to differences in wind at the anemometer position and at the position of the tree. This time-series validation is similar to that given in Moore & Maguire (2008) and Sellier, Brunet & Fourcaud (2008). It is useful to demonstrate that the modelled response resembles that of the actual trees, but only applicable at short distances from the anemometers due to the spatial variability of wind speeds.



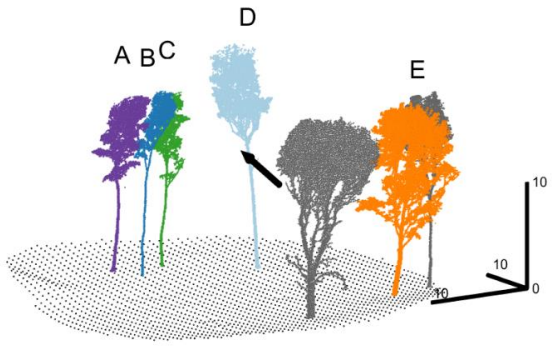


Figure 3 – Above – TLS data showing trees near the canopy walkway. The coloured trees are the ones used in this analysis. The black arrow shows the prevailing wind direction and is located at the point of the wind measurement. Left - simulated strain (coloured lines) against field data (black lines, inverted for clarity). The time-lag (field strain – simulated strain) as well as the cross correlation co-efficient are given for each signal.

Hourly maximum strain validation

This section examines the model's accuracy in predicting the strains produced by wind speeds of 5 and 15 ms^{-1}, and in extrapolating up to the critical wind speed (Figure 4). It is important to note that, in the case of CWS, both the x and y axes are estimates, since the CWS was estimated from field data by extrapolating beyond the available measurements. Therefore, this is not a straightforward validation but rather a demonstration that predictions from field and model approaches are correlated. We used hourly maximum wind speeds (highest 5 s mean per hour) measured at the nearby meteorological station, since this avoids the need for a multiplication factor (gust factor). A more detailed discussion of the data analysis choices relating to the wind data is given in SI-2.

The model predicted the strain produced at 5 ms^{-1} with an R^2=0.81 and concordance correlation coefficient (CCC) of 0.91. At 15 ms^{-1} wind speed the fit was slightly reduced R^2=0.79 and CCC=0.89. CWS predictions from field data and the model displayed a worse agreement, R^2=0.40 and CCC=0.66, presumably because the model behavior departed from a pure square law before reaching the CWS (due to streamlining), while the best fit line derived from the field data does not. We saw no departure from a square law in our field data, but we did not have measurements at high enough wind speeds to test this.

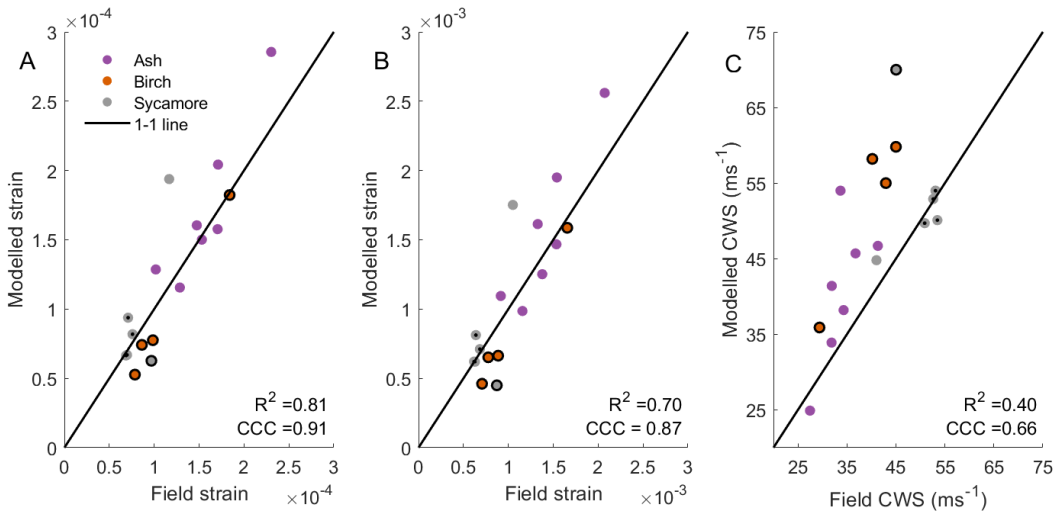


Figure 4 – Strain produced by wind speeds of 5 ms^{-1} (A) and 15 ms^{-1} (B) from field data and finite element analysis. C – critical wind speed estimates from field data and finite element analysis. Pearson's correlation coefficient and the concordance correlation coefficient (CCC) are given for all figures. Trees with an outer black circle are situated near the walkway, approximately 230 m from the other trees and were scanned in summer. The four trees that are independent stems of a large sycamore (branching below 1.3 m) tend to cluster together and are marked with a central black point (two stems overlap in panels A and B).

Fundamental frequency validation

We found that finite element analysis predicts the trend of fundamental frequency (f_0) correctly (R^2=0.38 and CCC=0.65, N=20). Using sample mean material properties, instead of the species-specific material properties which are often unavailable, only decreased the R^2 value by 0.05. Interestingly, there is a systematic under-prediction of f_0 across the 20 trees (Figure 5). This is likely due either to our simplistic treatment of material properties, which are constant throughout the tree, or our arbitrary trimming of all branches with a diameter under 2 cm. As noted in the figure legend, the fit is radically improved by removing the two birch trees whose fundamental frequencies were over predicted.

The free version of Abaqus can perform this analysis for any tree model consisting of fewer than 1000 beams. As previously noted this method predicts a dense distribution of modes about the main frequencies (M Rodriguez et al., 2012), representing the slightly different shapes or directions in which the tree can sway. In the field data, this takes the form of a wide resonance peak, instead of distinct modes.

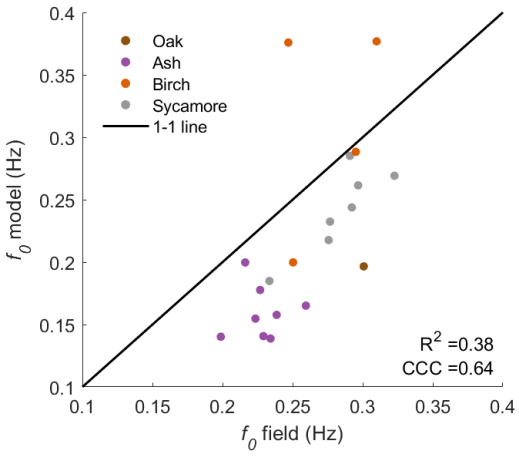


Figure 5 – Field measured fundamental frequency against modelled fundamental frequency for 20 trees (one tree was excluded due to errors in the simulation). The goodness of fit is highly sensitive to the two birch trees for which the fundamental frequency was overestimated. Removing these two trees increases the goodness of fit (R^2 to 0.66, CCC=0.83).

Sensitivity analysis

In this section, we examine the sensitivity of the model to the input parameters. We used three output variables as indicators of the models' response to a prescribed change in input parameters, the strain at a wind speed of 15 ms^{-1}, the critical wind speed estimate and the fundamental frequency (Table 2). The model was highly sensitive to the details of the QSM used as input. We found that the simplification step, used to reduce the number of cylinders in the original QSM for finite element analysis, has a large effect on the result. The second largest sensitivity was due to material properties, especially wood elasticity. Natural variation in wood elasticity, where data are available, is between 14% and 19%, which is comparable to the range of our sensitivity analysis. Unfortunately, green wood elasticity is not often measured and different measurement techniques are often not directly comparable (Ruel, Achim, Herrera, & Cloutier, 2010).

The beam type is a property of the finite element analysis and determines the solution method used to calculate the strains in each beam (Simulia Software Company, 2017). The choice of beam type is one of the smaller sources of sensitivity in the model. The drag factor, C_D, is an experimentally determined parameter which determines how much force is transferred to an object for a given wind speed (see equation 3). We treated the drag factor as a constant, following (J. R. Moore & Maguire, 2008; Sellier & Fourcaud, 2009; Ciftci, Brena, Kane, & Arwade, 2012; Kenneth R James et al., 2014), whereas in fact it changes with the Reynolds number of the flow (de Langre, 2008). These changes are small in the low wind speed regime

of our measurements and several projects are currently investigating the changes in the drag factor for trees at high wind speed. The model is insensitive to root parameters in this range, which are poorly constrained in the literature.

Parameter		Default (→ test)	Sensitivity – % increase for 20% increase in parameter		
			Strain at 15 ms^{-1}	CWS	f_0
QSM	Averaging iterations	1 (→ 2)	43	-14	-20
	Beam type	B31 (→ B33H)	-7	3	1
Wood properties	Green wood density, ρ_{gw}	Species specific	7	-2	-12
	Elasticity, E_{gw}	Species specific	-20	12	12
	Damping factor, α_W	0.2	0	0	0
Root model	Root elasticity, E_{root}	5e6 GPa	0	0	0
	Dashpot coefficient	10	0	0	0
Aeroy-namics	Drag coefficient, C_D	0.82	23	-9	0
	Wind decay, γ	0.05	-1.5	1	0

Table 2 – List of parameters used in simulations with sensitivity analysis results. Continuous parameters were increased by 20%, non-continuous parameters were varied as indicated in brackets (→ test value).

Discussion

Validation type		# Trees	Fit statistics
Time-series validation		5	Mean x-corr = 0.71
Hourly maxima	5 ms^{-1}	17	R^2=0.81, CCC=0.91
	15 ms^{-1}	17	R^2=0.79, CCC=0.89
	CWS	17	R^2=0.40, CCC=0.66
Fundamental frequency		20	R^2=0.38, CCC=0.65

Table 3 – Summary of validation results.

Overall, finite element analysis using QSMs from TLS data is a useful method for modelling the behaviour of trees in the wind (Table 3). It can predict the time-series of strain produced in the trunk of a tree, if the model is forced by wind speed data measured nearby. It can also predict the maximum strain for a given maximum wind speed, the critical wind speed at which the tree will break and the fundamental frequency of a tree. Since TLS data are becoming increasingly available for trees from a wide range of environments from tropical forests to city parks, this technique could now be used to model the dynamic behavior of a wide range of trees. This will allow us to revisit questions about the relationship between tree architecture and dynamics with realistic tree shapes instead of theory-based fractal or modelled trees. In particular, we could explore the relative importance of variations in material properties and tree architecture (Sellier & Fourcaud, 2009) and the differences between open grown trees and those in forests (Kane, Modarres-Sadeghi, James, & Reiland, 2014; Kenneth R James et al., 2014).

The characteristics of the high time-resolution response of a tree to wind are important, since it is at these scales that dynamic amplification and damping processes occur, which alter the likelihood of wind damage (K R James et al., 2006; Hanns Christof Spatz et al., 2007; Ciftci et al., 2013). However, wind speeds are highly spatially variable, so an array of anemometers is needed to represent the wind forcing. The variability of wind speeds can broadly be described by coherent gusts of approximately one tree height in the cross-stream direction and significantly longer in the stream-wise direction (J. Finnigan, 2000). In the current model, the wind regime at the position of each tree must be provided and we assume these wind regimes are identical. In the high-time resolution validation this led to some gusts hitting the trees which were not measured by the anemometer and vice versa.

The static response of the QSMs to an applied wind forcing was similar to the hourly maxima measured in the field. This is in agreement with recent work which demonstrated that, for *Pinus sylvestris*, a large part of the tree response was due to simple static effects (Schindler & Mohr, 2018). Within the range of wind speeds measured in this study the correlation between model and field data exceeded R^2=0.79, CCC=0.89. As the wind speed increased this correlation decreased, possibly because the model accounts for non-linear effects due to the displacement of the crown while the extrapolation from field data did not. The critical wind speeds were systematically overestimated by the simulation. It is important to note that there are likely to be further non-linear effects at high-wind speeds that are not accounted for in either the field data or the model. These are associated with changes in the drag factor, streamlining of the tree crown and possible plastic deformation of the wood. However, we

have no data with which to quantify these effects and assume they are small in comparison with the main effect of increasing wind speed.

The fundamental frequency is an important parameter since a lower fundamental frequency means that energy is more easily passed from the wind to the tree and the tree is at a higher risk of damage (Schütz, Götz, Schmid, & Mandallaz, 2006).The model predicted the fundamental frequency of trees with R^2=0.38, CCC=0.65, but displayed a clear negative offset. This offset is likely due to either our simplistic treatment of material properties or the simplification of the QSM. We do not possess independent validations of the accuracy of the QSM reconstructions and therefore cannot separate errors due the QSMs and those due to the treatment of material properties. A review of the material properties of trees worldwide (K. J. Niklas & Spatz, 2010) found a clear relationship between wood density and elasticity at the species level, but the potential for wide variation within species, especially in those selected for rapid growth, and within individual trees remains. Our sensitivity analysis shows that wood elasticity plays a larger role than wood density in driving tree dynamics, but it is also harder to measure (Ruel et al., 2010).

Previous authors increased the accuracy of the finite element analysis by adjusting the material properties in order to fit the model to static field tests performed on the tree (Sellier et al., 2006). This method could prove highly useful for small numbers of urban or valuable veteran trees where proposed treatments, such as removing a large branch or adding supports, can be tested in a model environment before being carried out. Another possible addition to the model would be a more accurate representation of leaves and twigs, which must influence the motion of the tree. This is currently limited by the difficulty of retrieving small twigs and leaves from TLS data, but a parameterization could possibly be developed using summer (leaf-on) data in combination with the winter (leaf-off) data.

Conclusion

Previously, finite element analysis of trees has been confined to a small number of relatively short or even idealized trees. We demonstrate that combining TLS data and finite element analysis allows us to model the detailed dynamics of realistic and complex broadleaf trees without manually mapping their 3D architecture. We show that this approach can model the strains produced in a tree for a given time-series wind forcing. Finite element analysis can also predict the effects of a static wind forcing, which was found to follow a similar trend to the hourly maximum strain - wind speed relationship. It can also predict the correct trend of fundamental frequencies for a set of trees given their geometry, although there is a systematic offset.

Several uncertainties remain, in particular relating to the accuracy of the TLS data in representing 3D tree architecture, the mechanical properties of roots, and the change in wind-tree interaction at high wind speeds. This approach is applicable in natural forest plots and would also be valuable in predicting the dynamics of park or city trees, and how they will respond to a proposed intervention.

Supplementary information

SI-1 Data treatment process

The raw strain data go through four processing steps before hourly maxima are selected. These steps are described below and data and scripts to apply the techniques described are available online.

1. The data are calibrated according to the size of the strain gauge caliper and the calibration coefficient of the strain gauge.
2. Next, the data are re-projected from the angles at which the strain calipers were placed on the tree to the Northward and Eastward directions.
3. The strain gauge responds to environmental factors and tends to develop an offset over time. This is partly corrected for in the field by adjusting a variable resistor in the wheat-stone bridge circuit, but it is necessary to further reduce this offset at the post-processing stage (S. E. Hale et al., 2012). We subtract a 5000-point (20.8 minute) running mode in this study.
4. The maximum strain on the circumference of the trunk at 1.3 m is calculated at each timestep, assuming the trunk is cylindrical.

At this point hourly maxima are selected. We tested a subsampling method (Cook 1986; Palutikof, Brabson & Lister 1999) for selecting maximum strain but found no increased accuracy over a simple maximum, although this led to systematically lower maximum strain values and correspondingly higher CWS estimates. We performed a sensitivity analysis on the parameters and choices involved in the process of CWS estimation from field data and found that the maximum strain selection method is by far the most important factor. Variations in offsetting window length make a small and uniform difference across the trees we studied.

Parameter	Range	ΔCWS
Offset window length (minutes)	4 → 20	2%
Maxima selection method	Simple → robust	68%

Table SI-1 – Data treatment parameters and the sensitivity of CWS estimates to changes in these parameters.

SI-2 Wind measurements and choice of time-resolution

In this study we used hourly maximum wind speeds from the local meteorological station since these data were readily available and easily comparable to our model output. We experimented with varying resolutions (i.e. using a one-minute mean wind speed and maximum strain) but found that this merely increased the noise without adding additional accuracy. Using an hourly value selects the outer envelope of the wind-strain relationship, which is the most relevant for wind-damage. Previous large scale critical wind speed estimates use the ten-minute mean wind speed multiplied by a gust factor (GF) to account for the higher resolution wind effects (S. A. Hale et al., 2015). Using maximum wind speed avoids the need for a gust factor. Using wind data from the meteorological station, instead of the data collected as part of this study, increased the number of hours of data available and avoided complications due to the change in wind regime in summer, since the anemometer is situated outside the forest.

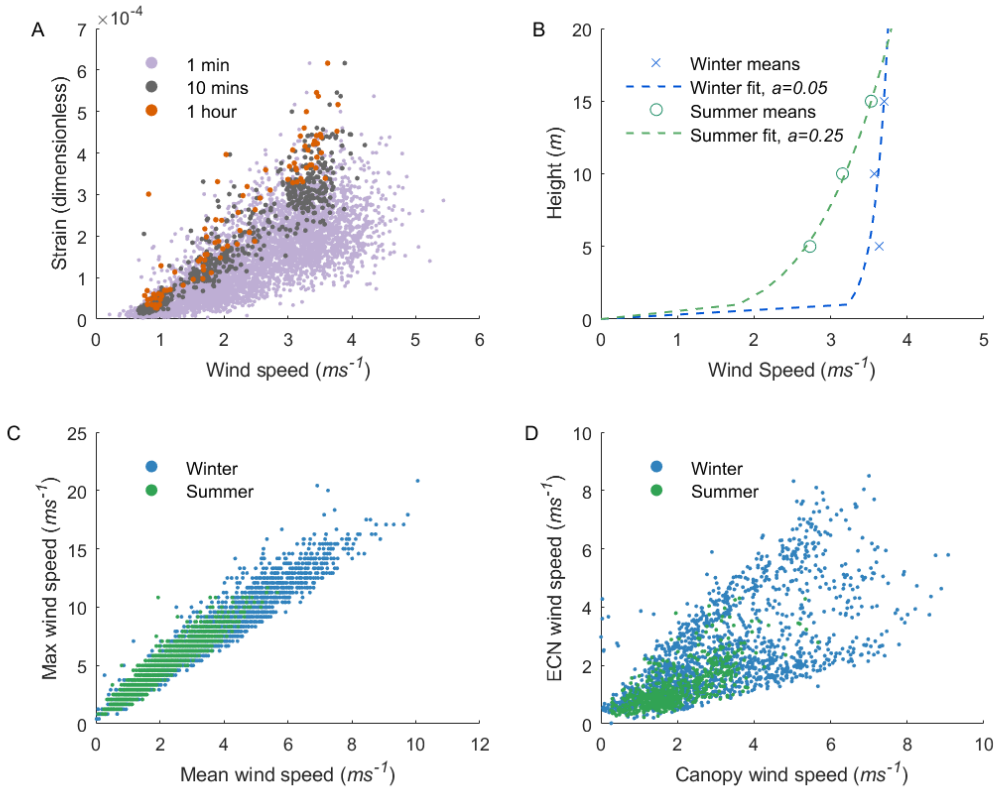


Figure SI-2 – A - Mean wind speed against maximum strain at varying temporal resolution. B – Vertical wind speed profiles in summer and winter, as measured from anemometers at 5, 10 and 15 m on the canopy walkway. The dashed lines represent the power law function used to model the vertical variation in wind speed, only the winter data was used in this study. C – Mean hourly wind speed against maximum wind speed, measured at 5 s resolution at the ECN

weather station. D – Hourly mean wind speed inside and outside the canopy, in summer and winter.

SI-3 Modelling the effect of gravity

The trees were scanned on calm days. The force of gravity is acting on the branches and their stiffness is keeping them in equilibrium by creating an equal and opposite force. In the finite element analysis, gravity must be defined as an external forcing. There are three options:

1. Run the simulations without gravity. In this case the trees do not experience self-weight or the additional force from their displaced crown as they lean in each direction.
2. Apply gravity directly to the model. This deforms the branches away from their scanned position slightly. This is small displacement and does not have a significant effect on the dynamics of the tree under wind forcing, but it is not fully realistic. Also, tree whose main stem leans significantly in the TLS scan could be deformed significantly by this forcing.
3. Apply a reversed gravity force, which causes the branches to deform upwards. These deformed positions are then saved and the analysis restarted using the deformed position. The restarted analysis then applies gravity according to option 2, which returns the branches to their resting position while maintaining the gravity load throughout all subsequent analysis. This is the most realistic option, although it does not take into account the non-uniform maturation strains which allow the branches to oppose the force of gravity normally. This is also the most computationally taxing approach since it requires two simulations per tree as well as a user defined subroutine to extract the deformed nodal positions.

The choice of treatment of gravity does not make a significant difference to the five-minute high-resolution simulation. However, the difference between option 1 (no-gravity) and options 2 and 3 (with gravity) is noticeable in both the frequency extraction and the critical wind speed estimation. As the tree bends in the wind, its centre-of-mass is displaced leading to an increased moment. This becomes significant at high displacements and can be seen as a slight deviation from the strict square law relationship between wind and strain.

To summarize, option 2 and 3 are similarly accurate for all the trees we tested, whereas option 1 produces less physical results in the case of large displacements. Option 3 is preferable since it more closely resembles the underlying physics

Paper 2

The second paper uses the techniques described in the previous paper and applies them to one ha of forest in Wytham Woods in order to explore the ecological role of wind damage risk. The previous paper found that finite element analysis is an accurate way of estimating the strain on different trees at a given wind speed, or the critical wind speed at which trees will break. Since trees must adapt their growth form in order to minimize the risk of damage, the critical wind speed may interact with other ecological variables. In addition to the modelling, field data collection was extended into summer in order to quantify the effect of leaves.

This paper fulfils thesis aims 2 and 3. I explore the differences in simulated CWS between species, across trees of different sizes and shapes and with different material properties. This paper also emphasises the seasonal nature of wind damage risk in this temperate deciduous forest. The presence of leaves in summer changes the tree's response to wind loading but also changes the distribution of wind speeds in and over the forest.

The idea for this paper was conceived by me and my supervisors while working on the previous paper. As in the previous paper, the TLS data collection was primarily carried out by co-authors from University College London and the National Physical Laboratory. TLS data processing was primarily carried out by co-author Kim Calders, and the resultant QSMs are freely available online. I performed the finite element analysis and the linear models on simulated critical wind speeds. The field data processing was carried out by me and Bavisha Kalyan, a summer student and a co-author on the paper. I wrote the initial manuscript and all co-authors contributed comments. The figures were much improved by helpful comments from an anonymous reviewer. This paper is published in Frontiers in Forests and Global Change

A new architectural perspective on wind damage in a natural forest

T. Jackson[1], A. Shenkin[1], B. Kalyan[2], J. Zionts[1], K. Calders[3], N. Origo[4,5], M. Disney[5,6], A. Burt[5], P. Raumonen[7], Y. Malhi[1]

1 – Environmental Change Institute, School of Geography and the Environment, University of Oxford, OX1 3QY, UK

2 – Civil and Environmental Engineering, University of California Berkeley, Berkeley, CA, USA

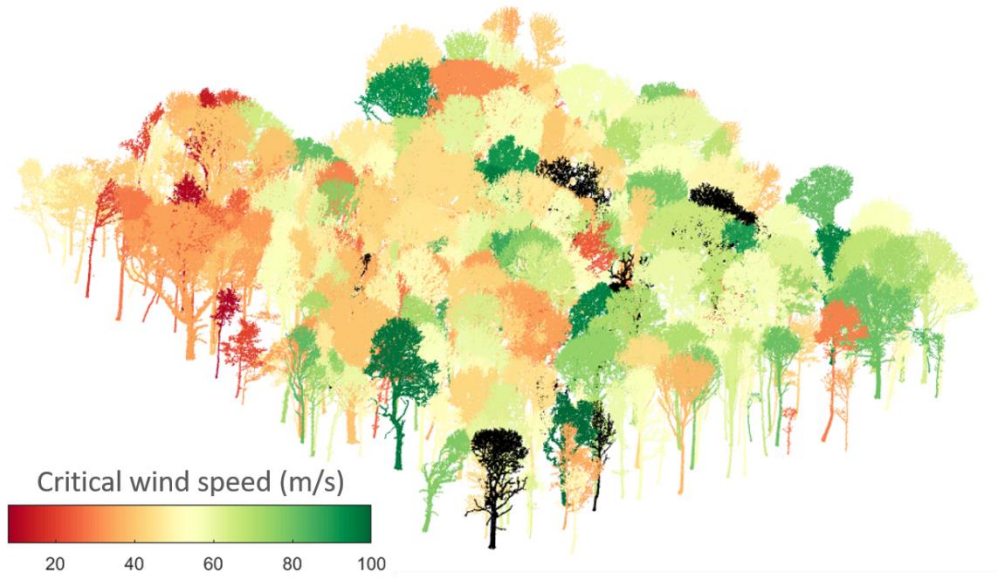
3 – CAVElab - Computational & Applied Vegetation Ecology, Ghent University, Belgium

4 – Earth Observation, Climate and Optical Group, National Physical Laboratory, Hampton Road, Teddington, Middlesex, TW11 0LW, UK

5– Department of Geography, University College London, WC1E 6BT, UK

6 – NERC National Centre for Earth Observation (NCEO), UK

7 – Tampere University of Technology, Korkeakoulunkatu 10, 33720 Tampere, Finland



Abstract

Wind damage is a significant driver of forest structure, ecology and carbon cycling in both temperate and tropical regions, but most of the literature on wind damage focusses on conifer plantations. Previous studies in broadleaf forests have been limited by a lack of data on tree architecture, a problem that is potentially overcome by terrestrial laser scanning. Here we apply novel approaches to estimate the critical wind speeds at which trees will break in a temperate, deciduous forest plot in Wytham Woods, UK, using a combination of field data and finite element analysis.

Ash trees *(Fraxinus excelsior)* tend to have lower critical wind speeds than sycamores *(Acer pseudoplatanus)*, while English oak *(Quercus robur)* are the most mechanically robust. This difference in critical wind speed is driven by tree size and architecture, rather than material properties. We observe a trade-off between critical wind speed and growth rate, both within and across species. Our estimates of critical wind speeds from field data are lower in summer than in winter, emphasizing the importance of the spring and autumn transition periods. Of the three species we studied, those with lower critical wind speeds drop their leaves earlier in autumn, suggesting that the timing of leaf shedding may be under selection pressure to minimize risk of tree damage from winter storms. These results are tentative, but also intriguing and intuitive.

Biomechanics, critical wind speed, wind damage, terrestrial laser scanning, TLS, phenology

- Highlights
    - We employ a novel laser scanning and finite element analysis approach to estimate critical wind speed for 397 trees, and to explore the influence of tree architecture
    - We find that critical wind speed is related to a number of key ecological variables such as tree species, size and growth rates.
    - Tree architecture is described in detail and shown to be an important driver of wind damage risk.
    - We find a tentative relationship between variation in the timing of leaf drop and critical wind speed. This suggests that a potential factor in timing of autumn leaf shedding is the reduction of damage risk from winter storms.

Introduction

Wind damage causes billions of euros of loss to the forestry sector (Schütz et al., 2006) and is a major focus of scientific attention. Previous work on forest wind damage risk has focused on relatively simple single-species, evenly-spaced plantation forests (B. A. Gardiner, 1995; S. A. Hale et al., 2015). However, wind damage is a major driver of the terrestrial carbon cycle in natural forests through its influence on the rates and patterns of tree mortality and branch loss. In the Amazon, wind damage rates have been estimated as 1.3 Pg carbon per year, compared to the 0.2 Pg carbon per year lost through logging in the 1990's (Espírito-Santo et al., 2014). Risk of wind damage is also a potentially limiting factor for maximum tree height and forest carbon storage, since trees sense their wind environment and respond with increased

diameter growth (K. J. Niklas, 2007; D. A. King et al., 2009; Bonnesoeur et al., 2016; Coomes et al., 2018).

The critical wind speed (CWS) is a common measure of a tree's susceptibility to wind damage (Gardiner, Peltola & Kellomäki 2000; Moore, Gardiner & Sellier 2018). CWS is defined here as the wind speed that would cause the tree to snap at 1.3m on the trunk. More generally, CWS estimates should take into account the risk of overturning (failure at the root soil boundary), but this requires extensive destructive tests, which have been carried out on some species of conifer but not broadleaf trees (Nicoll, Gardiner, Rayner, & Peace, 2006). However, mode of death surveys show that snapping and overturning occur at comparable rates across many forest types (Everham & Brokaw, 1996; N Gale & Hall, 2001; Chao et al., 2009; de Toledo et al., 2012), suggesting that CWS estimates will be broadly unaffected by this simplification. In order to fully understand wind damage risk we would also need information on wind exposure, which is affected by tree-level effects such as sheltering, which are beyond the scope of this study.

When modelling critical wind speeds, natural broadleaf forests present a challenge because of their more variable and complex tree architecture and forest structure. The links between a trees architecture and its response to wind forcing are poorly understood. There has been some important work on urban trees in the wind, which describes the effect of tree architecture, but usually only in a qualitative manner (Roodbaraky et al., 1994; Baker, 1997; Kane et al., 2014). Finite element modelling can overcome this difficulty by explicitly modelling the effect of the branches on tree sway. However, finite element analyses have mostly been limited to single tree studies due to the difficulty of accurately mapping the 3D architecture of trees (J. R. Moore & Maguire, 2008; Sellier & Fourcaud, 2009; Ciftci et al., 2013). This limitation is being overcome by recent advances in terrestrial laser scanning (TLS) and associated data processing techniques, which have the potential to give us access to large-numbers of accurately mapped 3D tree models (K Calders et al., 2015; Raumonen et al., 2015; Burt, 2017; Åkerblom, 2017; Malhi et al., 2018). These 3D model trees can be used as the basis of a finite element analysis (Jackson et al., 2019).

In this paper, we present a novel exploration of CWS in the context of a natural mixed-species and mixed-age woodland. We first estimate CWSs from field measurements of tree strain in summer and winter for 13 trees, in order to explore the effect of leaves. Next, we conduct a finite element analysis for each tree in the 1ha plot, a total of 397 trees for which TLS data are

publicly available (Kim Calders et al., 2018). We then use our model predictions of CWS to explore three questions about the ecological relevance of wind damage risk:

(1) What drives critical wind speed? We use generalized linear models to test the relative importance of tree size, shape and material properties as drivers of CWS.

(2) Is there a trade-off between growth rate and critical wind speed? Trees which grow tall quickly, driven by competition for light, necessarily invest less in diameter growth. As a result, these slender trees seem likely to be most at risk from wind damage.

(3) Is there a relationship between critical wind speed and the timing of autumn leaf drop? It has been often observed in urban settings that more trees snap or uproot during early winter storms than in mid-winter (Wessolly & Erb, 2016). There are a number of mechanisms that drive leaf bud in spring, including the trade-off between maximizing growth while avoiding damage risk from late spring frosts (Vitasse, Delzon, et al., 2009; Vitasse, Porté, Kremer, Michalet, & Delzon, 2009), but the factors driving the exact timing of leaf drop in autumn is less well understood and may be partly driven by a need to reduce risk of damage from early winter storms.

Materials and Methods

Field data and critical wind speed estimates

The field study was conducted in Wytham Woods, Oxford, a mature temperate woodland in southern England (51°46'27.2"N 1°20'20.1"W). The woodland contains approximately 950 trees per hectare and the dominant species are sycamore *(Acer pseudoplatanus)*, ash *(Fraxinus excelsior)*, birch *(Betula spp.)* and English oak *(Quercus robur)*. Wytham Woods has long been a testbed for ecological experiments and numerous complementary data sets are available. Most important for this study are the 10 years of census data from the 18 ha plot (Butt, 2009) and a co-located TLS scan conducted in 2015-2016 (Kim Calders et al., 2018). This TLS data set is of very high quality, since it was conducted in the absence of leaves and at high scanning resolution, using a Riegl VZ-400 and based on a 10 m grid with 0.04 degrees angular resolution (Wilkes *et al.* 2017).

We collected long-term field data on the wind speeds and strains (extensions / original length) produced in the trunks of 17 trees Wytham Woods, Oxford. We measured the bending strains in these trees at 4Hz for a period of 8 months from October 2015 to June 2016. Strain was

measured using the sensors and method developed by Blackburn (1997) and Moore et al. (2005), details are given in (Jackson et al., in review) and the data are available online (T Jackson, 2018). Local climate data are available through a meteorological station approximately 1km away, just outside the forest, operated by the Centre for Ecology and Hydrology (Figure SI-1). This station records mean hourly wind speed as well as the maximum 5s mean within that hour (5s maximum gust speed).

We used these data to estimate CWS for 17 trees. It is important to note that none of the monitored trees snapped during the experiment and, as in previous studies (S. E. Hale et al., 2012; Peltola, Gardiner, & Nicoll, 2013), we rely on extrapolation from field data to estimate the critical wind speed. Our estimates should, therefore, be looked upon as a means to compare the vulnerability of different trees to wind damage, rather than a rigorous determination of CWS.

The wind-strain relationship follows a power law $\varepsilon = av^2$, where ε is strain and v is wind speed (Gardiner 1995). We separated the data into summer and winter sections, avoiding the transition period, and fitted a linear model to the strain against squared wind speed relationship. We used the fits to extrapolate up to the breaking strain, which was calculated from literature values on the strength of green wood (SI-2) (Niklas & Spatz 2010). This approach assumes that the wind-strain relation follows a similar relation for low wind speeds and high wind speeds. There are likely to be non-linear effects at high wind speeds associated with change in the aerodynamic drag factor and crown streamlining, but these are beyond the scope of the current study.

We investigated the relationship between growth rates and critical wind speed using the repeat *dbh* measurements available at Wytham Woods. In order to test whether leaf phenology was related to critical wind speed, we estimated the leaf-on and leaf-off timings of the three main tree species in this study: ash, English oak and sycamore using data collected by the Woodland Trust's citizen science project 'Nature's Calendar' over the last 10 years (Woodland Trust, 2014).

Model-based critical wind speed predictions

Individual trees in the 1 ha plot were automatically extracted from the plot level point cloud and 3D cylinder models fitted to each of these (Åkerblom, 2017; Calders et al., 2018). The 3D model trees were then simplified by removing cylinders under 2 cm in diameter and combining neighbouring cylinders to reduce the number of cylinders and increase their length to radius

ratio. We then used the finite element method to estimate the CWS of 3D model trees from TLS data (Jackson et al., in review). We exposed the model trees to an artificial wind forcing, consisting of a stepwise increasing wind speed (Figure 1), and extracted the strain at each wind speed. We then interpolated between these points to find the wind speed at which the strain on the basal cylinder (corresponding to the position of our strain gauges in the field) equaled the literature-reported breaking strain, this was designated as the CWS. If the breaking strain was not reached by the maximum wind speed of 100 ms^{-1} the CWS was not determined, we did not attempt to estimate CWS higher than 100 ms^{-1}.

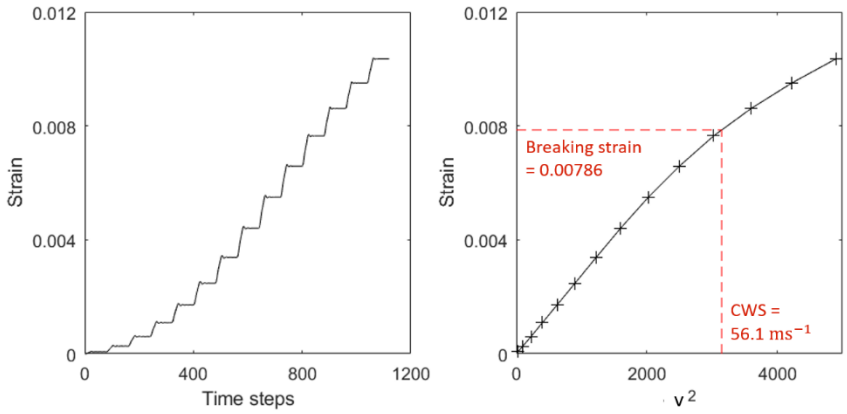


Figure 1 – Left – Raw strain output from simulation showing steps of increasing strain, corresponding to the stepwise wind ramp used to force each tree. Right – Strain against squared wind speed. The red line indicates the breaking strain and the point at which it intersects the interpolation is the critical wind speed. No breakage condition was included in the finite element analysis, but values beyond the critical wind speed are unreliable and non-linear effects, presumably due to large deformation in the tree, are apparent.

Recent work has shown that such simplified treatment of wind forcing, as opposed to a turbulent wind forcing and dynamic tree response, dominated the motion of four *Pinus sylvestris* trees in Germany (Schindler & Mohr, 2018). The 1 ha area we studied had a ground height range of 20 m and was surrounded by forest for at least 20 tree heights in all directions. The vertical wind profile applied in the model was fitted to wind speeds measured at 5, 10 and 15 m within the forest and the wind amplitude was defined at a resolution of 10Hz. The TLS scan mapped 557 trees in this 1ha area (Kim Calders et al., 2018). We filtered out trees under 5m tall, species with under five individuals, those whose CWS was not reached by 100 ms^{-1}, and those which produced errors giving 397 trees in total (330 sycamore, 44 ash and 23 oak trees).

Importantly, each tree was simulated individually so stand level effects such as sheltering were not included. However, trees are likely to respond to their local wind environment through

changes in growth patterns (Bonnesoeur et al., 2016). These will be captured by the TLS data and so included in the finite element analysis. To test the significance of this neighbourhood effect, we calculated a competition index for each tree by finding all trees within a 10 m radius and taking the sum of their diameters divided by their distance from the focal tree (S. E. Hale et al., 2012). We used this competition index as a crude test of whether residual variation is explained by the trees immediate surroundings. In order to test the influence of material properties on CWS, we first applied identical material properties, those of a sycamore tree, to all our model trees. Secondly, we applied the species-specific material properties to the oak and ash trees (K. J. Niklas & Spatz, 2010). We assumed isotropic material properties throughout the tree due to a lack of data on wood material properties, although wood is in fact a highly complex material (Mackerle, 2005).

Tree architecture

Previous studies have found that the dynamics of trees in the wind are determined mostly by tree architecture, rather than material properties (Sellier & Fourcaud, 2009; Kenneth R James et al., 2014). In order to test whether architecture drives CWS we extracted architectural measures from the cylinder models. The architectural measures we used were:

- Sail area – The total area of the cylinders (branches) projected into the x-y plane, i.e. the 2D area upon which wind drag is incident.
- Crown volume ratio (CVR) – the ratio of woody volume in the crown to that in the stem.
- Crown asymmetry – the ratio of mean to maximum woody volume contained in each segment of crown. These segments are defined by splitting the crown into eight 'pizza-like' slices, centered on the stem.

Generalized linear model selection

In order to test what drives CWS, we used the *fitglm* function in matlab (Mathworks, 2017) to fit generalized linear models of the form $CWS \sim Height * dbh + Species + Architecture$. Prior to model fitting, all variables were centered and scaled to a standard deviation of 1. Sail Area and CVR were log transformed. We selected models with highest coefficient of determination (R^2) and lowest Akaike's information criterion (AIC). The results of these model fits are summarized in Table 1 and further information is given in SI-4.

Results

The effect of leaves on critical wind speed

We first review the CWS estimates from our field data in summer and winter. Our hourly CWS estimates from field data range from 28-56 ms^{-1} in winter and 23-53ms^{-1} in summer (Figure 2). On average, each tree's CWS decreased by 9% in summer. The fact that CWS estimates were generally lower in summer means that trees are at a higher risk of breaking for a given wind speed in when in full leaf. This is presumably due to the additional drag from the leaves transmitting a higher force to the trunk. However, the role of leaves in wind damage is complex, since they also lower the tree's fundamental frequency and alter the wind regime. The likelihood of strong winds is much higher in winter than in summer, demonstrating CWS is not an absolute measure of damage risk. However, this difference between summer and winter suggests that the transition periods are likely to be significant, we discuss this further in section 4.4.

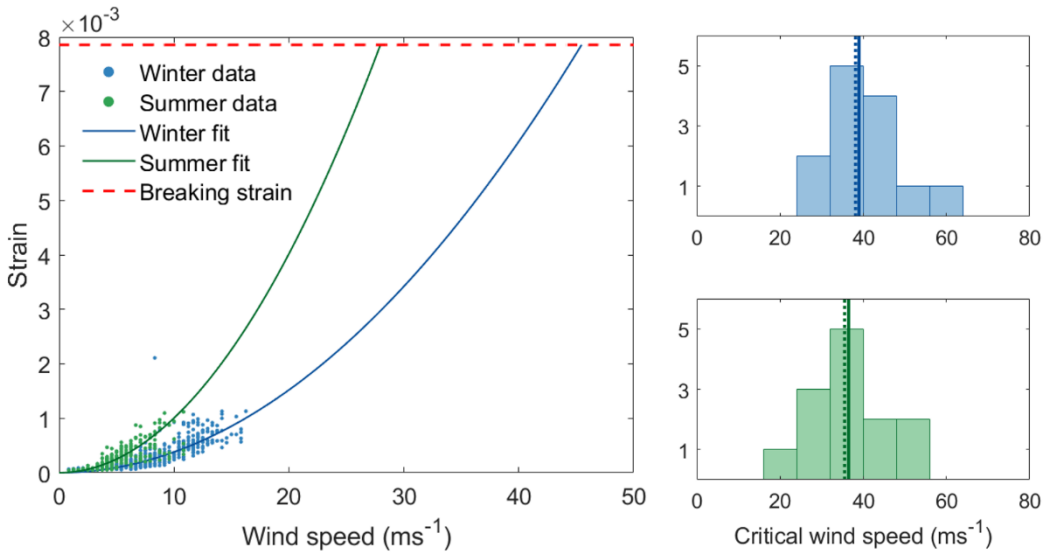


Figure 2 – Left: Critical wind speed estimates from field data in summer and winter using mean hourly wind speeds. Right: Histograms of CWS estimates from field data in winter (above) and in summer (below). The solid line through the histograms represent the mean and the dotted line the median.

Jackson et al (in review) showed that finite element analysis predicts the field estimated CWS with R^2=0.40 and concordance correlation coefficient (CCC) of 0.66, for 17 trees in Wytham Woods. At lower wind speeds the model predicts the strains produced in the tree more

accurately (R^2=0.81, CCC=0.91 at 5 ms^{-1} and R^2=0.79, CCC=0.89 at 15 ms^{-1} wind speed). It is in the high wind speed regime (*i.e*. the part where we do not have field data and are extrapolating) that the model and field predictions diverge. The model tends to estimate a higher CWS than the extrapolations from field data. Importantly, the modelled wind speed is a steadily increasing wind ramp applied at the position of the tree, whereas the field data wind speeds were measured approximately 1 km away and the extrapolation relates hourly wind speeds to hourly strain values. Also, the geographical separation of the two groups of trees used for validation is much larger (approx. 350 m) than the total size of the 1 ha plot. The fact that, despite these significant differences, a similar pattern of CWSs was estimated from both field data and finite element analysis shows that the two methods are comparable.

What drives critical wind speed?

The three species in our plot had significantly different CWSs, with oak having the lowest risk of wind damage and ash the highest risk, for a given wind regime (Figure 3). This difference was evident in both the constant material properties simulations (oak CWS=72±20 ms^{-1}, sycamore CWS=50±15 ms^{-1}, ash CWS=35±19 ms^{-1}, where the values given are mean ± standard deviation) and in the species-specific material properties simulations (oak CWS=72±20 ms^{-1}, sycamore CWS=50±15 ms^{-1}, ash CWS=37±19 ms^{-1}). This suggests that it is the size and shape of the different species that drive differences in critical wind speed, rather than their wood properties.

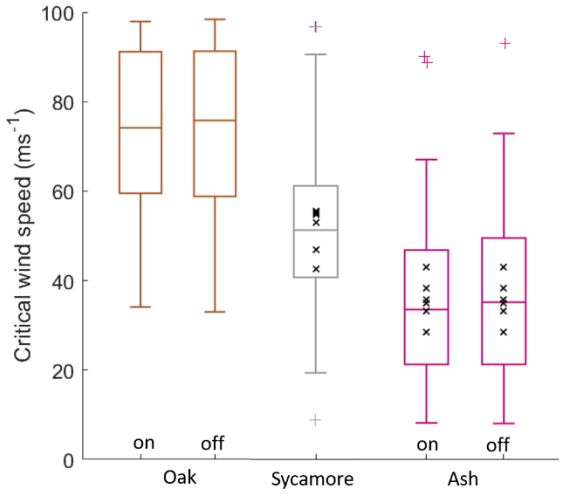


Figure 3 –Simulated critical wind speeds for the three species in our 1ha plot, 'on' signifies species-specific material properties, 'off' represents uniform material properties across all species. The black 'x' markers are field data overlaid for sycamore and ash trees. CWS estimates above 100 ms^{-1} were excluded.

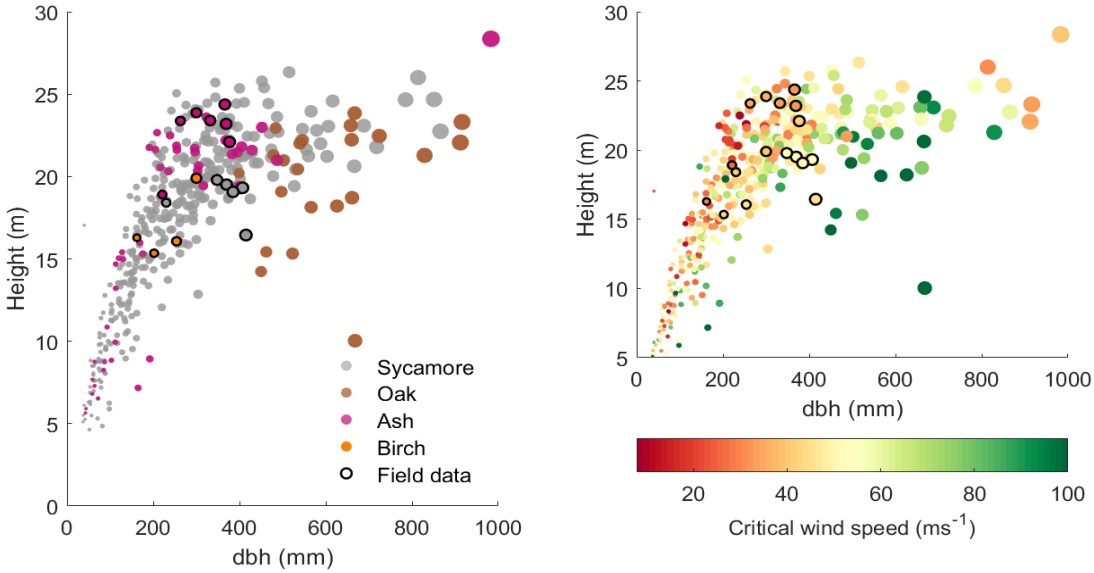


Figure 4 – Left – Tree height against dbh for 397 model trees from the 1ha plot and the 17 trees for which we have field data. The points are scaled by dbh and coloured by species. Right – Tree height against dbh for the same trees, but coloured by simulated CWS (with species-specific material properties).

Figure 4 clearly shows that the different species in our plot occupy different height ranges for a given *dbh*: oak trees tended to have a large *dbh* for their height, whereas ash trees tend to be tall and slender. This range reflects both the growth form of that species and the age of the trees in this plot. There is also a range of heights for a given *dbh* within each species, most clearly in the sycamores that dominate this plot. More slender trees tend to have a higher risk of wind damage and are concentrated on the upper edge of this height to *dbh* relationship.

The results for species-specific material properties and uniform material properties simulations were similar (Table 1), we discuss the former. We found that the competition index accounted for only 4% of the variation in CWS. Tree size, modelled as the interaction of height and *dbh,* and species accounted for 23% and 19% of the variation in CWS, respectively. However, when combined the prediction accuracy increased only slightly, showing that tree size and species explain much of the same variation, as expected from Figure 4. The addition of architectural measures significantly increased the model accuracy. The most significant architectural measure was the crown volume ratio (CVR), which describes the size of the crown relative to the stem, but sail area also increased the prediction accuracy significantly. Crown asymmetry

was not strongly correlated with CWS. As in the case of species and tree size, the architectural measures tended to covary (Figure SI-5). See Figure SI-4 for estimates of effect size for each continuous variable. Overall, this shows that measures of tree architecture, in addition to the commonly measured tree height and *dbh,* are needed to accurately predict CWS in natural forests.

Model specification	Species-specific material properties		Uniform material properties	
	R^2	ΔAIC	R^2	ΔAIC
$CWS \sim Competition$	0.04		0.04	
$CWS \sim Species$	0.19	-66	0.18	-62
$CWS \sim H * dbh$	0.23	-88	0.23	-86
$CWS \sim H * dbh + Species$	0.28	-110	0.27	-104
$CWS \sim H * dbh + Sail\ Area + Species$	0.45	-220	0.44	-213
$CWS \sim H * dbh + CVR + Species$	0.49	-249	0.48	-242

Table 1 – Generalized linear model results showing the key drivers of simulated critical wind speeds. Models are specified in Wilkinson notation.

Is there a trade-off between growth rate and critical wind speed?

Figure 5 shows that faster growing trees tended to have a higher risk of wind damage, for a given wind regime. Ash trees are the fastest growing in our sample and had the lowest CWSs, whereas the slow growing oaks had a larger mechanical safety margin. The sycamore trees occupied the middle ground, and are the most abundant species in this plot. Interestingly, plotting only the larger trees (*dbh>40 cm,* Figure 5B) shows a clearer relationship between growth rate and CWS. This suggests that it is not tree size which is driving this relationship. However, the growth rate data relies on repeat *dbh* measurements and so only reflects radial growth. We therefore cannot determine whether a high growth rate is the cause or the effect of low critical wind speed.

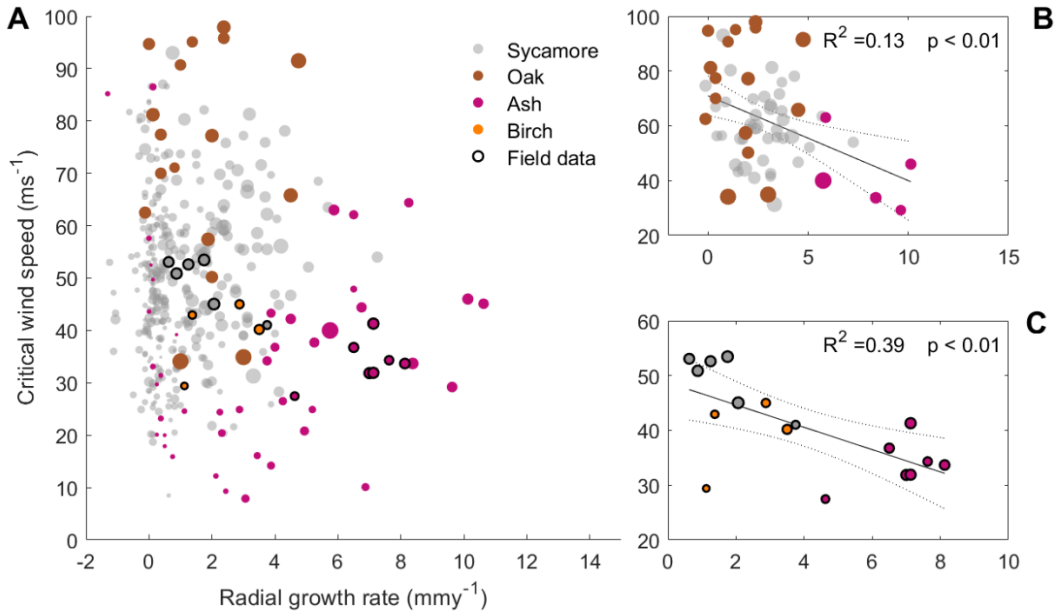


Figure 5 – A: Critical wind speed against radial growth rate for the 397 trees modelled in the 1ha plot with the trees measured in the field overlaid. The marker size represents the tree dbh. B: subset of A, with modelled trees over 40cm dbh only and a best fit line overlaid. C: subset of A, with field data trees only and a best fit line overlaid. All plots have the same axes

Is there a relationship between critical wind speed and the timing of autumn leaf drop?

We found that the leaf-on and leaf-off timings of our three species differ significantly (Woodland Trust 2014). Figure 6 overlays these timings onto a graph of the wind regime in Wytham Woods (defined as the maximum wind speeds for the last 10 years). In autumn, the order of leaf senescence between the three species reflected that of decreasing wind damage risk – as calculated both from both field and modelling work. Ash trees, the most at risk of wind damage for a given wind regime, drop their leaves first and so expose themselves to lower risk from early winter storms. Of the three species we measured, oak trees, the least at risk of wind damage, consistently drop their leaves last. The same ordering does not occur in spring, when other factors are known to drive the timing of bud burst (Vitasse, Delzon, et al., 2009; Vitasse, Porté, et al., 2009).

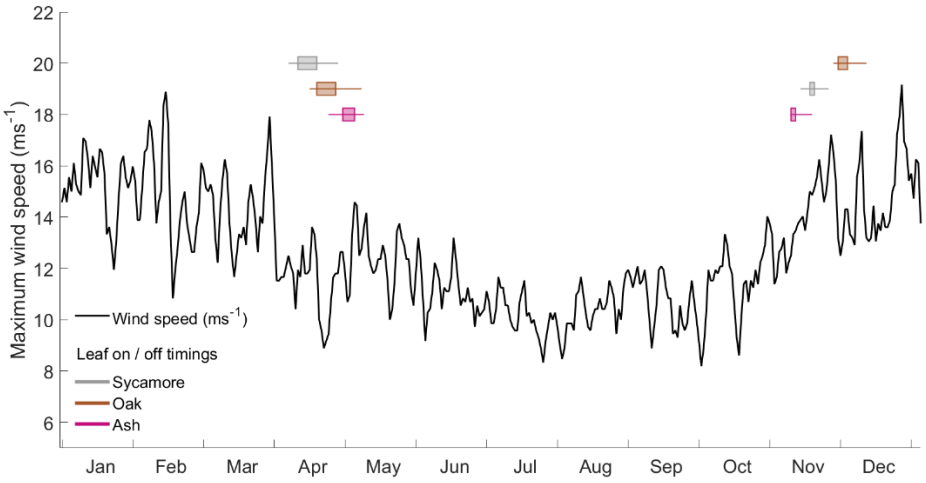


Figure 6 – Wind speed, measured as the maximum occurring in each hour from 2008-2017 at the ECN weather station at Wytham Woods. Overlaid box and whisker plots represent leaf-in / leaf-out timings for the same period.

Discussion

We present a plot-scale estimate of critical wind speed in a natural forest. This study demonstrates the potential of terrestrial laser scanning data to bring new insights into forest ecology by accurately mapping tree architecture and allowing us to question how tree form affects function. Understanding the relationship between critical wind speed and other ecological processes is essential in predicting how forest ecosystems will respond to climate change.

Limitations

Since no field study has witnessed a tree breaking in the wind, estimating CWS necessarily involves extrapolation beyond the range of field data (S. E. Hale et al., 2012; J. Moore et al., 2018). In the eight months of data collection the maximum recorded wind speed was 15ms^{-1}. Within this range of wind speeds, we found that the wind-strain relationship follows the square law predicted by theory, but were unable to test if non-linear effects are significant beyond this range. Finite element predictions of CWS are also uncertain, but follow a similar trend to those from field data. We therefore use finite element analysis to scale-up to the plot level. We do not intend our CWS estimates as predictions for management purposes, but rather as a useful measure with which to compare relative wind risk between trees and to gain ecological insight into the role of wind damage risk as a driver of ecosystem structure.

One source of uncertainty in the finite element prediction of CWS is the treatment of material properties. We use uniform material properties throughout each tree and across all trees of the same species (SI-2). In reality, material properties vary within individual trees, within species and also between species (Lavers, 1983; K. J. Niklas & Spatz, 2010). A sensitivity analysis showed that the most important material property driving the variation in response to wind forcing is green wood elasticity (Table SI-2). The inter-specific variation in elasticity is 25% for the four species in this study, and the intra-specific variation in elasticity is lower than 20%. Changing the model elasticity by this amount caused a 12% change in CWS (Table SI-2), compared to the two-fold variation in CWS for trees of similar sizes evident in Figure 4. In line with previous studies, our sensitivity analysis shows that architecture is a stronger driver of trees response to wind than material properties (Sellier & Fourcaud, 2009; Kane et al., 2014).

Another important limitation of this study is that local wind sheltering effects are not accounted for. The effect of sheltering between trees cannot be explored without intensive wind speed measurements at multiple locations within a forest plot. In this study all trees were forced with an identical wind forcing (SI-3). In reality trees growing close to large neighbouring trees may be sheltered from the full force of the wind (S. E. Hale et al., 2012; MacFarlane & Kane, 2017). Finally, we assume that cylinder reconstructions from TLS data accurately represents tree architecture, but we do not validate this. A number of studies have used these 3D cylinder model trees under the same assumption and found that they can predict tree biomass, and even differentiate between different species (K Calders et al., 2015; Åkerblom, Raumonen, Mäkipää, & Kaasalainen, 2017; Disney et al., 2018). A direct validation of TLS derived tree architecture using field data would be very useful, but highly time-consuming.

Seasonality

The interaction between wind damage risk and the presence or absence of leaves is complex, since leaves alter the wind regime as well as the trees response to wind forcing (Roodbaraky et al., 1994; J. Finnigan, 2000). Our field data predicted lower CWS in summer than in winter, meaning that trees were at a higher risk from the same wind speed in summer. This is not a measure of absolute risk, and Figure 6 clearly shows that wind speeds are generally much lower in summer, but it does emphasize the importance of transition periods when trees are either growing or losing their leaves. In these transition periods, early or late winter storms can bring strong winds and, if a tree still has increased sail area due to leaves, it may be at a higher

risk of damage. To add to this effect, if the surrounding trees have lost their leaves, wind will more easily penetrate into the canopy and the total drag force will be higher.

The three species in our plot display distinct leaf phenology, particularly in autumn (Woodland Trust, 2014). The timing with which they drop their leaves reflects their predicted critical wind speeds, with the ash trees being the most at risk and dropping their leaves first, while the oaks keep their leaves the longest. As would be expected, this order does not hold in spring when other factors (e.g. avoidance of frost risk) determine leaf out timing (Vitasse, Delzon, et al., 2009; Vitasse, Porté, et al., 2009). As we have only studied three species our conclusion is highly tentative, but our findings provide a novel strand of evidence that the timing of leaf drop in autumn may be a trade-off between decreasing marginal returns on photosynthesis and increasing risk of wind damage from winter storms. These findings need to be further explored with other tree species and in other forests. This hypothesis could be tested at scale by analyzing remotely sensed leaf phenology in combination with wind field data.

Drivers of CWS

Tree size and architecture were the main drivers of CWS in this study. Specifically, crown volume ratio was positively correlated with CWS while total sail area was negatively correlated with CWS (Figure SI-4). We saw clear differences in CWS between species, but also a wide range within each species (Figure 3). This was partly driven by tree slenderness, the thinner ash trees having a lower critical wind speeds than the wide oaks (Figure 4). Trees with a higher radial growth rates tended to have lower critical wind speeds. However, repeat *dbh* measurements alone cannot disentangle the cause from the effect in this process, since height growth and *dbh* growth are confounded. A high radial growth rate may indicate fast height growth, leading to low critical wind speed. On the other hand, trees with a high risk of damage will tend to increase their radial growth rate (Bonnesoeur et al., 2016), giving the same pattern. This interplay demonstrates the balance between competition for light and risk of damage from wind storms that trees must maintain to endure wind storms and survive within a forest ecosystem.

Supplementary materials

SI-1. Map of the field site

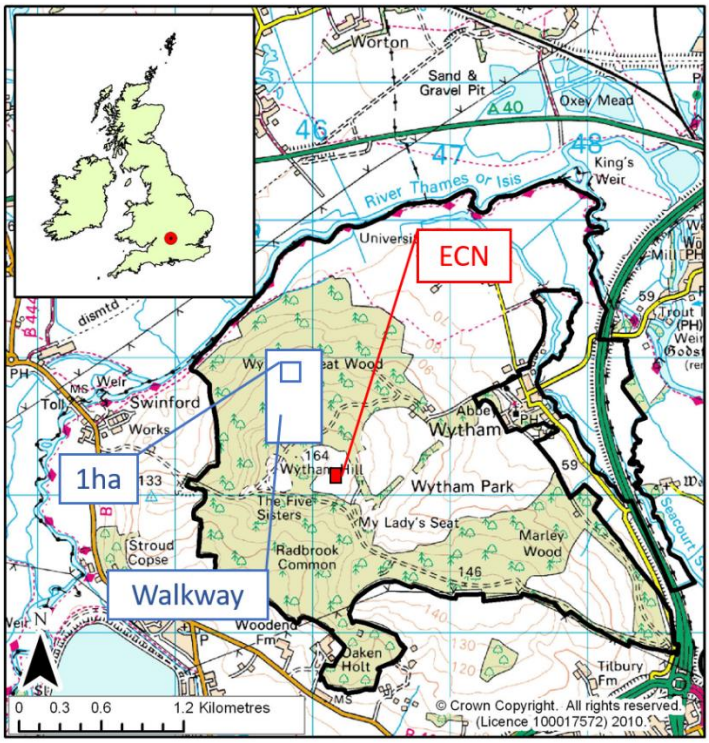


Figure SI-1 – Wytham Woods and surrounding area, showing the ECN weather station, the 18ha permanent Smithsonian plot and the two areas within it in where data were collected for this study. Adapted from (Butt, 2009).

SI-2. Material properties

The species-specific material properties used in the simulations are given below (K. J. Niklas & Spatz, 2010). In the case of the uniform material properties simulations all the trees are assigned the elasticity, density and breaking strain of sycamores.

Latin Name	Common Name	Density (kgm^{-3})	Elasticity (MNm^{-2})	MOR (MNm^{-2})
Acer pseudoplatanus	Sycamore	721	8400 (1340, 43)	66 (8.8, 43)
Fraxinus excelsior	Ash	801	9500 (1880, 204)	66 (10.9, 204)
Quercus robur	English oak	865	10500	72
Betula spp.	Birch	801	9900 (410, 6)	63 (5.1, 6)

Table SI-2 – Material properties of the dominant species in Wytham Woods, Oxford. The values in brackets are the standard deviations and number of samples for each of the measurements respectively.

SI-3. Finite element analysis sensitivity

We conducted a model sensitivity analysis by altering the parameters by 20% (in the case of continuous parameters) and testing the effect on model predictions (Table SI-3). This 20% variation is comparable to the actual range of material properties as measured by (Lavers, 1983).

	Parameter	Default value	ΔCWS (%)
QSM	Averaging iterations	1 (→ 2)	-14
	Beam type	B31 (→ B33H)	3
Wood properties	Green wood density, ρ	Species-specific	-2
	Elasticity, E	Species-specific	12
	Damping factor, α	0.2	0
Root model	Root elasticity	5e6 GPa	0
	Root dashpot	10	0
Aerodynamics	Drag coefficient, C_D	0.82	-9
	Wind decay, μ	0.05	1

Table SI-3 – Sensitivity analysis of the finite element model. Change in critical wind speed prediction when continuous parameters were increased by 20% and discrete parameters changed to the value indicated in brackets.

SI-4. Linear model effect sizes

Table 1 gives an overview of the model fits. In order to show clearly the effect sizes associated with each continuous variable we fit the linear model $CWS \sim Height * dbh + CrownAsymmetr + Sail\ Area + CVR$, leaving out the effect of species. We use the interactive term $Height * dbh$ as the first predictor, since these variables are often available for a monitored forest plot, and because they account for the variation in tree size.

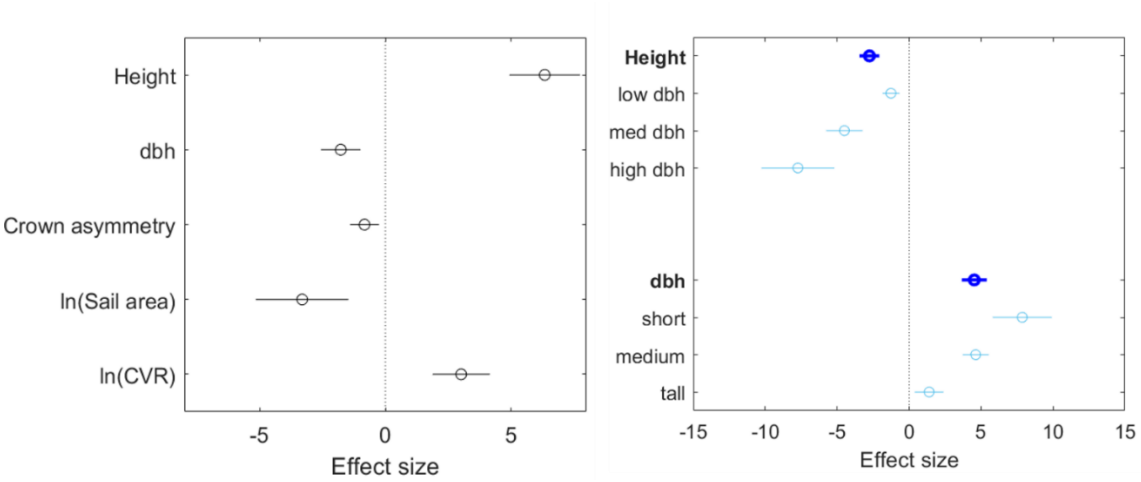


Figure SI-4 – Left: Magnitudes of the effect sizes of height, dbh and the architectural terms in a linear model for CWS. Right: Interaction between tree height and dbh in the linear model for CWS.

Figure SI-5 shows the effect of each predictor variable, added in order of its significance to the generalized linear model. We find that, after tree size, the first architectural measure explains more variation than species. This holds true for both sail area and CVR but the effect of the second architectural measure is small. This shows that these architectural measures explain similar variation in CWS, i.e. that they covary.

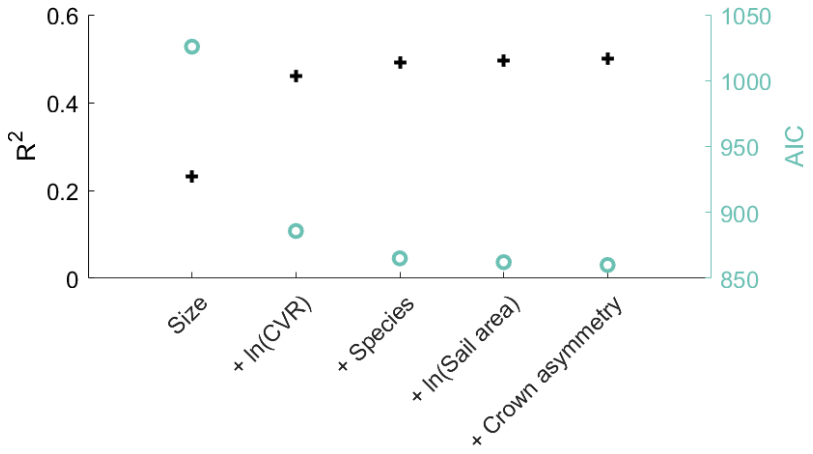


Figure SI-5 – Change in Pearsons correlation coefficient and Akaike's information criterion as predictor variables are added to the generalized linear model. Note that the x-axis is cumulative, so the third entry (+ species) corresponds to a generalized linear model containing tree size, CVR and species.

Paper 3

This paper focuses on the fundamental frequencies of broadleaf trees. The premise is that the complex architecture of broadleaf trees makes them unlikely to sway in as predictable a way as plantation conifers, which can be approximated as cantilever beams. In order to explore this hypothesis, I collated field data on fundamental frequencies of broadleaf trees from all the published sources I could find, and also received unpublished data from two co-authors. These field data are used to test the cantilever beam assumption, but no quantitative measure of tree architecture is available for these trees. Therefore, I also collected a large data set of QSMs of broadleaf trees from many different forests and explored the relationship between architecture and fundamental frequency using finite element analysis, thus building on paper 1. Finally, this paper shows the change in fundamental frequency that occurs when temperate deciduous trees lose their leaves in winter. This paper primarily fulfils thesis aim 3, since it is almost exclusively an exploration of the relationship between tree architecture and fundamental frequency.

The idea for this paper was conceived by me and my supervisors. Most of the field data was collected by co-authors and I brought it together and carried out the statistical analysis. This paper uses field data collected by me in both Wytham Woods and Danum Valley. The TLS data was also mostly collected and processed by co-authors. I extracted tree architectural indices from the QSMs, then converted the QSMs for finite element analysis and carried out the statistical analysis. All of the co-authors contributed meaningfully to the numerous versions of this manuscript. It is currently under review in the Royal Society Interface journal.

An architectural model of resonant frequencies in trees

T. Jackson*[1], A. Shenkin[1], J. Moore[2], A. Bunce[3], T. van Emmerik[4], B. Kane[5], D. Burcham[6], K. James[7], J. Selker[8], K. Calders[9], N. Origo[10,11], M. Disney[11,12], A. Burt[11], P. Wilkes[11,12], P. Raumonen[13], J. Gonzalez de Tanago Menaca[14,15], A. Lau[14,15], M. Herold[14], R. C. Goodman[16], T. Fourcaud[17], Y. Malhi[1]

1 – Environmental Change Institute, School of Geography and the Environment, University of Oxford, OX1 3QY, UK

2 – Scion, 49 Sala Street, Rotorua 3010, New Zealand

3 – Department of Natural Resources, University of Connecticut, CT 06269, USA

4 – Water Resources Section, Delft University of Technology, Stevinweg 1, 2628 CN, Delft, Netherlands

5 – Department of Environmental Conservation, University of Massachusetts, MA 01003, USA

6 – Centre for Urban Greenery and Ecology, National Parks Board, Singapore 259569

7 – School of Ecosystem and Forest Sciences, Faculty of Science, University of Melbourne, Australia

8 – Oregon State University, Corvallis, OR 97331, USA

9 – CAVElab - Computational & Applied Vegetation Ecology, Ghent University, Belgium

10 – Earth Observation, Climate and Optical Group, National Physical Laboratory, Hampton Road, Teddington, Middlesex, TW11 0LW, UK

11 – Department of Geography, University College London, WC1E 6BT, UK

12 – NERC National Centre for Earth Observation (NCEO), Leicester, UK

13 – Tampere University of Technology, Korkeakoulunkatu 10, 33720 Tampere, Finland

14 – Laboratory of Geo-Information Science and Remote Sensing, Wageningen University, Droevendaalsesteeg 3, 6708 PB Wageningen, the Netherlands

15 – Center for International Forestry Research (CIFOR), P.O. Box 0113 BOCBD, Bogor 16000, Indonesia

16 – Department of Forest Ecology and Management, Swedish University of Agricultural Sciences, Umeå, Sweden

17 – AMAP, University of Montpellier, CIRAD, CNRS, INRA, IRD, Montpellier, France

*Corresponding author – tobydjackson@gmail.com

Abstract

Wind damage is a significant driver of forest ecosystem structure and the terrestrial carbon cycle, but the rate of wind damage is uncertain. Trees exhibit resonant frequencies and damping processes that are important in understanding wind damage. We present a comprehensive view of resonant frequencies in broadleaf trees, combining new and existing field data with structurally detailed tree dynamics simulations. We compile a dataset of field measurements of tree fundamental frequencies, spanning conifers and broadleaves, tropical and temperate forests. The field data show that a cantilever beam approximation adequately predicts the fundamental frequency of conifers, but not that of broadleaf trees. We also use a new approach to test fundamental assumptions underpinning resonant frequency models of trees. We model the dynamic properties of >1000 trees using a finite-element approach

based on accurate 3D model trees derived from terrestrial laser scanning data. We show that residual variation in fundamental frequencies of broadleaf trees is driven by their architecture. We also show that slender trees behave like a simple pendulum, with a single resonant mode dominating their motion, which makes them vulnerable to wind damage. Finally, we find that the presence of leaves decreases the fundamental frequency and decreases the damping ratio. These findings demonstrate the value of new 3D measurements for understanding wind impacts on trees and suggest new directions for improving our understanding of tree dynamics from conifer plantations to natural forests.

Resonant frequencies, fundamental frequency, tree architecture, TLS, finite element analysis, wind damage

Introduction

Is resonance relevant?

The dynamics of trees in the wind has interested observers for centuries, but detailed studies are relatively recent (Mayer, 1987). All moving structures, including trees, possess resonant frequencies, but resonance only occurs when a periodic forcing approaches one of these frequencies. The fundamental frequency (f_0) of any structure is particularly relevant for wind damage risk, since wind energy is concentrated at low frequencies and passes to the structure most efficiently in this range (J. Finnigan, 2000; Peltola et al., 2013). Importantly, no field study has recorded a tree breaking or uprooting under wind forcing, and no wind-tree resonance has been observed (J. Moore et al., 2018). Therefore, the relevance of resonance in wind damage processes is a subject of ongoing debate in the literature (Hanns Christof Spatz et al., 2007; Ciftci et al., 2013; J. Moore et al., 2018; Schindler & Mohr, 2018).

Previous work found an empirical relationship between f_0 and tree height for 603 conifers in the UK and North America that closely followed the cantilever beam approximation (equation 1, black text) (B. A. Gardiner, 1992; J. R. Moore & Maguire, 2004). If this approximation holds more generally, f_0 will decrease with increasing tree height leading to a more efficient transfer of energy from the wind to the tree, increasing the likelihood of uprooting or stem breakage (Kenneth R James et al., 2014). The cantilever beam approximation assumes that the tree can be represented by a vertically oriented cylinder with uniform radius and material properties. We employ this relationship as a starting point, appropriate to the simple architecture of many conifers, and add additional terms to explain

residual variation caused by the complexities of broadleaf trees (equation 1, green text). Our updated equation takes the form:

$$f_0 \propto \left(\frac{dbh}{H^2} \sqrt{\frac{E}{\rho}} \right) A \times L \qquad [1]$$

where *H* is tree height and *dbh* is the diameter at breast height, measured at 1.3 m, and E/ρ is the ratio of green wood elasticity to density. The additional terms *A* and *L* represent the effect of tree architecture and leaves, respectively, which are explored in this paper.

In addition, an understanding of the resonant modes of a structure allows for a detailed model of the structure's dynamics under forcing. In the case of conifer trees in the wind, data on f_0 provided the basis for an accurate model of tree motion under wind forcing at the plot level (Dupont et al., 2015). This was possible because the dynamics of conifers are, in uniform plantations, dominated by the fundamental mode (f_0) due to their simple architecture. However, the dynamics of broadleaf trees are likely to consist of multiple significant modes and be dependent on tree architecture and the presence or absence of leaves (Schindler, Schönborn, Fugmann, & Mayer, 2013; Kane et al., 2014).

Tree architecture and finite element analysis

The effectiveness of tension-wood as a support mechanism enables angiosperms to grow in a wide variety of excurrent architectural forms (Loehle, 2016). The difficulty of obtaining detailed maps of tree architecture has, until recently, been a barrier to exploring the complex swaying behaviour of broadleaf trees. Analytical functions can describe both the architecture and arrangement of resonant modes in idealized fractal trees (Mathieu Rodriguez et al., 2008), but real trees require finite element techniques (M Rodriguez et al., 2012; Ciftci et al., 2013). Recently, terrestrial laser scanning (TLS) has revolutionised the mapping of tree architecture (K Calders et al., 2015; Gonzalez de Tanago Menaca et al., 2017; Disney et al., 2018; Malhi et al., 2018). 3D cylinder models, or quantitative structure models (QSMs), are fit to the point cloud data, from which architectural indices can be computed. These QSMs can also be used in a finite element analysis (figure 1), a computational technique capable of simulating the dynamics of structures and the de facto investigation tool used to isolate mechanisms related to branched structures (J. R. Moore & Maguire, 2008; Sellier et al., 2008; Théckès et al., 2015; J. Moore et al., 2018).

We focus on two dynamic properties of trees, which can be easily calculated using the finite element method: the fundamental frequency, f_0, and the dominance of the fundamental sway mode, D_0. Trees with $D_0 > 90\%$ behave like a simple pendulum, with a single dominant resonant mode, while lower D_0 values correspond to increasing significance of higher order resonant modes in the overall motion of the tree. Trees with multiple significant resonant modes can exhibit multiple resonance damping, a dynamic process whereby dangerous energy in the stem is dissipated by the movement of the branches (H. Spatz & Theckes, 2013; Théckès et al., 2015). For a review of multiple resonance damping (also referred to as structural damping or damping by branching) see (H. Spatz & Theckes, 2013). The existence of this damping mechanism underlines the relationship between wind damage risk and tree architecture: trees with certain architectures will dissipate dangerous sway energy more efficiently and so reduce their risk of damage in storms.

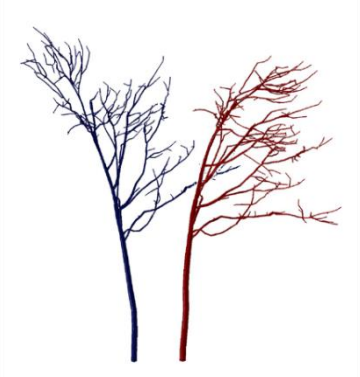


Figure 1 – Simulated fundamental sway frequency of a tree*. Finite element analysis output showing the two extreme positions (blue and red) for a QSM model sycamore tree (Acer pseudoplatanus) swaying in its fundamental mode, f_0 =0.26Hz.*

Structure of the paper

An overview of the analysis and workflow is given in figure 2. In this paper, we:

1. Test the applicability of the cantilever beam approximation to broadleaf trees using field data. Our collated data set consists of 163 broadleaf trees spanning open-grown conditions, tropical forests, temperate forests, and a height range of 4.7 m to 55.7 m.
2. Explore the variation in tree architecture across the 1083 QSMs using a principal component analysis and test for covariance between these architectural explanatory variables.

3. Quantify the architectural term, *A (equation 1)* in a model environment. We use finite element analysis to extract f_0 for each of the 1083 QSMs and test how well the cantilever beam approximation holds. We then test how much of the residual variation in simulated f_0 can be explained by tree architecture.
4. Next, we investigate the range of D_0 across the QSMs and test how it is related to tree architecture.
5. Finally, we return to our field data to quantify the effect of leaves, *L* (*equation 1*) on the dynamic properties of deciduous broadleaf trees.

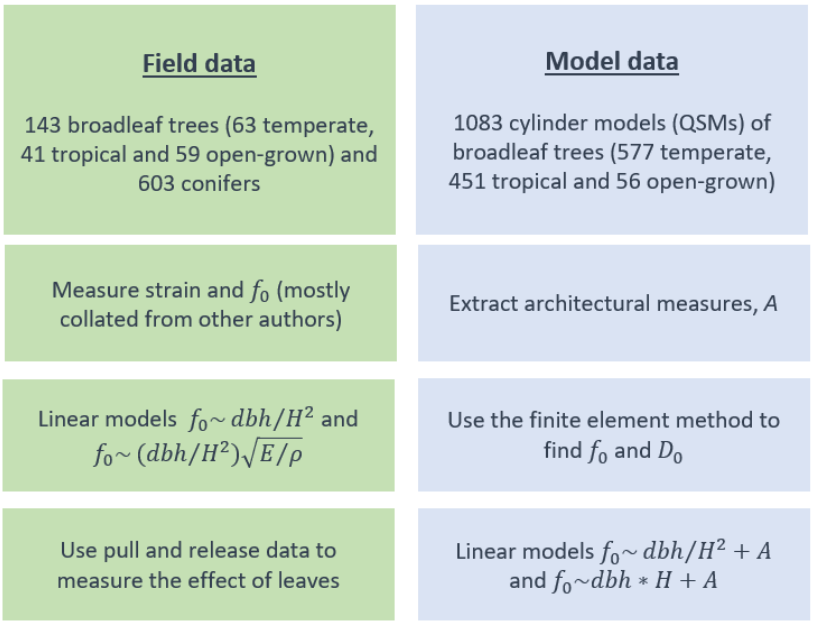


Figure 2 – Workflow diagram

Materials and Methods

Analysis of field data

In order to extract field data on fundamental frequency we measured strain (extension / original length) (following Moore et al., 2005) for a period of 8-months (spanning winter and summer) at 1.3 m height on the trunks of 18 trees (21 stems) in Wytham Woods, UK, and for 3-months on 20 trees in Danum Valley, Malaysia. We separated the strain data into hourly blocks and analysed them using a Welch's power spectral density function. We smoothed the resulting spectra and extracted the peak frequencies. We then took the mean of all the hourly frequencies in summer and winter. Resonant frequency extraction from previous studies are described in the original publications (Baker, 1997; Kane & James, 2011; Bunce, 2017; Van Emmerik et al., 2017).

To investigate the damping effect of leaves, we conducted pull and release tests on four trees in Wytham Woods in February 2016 (leaf-off) and June 2016 (full-leaf), repeating the tests multiple times per tree in perpendicular directions. In pull and release tests the tree behaves like a damped harmonic oscillator, we therefore fit functions of the form

$$\varepsilon = \varepsilon_0 e^{-\lambda t} \cos(2\pi f_0 t + \theta) \qquad [2]$$

to the data, where ε is strain, ε_0 is the initial amplitude, λ is the decay exponent, *t* is time and θ is the phase offset at time *t=0.* The direct effect of damping on the fundamental frequency is given by

$$f_0^d = f_0^u \sqrt{1 - \left(\frac{\lambda}{2\pi f_0^u} \right)^2} \qquad [3]$$

where f_0^d and f_0^u are the damped and undamped fundamental frequencies, respectively.

We were unable to robustly calculate D_0 from field data. We observed multiple resonant peaks in the data (not shown) but any metric based on ratios of peak heights was strongly influenced by data quality, which varied widely across our sample. Instead, we examined D_0 across our QSMs through finite element analysis.

Tree architectural indices

We used QSMs derived from TLS data to test how tree architecture affects f_0 and D_0. The QSMs were sourced from existing publications and ongoing projects (K Calders et al., 2015; Gonzalez de Tanago Menaca et al., 2017; Disney et al., 2018; Kim Calders et al., 2018; Philip ;

Wilkes, Disney, Boni Vicari, Calders, & Burt, 2018). These QSMs were generated using a cylinder fitting algorithm applied to TLS data (Åkerblom, 2017). We applied a simplification step in order to prepare the trees for finite element analysis. This step removes branches under 2cm diameter and child branches whose diameter is less than 30% of its parent branch diameter, since they are error prone (Phil Wilkes et al., 2017). It also averages neighbouring cylinders to increase their length to radius ratio. This simplification was applied to remove most of the variation that arises from uncertainties in the cylinder fitting process for smaller branches. The following architectural indices, in addition to tree height and dbh, were extracted from the simplified QSMs:

- Crown area – maximum ground area covered by the crown viewed from above.
- Crown aspect ratio – ratio of maximum crown width to crown height.
- Crown volume ratio (CVR) – ratio of total woody volume in the crown to that in the stem. This is a measure of how 'top-heavy' the tree is.
- Crown volume asymmetry – the ratio of mean to maximum woody volume contained in each segment of crown, which are defined by splitting the crown into eight azimuthal segments, centered on the stem.
- Path fraction – ratio of mean to maximum base-to-twig path length, this is considered a proxy for water use efficiency (Savage et al., 2010; Bentley et al., 2013).
- Mean branching angle – the average angle between two cylinders at each branching point.
- Total volume – total volume of all the cylinders that make up the tree.

No validation of these architectural indices was possible since measuring tree architecture in the field is extremely slow and difficult. Indeed, it is exactly this difficulty that has hampered previous studies on tree architecture, which are now possible through TLS (Malhi et al., 2018). Previous work found that these QSMs are accurate enough to extract architecture information sufficient to identify species in a 3-species environment (Åkerblom et al., 2017).

Finite element analysis

The QSMs were then imported into Abaqus (Simulia Software Company, 2017), with each cylinder represented as a beam. First, a gravitational force was applied to the trees, which caused a number of simulation failures due to poorly connected beams. This reduced the sample size from 577 to 568 for the temperate trees, 451 to 348 for the tropical trees and 56 to 52 for the open-grown trees. A subspace method was employed to extract the resonant frequencies (Viberg, 1995) and D_0 was calculated as the percentage of generalized mass

contained in the fundamental mode. See Jackson et al. (in press) for a detailed description of the finite element process. Due to the difficulty of co-locating TLS and census data, we could not determine the species of trees represented by the QSMs. Therefore, green wood density and elasticity were kept constant for all simulations at 800 kgm^{-3} and 9.5 *GPa* respectively (K. J. Niklas & Spatz, 2010), except when conducting the sensitivity analysis. The range of sites included in this analysis ensures that our results are not site- or species-specific. We test the sensitivity of the fundamental frequency prediction to finite element parameters in table S2. Importantly, the same simplified model trees were used for the finite element simulations and to extract the architectural indices, so our linear models predicting f_0 and D_0 from architecture are internally consistent.

Statistical analysis

We used ordinary least squares linear regression models for all the statistical analysis in this study. For the field data, we tested models of the form $f_0 = 1 + dbh / H^2$ for each subset of trees, allowing the intercepts to vary between subsets. Where information on material properties was available, we tested a linear model of the form $f_0 = 1 + (dbh / H^2)\sqrt{E/\rho}$. For the model trees (QSMs), for which we had both architectural information and simulated f_0 and D_0, we used linear models of the form $f_0 = 1 + dbh / H^2 + (A_1 + A_2 + A_3)$ and $f_0 = 1 + dbh / H^2 + dbh / H^2 : (A_1 + A_2 + A_3)$ to predict f_0 for each subset of trees, allowing the intercept to vary between subsets (linear models specified in Wilkinson notation). The same method was used for D_0 except that in this case $H + dbh$ was the primary predictor variable. See figures S1-4 for full details of the linear models and their outputs.

Results

Patterns in f_0 from field data

Unsurprisingly, conifers, forest broadleaf trees, and open-grown broadleaf trees have quite distinct ranges of f_0 (figure 3). Moore and Maguire (2004) found that f_0 is strongly related to dbh / H^2 for conifers, indicating that the cantilever beam approximation is accurate. This relationship is weaker for broadleaf trees (figure 3A, see table 1 for fit statistics) presumably due to their more varied architectures. This is to be expected, since trees with multiple stems or large branches clearly do not conform to the cantilever beam model. Differences between

tropical and temperate broadleaf forest trees are not statistically robust in this limited sample. Surprisingly, f_0 for open-grown broadleaf trees was well predicted by the cantilever beam approximation (table 1), even though these trees typically display the least 'beam-like' architecture. This is partly driven by the large range of f_0 and tree size in our open-grown tree sample. In addition, this high predictability could be due to a smaller range of architectures in open-grown trees.

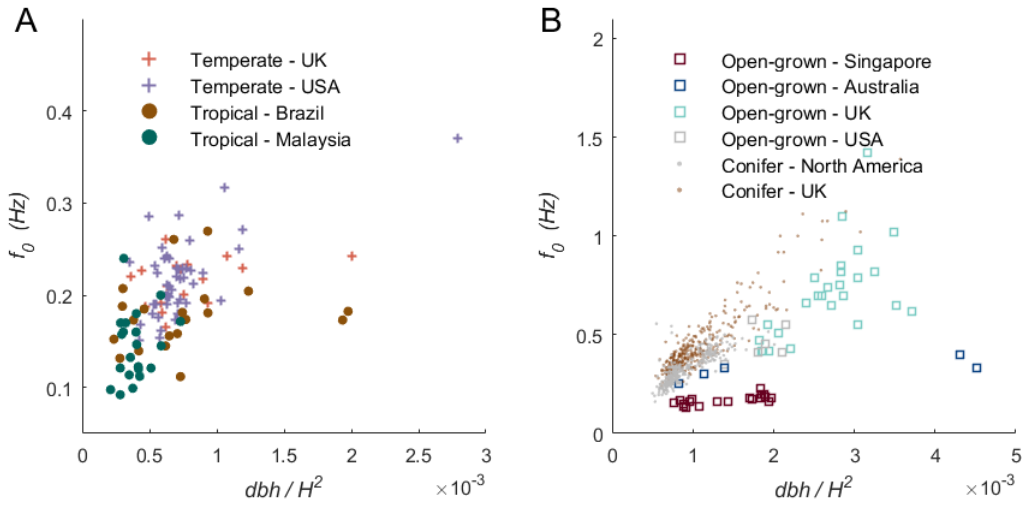


Figure 3 – Fundamental frequencies from field data. *f_0 against dbh/H^2 for A – broadleaf forest trees from temperate and tropical forests and B – open-grown broadleaf trees and plantation conifers. Note the difference in y-axis range.*

As a first order test of whether material properties explain the residual variation in f_0, we collated data on the material properties for a subset of 40 broadleaf trees. We found that fitting models of the form $dbh/H^2\sqrt{E/\rho}$ (equation 1, black text) actually lowered the Pearson correlation coefficient (R^2) value (table S1). This is likely due to the large range of inter- and intra-specific variation in material properties that is not accounted for in this simplistic approach (Hanns Christof Spatz et al., 2007; K. J. Niklas & Spatz, 2010). Also, measurements on small wood samples using a 3-point bending test are not representative of the whole tree elasticity (Ruel et al., 2010; Kane, 2014).

Tree architecture

In this section we use TLS-derived QSMs to explore our seven architectural indices.

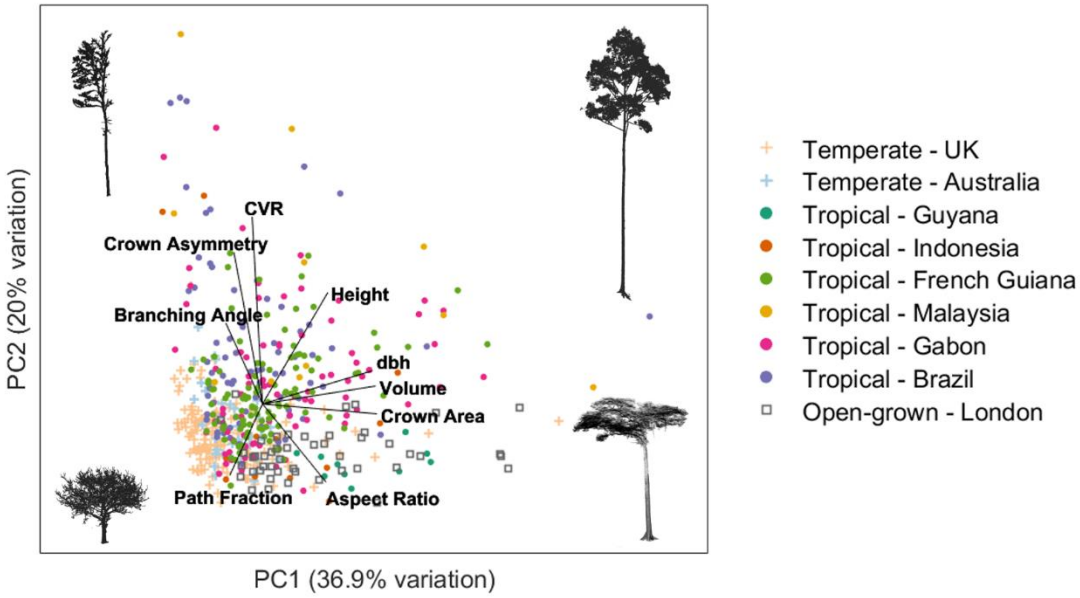


***Figure 4 – Tree architectural indices**. Principle component analysis of the architectural indices extracted from QSMs. Only trees with dbh > 30 cm were included in this analysis for clarity, this did not significantly change the result. The images of trees overlaid were selected as characteristic examples of the architecture expected at their position in the diagram.*

Instantly apparent from figure 4 is the large range of architectural variation in the tropical trees, as compared to the temperate or open-grown trees. This could be driven by the diversity of tropical forests or by the relative number of sites in our sample. The primary axis of variation is driven by tree size: Total volume, dbh and crown area are closely aligned and they account for much of the separation between the relatively small trees from a temperate forest in the UK and the large tropical trees. The second axis of variation is driven by crown properties, specifically the crown volume ratio (CVR) and crown asymmetry. This suggests that tropical some tropical trees have crowns which are both asymmetric and heavy relative to their stem, and that this does not occur at all in the open-grown trees in our sample. Instead, open-grown trees tend to have large, wide crowns and high path fractions. These are both traits we would expect in the absence of competition for light or resources since a large crown captures more light and a high path fraction is the optimum architecture for hydraulic transport (Savage et al., 2010),

Importantly, the TLS data quality differs systematically between study sites due to differences in forest structure (Phil Wilkes et al., 2017). Simple architectural indices such as crown area are likely to be robust, but more complex measures such as crown asymmetry may be less accurate in tall dense forests. A validation study of these, and other, TLS-derived

architectural indices across different forest types would be highly valuable, albeit extremely time consuming.

The effect of tree architecture on f_0

In this section we test whether simulated f_0 follows the cantilever beam approximation, and whether the residual variation in f_0 is driven by architecture.

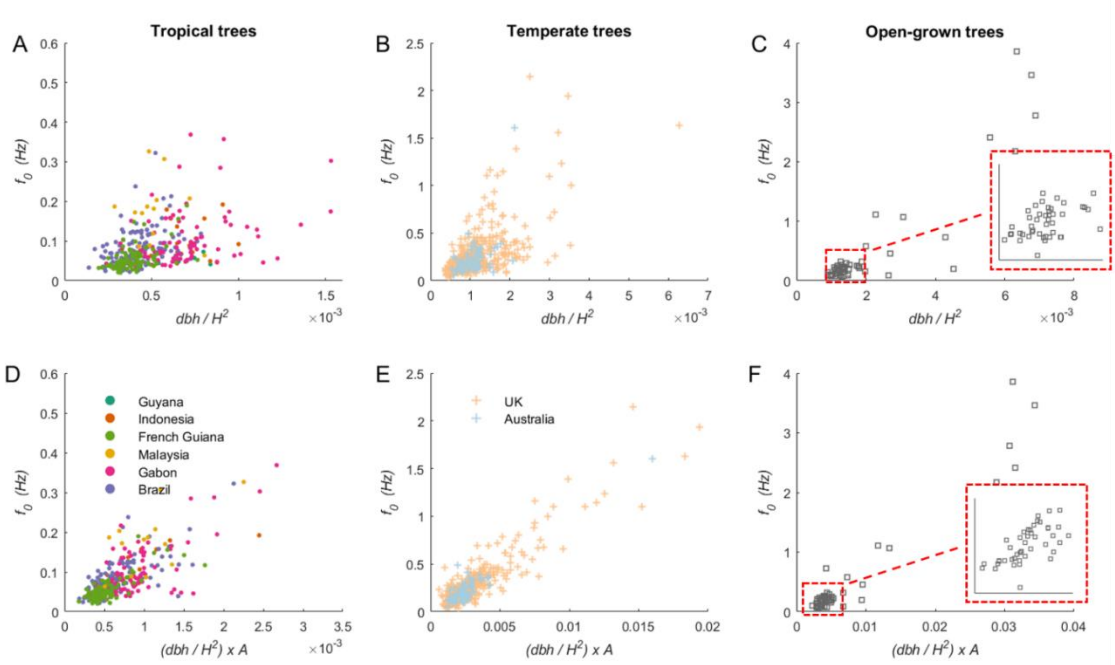


Figure 5 – Simulated fundamental frequencies. *(A-C) Cantilever beam approximation predicting simulated f_0. (D-F) Predicting simulated f_0 using architectural information. Here $A = (CVR + crown\ asymmetry + aspect\ ratio)$. Panels A and D are tropical forest trees, B and E are temperate forest trees and C and F are open-grown trees. Note the difference in y-axis ranges.*

Across all the simulations, linear models show that dbh / H^2 is the primary driver of f_0. Slender trees tend to have low f_0, and will therefore efficiently absorb wind energy which is concentrated at low frequencies. This relationship is weakest for the tropical trees (figure 4), presumably due to the higher range of architectures in this sample. The architectural term, *A,* improves f_0 predictability in all samples (figure 5). The predictability increased by approximately 40% in both temperate and tropical trees (table 1). All three of the architectural indices in the optimal model focussed on crown architecture. Trees with a large crown volume ratio (i.e. top-heavy trees) tended to have lower fundamental frequencies.

This is unsurprising since the same thing happens in pendulums. Less intuitive was the positive correlation between f_0 and both crown asymmetry and aspect ratio. This is consistent with the field data in that open-grown broadleaf trees, which have wider crowns, were found to have much higher f_0 than the forest-grown broadleaf trees (figure 3). As in the field data (figure 3B), open-grown trees were surprisingly well approximated by the cantilever beam model, but this was complicated by the un-even distribution of tree sizes in our open-grown tree sample (figure 5C).

In the above we used the model with highest predictive power and lowest Akaike information criteria (AIC) (see figure S1), which was a three-parameter model focussing on crown architecture. However, all of our architectural indices improved the predictability of f_0 to different extents (see SI) and the key message is that any architectural information is useful when attempting to predict tree dynamics.

Dominance of the fundamental mode

Linear models show that height and diameter explain 26% of the variation in D_0 across all QSMs (table 1). Taller trees tended to have higher D_0, while a higher dbh resulted in a lower D_0 (figure S4). This suggests that slender trees behave more like a simple pendulum, with the fundamental mode accounting for the majority of the motion. This means that slender trees are more suitable for simpler modelling techniques, similar to that of (Dupont et al., 2015) and are less likely to dissipate dangerous sway energy through multiple resonance damping (Hanns Christof Spatz et al., 2007).

Architectural indices did not improve our ability to predict of D_0 as much as we expected, accounting for only 14% of the residual variation. Despite the fact that 3D tree structure was fully mapped and specified in a virtual environment, we were not able to satisfactorily explain the resulting variation of D_0 using our architectural indices. This result suggests that D_0 is driven by finer scale properties, such as the presence of a single large branch, that are not captured by our tree-level architectural indices (Sellier & Fourcaud, 2005). Within our small subset of open-grown trees it was possible to predict D_0 from tree height, dbh and total volume (table 1) but further work is needed to robustly explore this relationship.

	Field data		***Model results***				
	N	$f_0 \propto dbh/H^2$	**N**	$f_0 \propto dbh/H^2$	$f_0 \propto dbh/H^2 \times (A_1 + A_2 + A_2)$	$D_0 \propto H + dbh$	$D_0 \propto H + dbh + A_1 + A_2$

Broadleaf	**Temperate**[i]	**63**	0.32	**568**	0.42	0.83	0.09	0.12
	Tropical	**41**	0.09	**348**	0.16	0.56	0.16	0.29
	Open-Grown	**59**	0.45	**54 (42)**	0.82 (0.18)	0.93 (0.42)	0.29	0.69
Conifers		**603**	0.77	**-**	-		-	-
All Trees		**765**	0.55	**970**	0.62	0.86	0.26	0.40

Table 1 – Summary of linear model predictions of f_0 and D_0. *The entries are adjusted R^2 values for ordinary least squares linear model fits* ***and the linear models are specified in Wilkinson notation****.* [i]*For temperate deciduous trees the field data were measured in full-leaf. In the case of f_0, the three architectural indices are crown volume ratio, crown asymmetry and aspect ratio. In the case of D_0, the two architectural indices are total tree volume and crown area. The numbers in brackets for the open grown trees correspond to the insets in figure 5, they demonstrate the sensitivity of linear models to outliers in this sample. For more details on linear models see figures S1-4.*

The effect of leaves

The swaying behaviour of deciduous trees changes as leaves senesce. The reduction in crown mass leads to an increase in f_0, amplified by the fact that leaf mass is concentrated above the centre of mass of the tree. We found that the mean f_0 increased by 19.4% in winter in Wytham Woods (figure 6). A similar result, a 17.2% increase, was found in the deciduous forests of Connecticut (Bunce, 2017) and previous studies have found comparable results (Kane & James, 2011; Reiland et al., 2015). These variations in mean f_0 are small compared to the range of values measured across different trees, but any decrease in f_0 will lead to more efficient transfer of energy from the wind to the tree, and so increase the risk of damage for a given wind speed. Interestingly, these changes are nearly uniform and can easily be parameterized. If we define L (equation 1) as the increase of f_0 in winter, then $L = 1.18 \pm 0.12$. We expect that this magnitude of this term will be influenced by total leaf biomass, which varies from site to site. For comparison with other forest plots, the leaf mas per unit ground area in Wytham Woods was measured to be 0.35 ± 0.02 kgm^{-2} (dry weight) through direct measurement of cumulative autumn litterfall.

Repeated pull and release tests on the same four trees in summer and winter determined the summer damping ratio to be 8.6±2.2% and the winter damping ratio to be 3.9±1.3%. If we assume that changes in temperature and air density do not have a significant effect on damping, we find that the leaves contributed a damping ratio 4.7±2.5% or approximately half the full summer damping ratio. The direct effect of this damping on f_0 is less than 1% (equation 3). This means that the change in f_0 is due to the mass of the leaves, not their aerodynamic drag. Additionally, both water uptake and soil state can alter f_0 (Bunce, 2017; Van Emmerik et al., 2017). However, predicting leaf mass or volume of water uptake by the changes they cause in f_0 is difficult, since it is highly sensitive to the mass distribution of water or leaves on the tree.

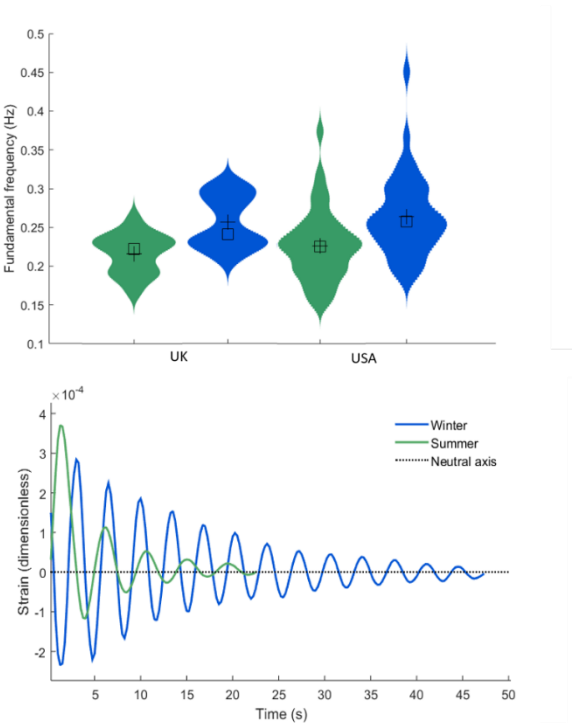


Figure 6 – The effect of leaves on tree sway*. Top: Violin plots of fundamental frequency in summer (green, full-leaf) and winter (blue, leaf-off), from Wytham, UK (left pair) and Connecticut, USA (right pair). Bottom: Summer and winter pull and release test for a single sycamore tree in Wytham Woods, Oxford.*

Discussion

By utilizing novel tools and sensors, particularly a large number of detailed 3D measurements of individual tree structure across biomes, we have improved our understanding of the dynamic behaviour of broadleaf trees. In particular, we have introduced a new way to quantify the impact of tree structure on wind effects. The improved predictability of f_0 is a step towards modelling wind damage for natural broadleaf forests, which plays a vital role in the terrestrial carbon cycle (Espírito-Santo et al., 2014). We show that most trees exhibit a clear fundamental frequency, which is related to dbh / H^2 as expected from the cantilever beam approximation (equation 1, black text). In the case of broadleaf trees, and especially tropical broadleaf trees, there is significant residual variation in f_0. Our modelling work shows that in these cases, tree architectural information can increase the predictability of f_0 by approximately 40%. However, the range of D_0 values and the amount of unexplained

variation in D_0 demonstrates that significant uncertainties remain. Our results on the effect of leaves were relatively simple, leaves cause an 18% increase in f_0 and a doubling of damping efficiency in Wytham Woods.

In general, tall, slender trees tended have higher D_0 and lower f_0, making them both potentially more vulnerable to wind damage and easier to understand using a simple model (Pivato, Dupont, & Brunet, 2014). These tall trees store the majority of carbon in tropical forests and have a high conservation value (Slik et al., 2013). As a result, improved predictions of the likelihood of wind damage to tall tropical trees would be highly valuable.

One key limitation of this study is the lack of accurate green wood material properties data. Material properties vary significantly within individual trees, between individuals of the same species and across species (K. J. Niklas & Spatz, 2010). Our sensitivity analysis (table S2) showed that species level uncertainty is unlikely to affect our predictions of f_0. This is in agreement with Sellier and Fourcaud (2009) who found that the effect of material properties on tree dynamics is likely to be secondary to that of tree architecture. However, tree level variation in material properties may be important all aspects of tree motion. Unfortunately, field data on the variation of wood density and elasticity within trees is scarce.

Our modelling approach, combining TLS data with finite element analysis, could be useful for important open-grown trees, to inform risk assessments and test proposed interventions. The open-grown trees in this study displayed surprising predictability in both f_0 and D_0, although a larger sample size would be needed to robustly test this result.

This paper also explores the range of tree architectures using TLS data. The primary axis of variation was driven by tree size and the secondary axis of variation by crown shape. Interestingly, open grown trees tended to cluster around high path fraction and aspect ratio, which suggests efficient hydraulics and light capture. More work is needed to validate these architectural measures and explore their sensitivity to TLS data processing parameters.

Overall, we show how detailed measurements of tree architecture, such as those just becoming available due to advances in terrestrial laser scanning, give us new insight into the dynamic properties of trees. Our work has quantified the relative importance of tree architectural indices in predicting resonant frequencies, while also highlighting the greater challenge of developing a general model for energy dissipation in complex tree architectures. With TLS-derived tree architectural information now becoming widely available, this is an area ripe for further inquiry.

Supplementary Materials

Material properties

We collated data on green wood material properties for the trees for which we have fundamental frequency data. We found that reliable data on green wood elasticity was sparse and different sources used different measurement techniques. This led to our decision to use values from a single publication only (K. J. Niklas & Spatz, 2010). This publication contained information on 11 of the 59 broadleaf species for which we have field data, representing 40 out of 163 trees. We tested whether the material properties data improved the model for the subset of 40 trees and found no significant change.

Linear models	**N**	**R^2**
All broadleaves $f_0 \sim dbh / H^2$	163	0.25
Subset $f_0 \sim dbh / H^2$	40	0.33
Subset $f_0 \sim dbh / H^2 \sqrt{E/\rho}$	40	0.31

***Table S1 – Variation in f_0 explained by material properties**. Linear model summaries for the broadleaf trees with, and without, material property information.*

Finite element parameters and sensitivity analysis

The finite element simulations represented each tree as a series of beams, a quantitative structure model (QSM), with a uniform density and elasticity, 800kgm^{-3} and 9.5GPa respectively. The root-soil boundary is modelled by a dashpot-spring system. We extracted all the undamped sway modes using a subspace method. This analysis can be done in the free student version of Abaqus as long as the tree model consists of less than 1000 nodes. The parameters used in the simulation and the sensitivity of fundamental frequency on these parameters are given in table S2. The model proved sensitive to green wood density and elasticity, which have opposite effects on f_0 as expected from equation 1.

Parameter	Values	Δf_0 (%)
Radius limit	2cm → 4cm	17
Averaging iterations	2 → 1	18
Beam type	B31 → B33H	1
Green wood density, ρ	800 kgm^{-3}	-15
Elasticity, E	9.5*GPa*	12
Root elasticity	50*MPa*	0.3

Table S2 – Finite element parameters and sensitivity. *Parameters used in finite element analysis and sensitivity of fundamental frequency extraction on these parameters. The sensitivity is measured by increasing each parameter value by 20% and re-calculating f_0. Non-continuous variables were changed as indicated.*

Choice of linear model for the effect of architecture on f_0

The main conclusion of this paper is that architectural information helps explain variation in simulated $\boldsymbol{f_0}$. Detailed conclusions about which architectural indices are most important depend on the selection of an appropriate linear model. We do not discuss all possible models in the main text since there are seven architectural indices in addition to dbh/H^2 and a number of models give similar results. We added architectural indices to the linear model one-by-one, each time choosing the one that explained the most residual variation in $\boldsymbol{f_0}$. The result is shown in figure S1.

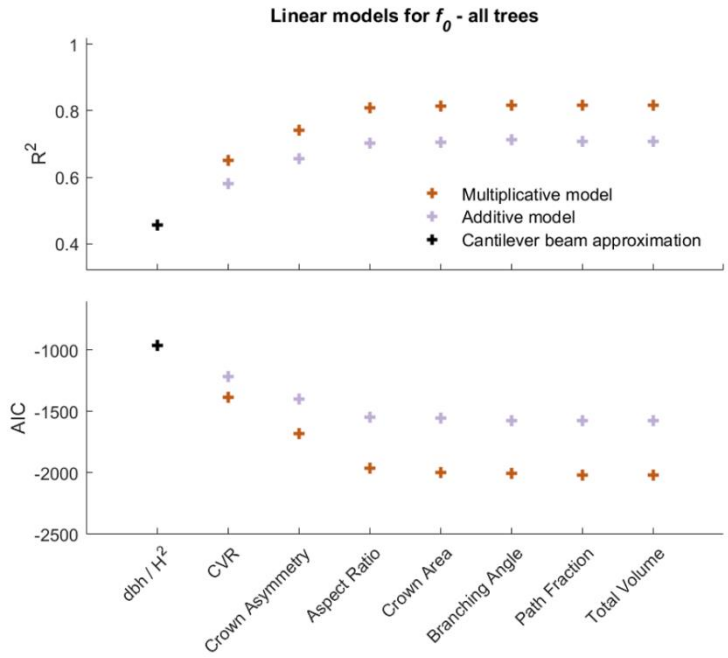


Figure S1 – Summary of linear models for f_0. *The x-axis for both panels represents the architectural indices added cumulatively to the linear model (i.e. the model at denoted 'Path Fraction' contains all architectural indices up to and including Path Fraction). Top panel – Pearson's correlation coefficient (R^2) each linear model. Lower panel – Akaike's information criterion (AIC) for each linear model. Architectural indices were added in the order in which they increase the R^2 by the largest amount.*

Multiplicative models outperform additive models, both in terms of R^2 and AIC. We find that three architectural indices (as presented in the main text) account for most of the variation in f_0 and that further architectural indices are unnecessary. The coefficients of the predictor variables in the best three-parameter model for each subset of trees are presented in figure S2.

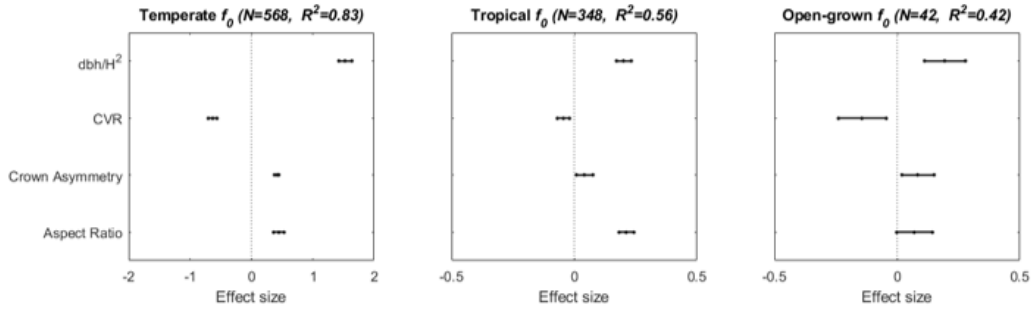


Figure S2 – Effect sizes in selected multiplicative models for simulated f_0. *The central vertical line represents the mean value and the horizontal lines represent the standard error.*

Choice of linear model for the effect of architecture on D0

With no theory to build from, we used $H + dbh$ as the basic term in linear model predictions, since these variables are readily available for many trees and also describe most of the variation in tree size. We then followed a similar approach to our prediction of f_0, adding architectural indices in order of variation explained. We did not use multiplicative models for D_0 since they performed poorly. The result is summarized in figure S3.

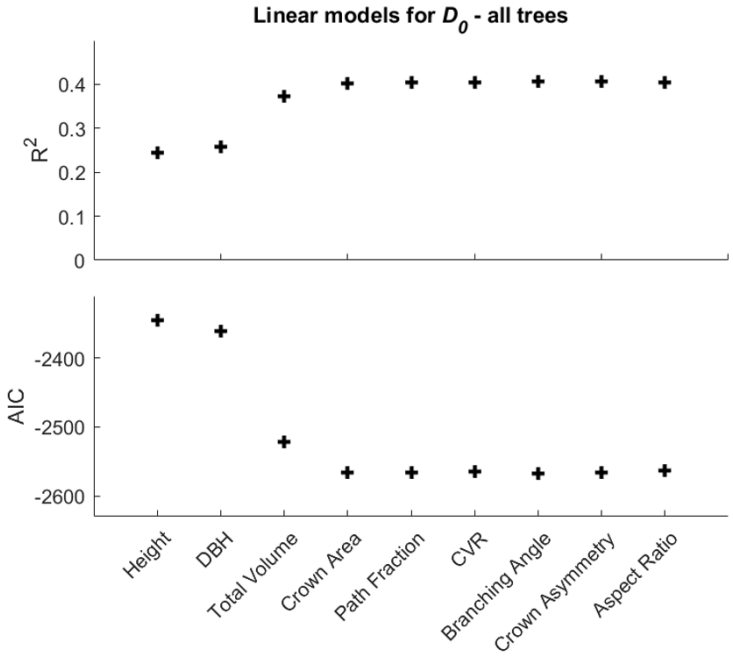


Figure S3 – Summary of linear models for D_0. *The x-axis for both panels represents the architectural indices added cumulatively to the linear model (i.e. the model at denoted 'Path Fraction' contains all architectural indices up to and including Path Fraction). Top panel – Pearson's correlation coefficient (R^2) each linear model. Lower panel – Akaike's information criterion (AIC) for each linear model. Architectural indices were added in the order in which they increase the R^2 by the largest amount. Note the difference in scale between this figure and the corresponding figure for f_0.*

D_0 proved less predictable than ***f_0***, and the various linear model forms tested for ***f_0*** made little difference to the accuracy of the prediction of ***D_0***. We found little support for including interaction terms in linear models of ***D_0*** and so present the architectural indices as purely additive in the main text.

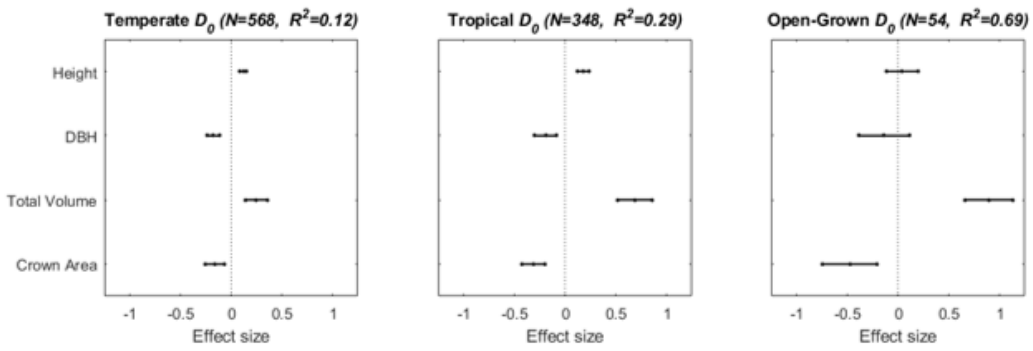


Figure S4 – Summary of architectural models for D_0. *Predicting D_0 from architectural indices for TLS derived QSMs. The central vertical line represents the mean value and the horizontal lines represent the standard error.*

Paper 4

This paper focuses on Danum Valley and thesis aim four. I re-visit the longstanding question 'what limits tree height?' with new techniques, namely strain gauges and TLS. I compare three gravitational stability models and update them using detailed tree architecture measurements based on TLS data. I also calculate the risk of wind damage based on strain gauge data and compare this to the gravitational stability. I attempt to use finite element analysis to model the effect of wind, thereby fulfilling thesis aim two, but find that the model does not agree with the field data, this is discussed in the paper. This paper builds on the finite element analysis and data processing in paper 1.

The ideas in this paper were conceived by me and my supervisors at the start of my PhD, and have been developed during the intervening time. I collected all of the strain gauge data in this study, with the help of two field assistants, and processed the data. I also assisted co-author Dr Andy Burt with the TLS data collection. I then manually extracted the trees from the plot level data, carried out the QSM fitting and all subsequent analysis. This paper has not yet been submitted for publication since I am awaiting comments from co-authors as well as additional TLS data to improve it.

The mechanical stability of the world's tallest hardwood trees

T. Jackson[1], A. Shenkin[1], A. Burt[2], Phil Wilkes[2], M. Disney[2,3], P. Raumonen[4], Y. Malhi[1]

1 – Environmental Change Institute, School of Geography and the Environment, University of Oxford, OX1 3QY, UK

2 – Department of Geography, University College London, WC1E 6BT, UK

3 – NERC National Centre for Earth Observation (NCEO), Leicester, UK

4 – Tampere University of Technology, Korkeakoulunkatu 10, 33720 Tampere, Finland

Corresponding author – tobydjackson@gmail.com

Abstract

The maximum height of trees and the factors which limit it are the subject of a longstanding debate in forest ecology. Previous work on the mechanical limitation of tree height has focussed on height-diameter allometries from forest plots, which miss the tallest trees and the mechanistic understanding of height limitation. We use novel techniques to map the 3D architecture of tall trees and monitor their response to wind loading. We find that gravitational risk decreases with tree height and is strongly affected by tree architecture. In contrast, wind damage risk increases with tree height. The larger diameters and higher wood elasticities of tall trees do not compensate for the increased wind loading experienced above the canopy. The strongest mechanical limitation on the world's tallest angiosperm is therefore likely due to wind loading. We estimate that this tall tree would snap at a wind speed of 24.1 ms^{-1}.

Introduction

Tall trees are an essential store of carbon and an inspiration to the public and to ecologists alike (Slik et al., 2013; Lutz et al., 2018). Competition for light drives increased height growth in densely populated stands (MacFarlane & Kane, 2017) but the processes which limit tree height have long been debated in the literature (McMahon, 1975; Koch, Stillet, Jennings, & Davis, 2004). The hydraulic limitation theory posits that as tree height increases, so does the weight of the root-to-leaf water column, the risk of embolism and the limitation of photosynthesis (Koch et al., 2004; Ishii, Azuma, Kuroda, & Sillett, 2014). This theory is supported by the fact that, at the global scale, canopy height is related to water availability (Moles et al., 2009; Klein et al., 2015). The mechanical limitation theory suggests that, as a tree grows taller the cost of support tissues increases disproportionately and the risk of buckling or wind damage rises.

The first aspect of mechanical stability is a tree's ability to support its own weight. Leonard Euler showed that, in order for a simple beam to avoid buckling under gravity, its height-

diameter allometry should follow $H \sim D^{2/3}$ (Greenhill, 1881) corresponding to elastic self-similarity (Dean & Long, 1986; K. J. Niklas, 1995). Record size trees do indeed follow this pattern, although with a significant safety margin (McMahon, 1975), and understory trees in the lowland, dipterocarp dominated forests of Malaysia have been shown to be close to their gravitational limits (D. A. King et al., 2009). Due to lack of data on tree architecture, most studies use the 'classical' form of Euler's equation which assumes the tree is cylindrical beam. However, other studies take into account the weight of the crown (King & Loucks, 1978) and the taper of the trunk radius and tree mass (Jaouen, Almeras, Coutand, & Fournier, 2007). Terrestrial laser scanning (TLS) data gives us access to realistic tree architecture information (Disney et al., 2018; Malhi et al., 2018) and allows us to compare these theories and assess the importance of tree architecture.

The second aspect of mechanical stability is resistance to snapping or uprooting due to wind loading (K. K. J. Niklas & Spatz, 2012). This is a more complex limitation since it depends on the frequency and intensity of extreme wind events. Also, trees are known to adapt to their local wind environment through increased diameter growth, a process known as thigmomorphogenesis (Telewski, 1995; Bonnesoeur et al., 2016). However, Givnish et al., (2014) showed that support tissue costs increase disproportionately with tree height, which limits the scope of these adaptations and so limits tree height. Recent work using airborne laser scanning has shown that canopy height does indeed track wind exposure in the Wellington region of New Zealand (Coomes et al., 2018). Wind is a key disturbance agent in forests (Magnabosco Marra et al., 2018) and post-damage surveys have shown that tall trees are particularly susceptible (Rifai et al., 2016). Wind risk estimation techniques have been developed for conifer plantations (B. A. Gardiner, 1995; S. E. Hale et al., 2012) and to a lesser extent for open grown trees (Roodbaraky et al., 1994; Kane et al., 2014). The current study is, to the best of our knowledge, the first to conduct these experiments in tropical forests.

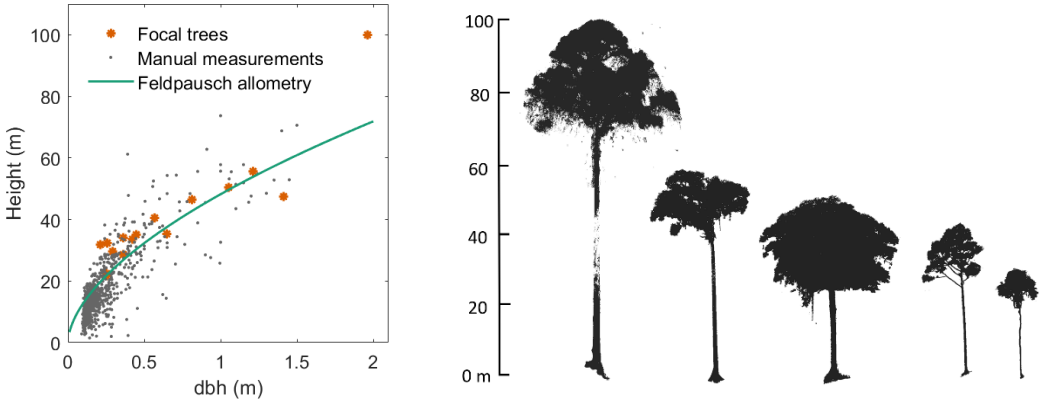


Figure 1 – Left: H-D allometry for trees in this study as well as manual measurements from the same plot (Sullivan et al., 2018) *and a regional allometry* (Feldpausch et al., 2011). *Note the extreme outlier, the world's tallest angiosperm. Right: TLS scans of five trees to demonstrate the height range of our sample. From left to right: Shorea faguetiana, Parashorea malaanonan, Eusidoxyleron zwageri, Shorea parvifolia and Pometia pinnata*

In this study we provide a quantitative analysis of the mechanical limitation of tree height in the tallest tropical forests on earth. We use terrestrial laser scanning (TLS) data to map the architecture of 16 trees, including the world's newly discovered tallest angiosperm, a 100 m *Shorea Faguetiana* (Fig 1). We also present novel field data on the wind-tree interaction for 19 trees. Our key questions are:

1. **Does gravitational stability vary with tree height?** Most studies using height-diameter allometry from plot data are biased towards small trees whereas our TLS data includes trees ranging from 17 m to 100 m in height. We also test whether material properties have a significant effect on gravitational stability.
2. **How does tree architecture influence gravitational stability?** TLS data allows us to specifically measure the stem taper and crown properties of tall trees. We compare (i) the classical cylindrical beam model, (ii) the tapering beam with a crown model and (iii) the model with independent radius and mass tapers.
3. **How does the risk of wind damage change with tree height?** Taller trees are exposed to higher wind speeds, but the resistance to bending scales with the trunk diameter cubed and taller trees may have high wood elasticities. We use field techniques developed for conifer plantations to explicitly test whether these effects balance out.
4. **Is the world's tallest angiosperm close to its mechanical limits?** We estimate the gravitational and wind risk factors separately and then use FE analysis to simulate the combined effect of wind and gravity for the world's tallest angiosperm.

Methods

Field data collection

The island of Borneo is host to the worlds tallest tropical forests. Danum Valley, Malaysia is situated in the state of Sabah (4°57'53.0"N 117°48'18.3"E) and is home to a permanent 50 ha forest monitoring plot. Within this plot all the trees with dbh > 10 cm have been tagged, identified to species level where possible and their dbh has been measured. For a subset, including the trees in this study, tree height and crown dimensions have also been estimated using a laser rangefinder (Sullivan et al., 2018). Our study site is located within a 1 ha intense monitoring carbon plot containing 450 trees > 10 cm dbh, a basal area of 32 m^2ha^{-1}, 178 known species and 50 trees whose species could not be determined (Riutta et al., 2018).

We attached pairs of strain gauges to the stems of 19 trees at approximately 1.3 m. We used three Campbell Scientific CR1000 data loggers and two CR23X data loggers to record the data, each data logger monitoring multiple strain gauge pairs from October 2016 until April 2017. The data loggers were placed at the base of the focal trees, selected for height and accessibility. To minimize the length of wire used for each strain gauge, subsequent trees were selected nearby each focal tree. The strain gauges were attached to the data loggers via wheat-stone bridge circuits to balance the inevitable offset in voltage. An excitation voltage was pulsed through the circuit at 4 Hz and the voltage across the strain gauges monitored at the same frequency. The limited storage capacity of the CR23X data loggers was supplemented using a Raspberry Pi, as in (Jackson et al., 2019). To reduce the power used by the Raspberry Pi, a trigger system was implemented so that it would only turn on and record data when the variance of the strain signal was high (i.e. windy periods). Unfortunately, the voltage offset increased further than expected due to temperature and humidity variations, and this led to a reduced data logger resolution, the failure of the trigger system and ultimately to loss of data. Nevertheless, we recorded some data for these CR23X logged trees and the CR1000 data loggers were unaffected by this, since they had sufficient internal storage.

Since there is no tower in the vicinity of this plot, anemometers were attached to tall trees (trees 1 and 6) boomed out from the stem and facing in different directions so that the sheltering effects of the stem would be different for each. In the case of tree 1, cup anemometers were mounted at 25 m and 35 m (Fig 3). In the case of tree 6 a cup anemometer was mounted at 19 m and a 2D sonic anemometer at 30 m. The cup anemometers were Vector

Instruments A100LK/5M and recorded wind speeds at 0.1 Hz, and the 2D sonic anemometer was a Gill Sonic 1, recording at 1 Hz.

Field data processing

The data loggers record two mV readings per tree at 4 Hz. We calculated a single maximum strain signal for each tree. This process involved (1) multiplying the raw strain signal by calibration coefficients to transform from units of mV to strain; (2) bandpass filtering the data to smooth out drift (3) re-projecting the signals onto into the North and East facing axes using measurements of the actual angles of attachment in the field; and (4) combining each pair of strain signals into a single maximum strain signal using Pythagoras theorem.

For the seven trees logged with CR1000 data loggers, we collected hundreds of hours of data and found a clear bending strain signal (Fig 2A). We also found clear signals for 9 of the 12 trees monitored with CR23X data loggers, although the data availability was lower and the data were noisier. This complicated the uncertainty estimates between trees and the error propagation for the combined wind-strain gradient against tree height model. The improvised wind speed measurement system proved useful and wind-strain gradients did not vary much whichever anemometer they were derived from (see S2 and S3). We compared the distributions of squared wind speed and bending strain at 1 Hz resolution, as a first order test of whether the dynamics of the tree amplify or damp the motion (Fig 2B). We also conducted a singular spectrum analysis, following Schindler and Mohr (2018), to test whether dynamic signals play a key role in the time-series (not shown). Finding that the effects of dynamics were small, we proceeded with a relatively simple static wind loading approach. We calculated the modal maximum bending strain (Wellpott, 2008) and absolute maximum wind speed for each aggregation period (10 or 1 minute). Using the maxima negates the need for a gust factor (Gardiner, Peltola & Kellomäki 2000) and focuses on the bending strains most relevant to wind damage. The length of the aggregation period influences the gradient of the wind-strain relationship, since longer periods focus more on the extreme values while shorter periods increase the number of data points available for fitting.

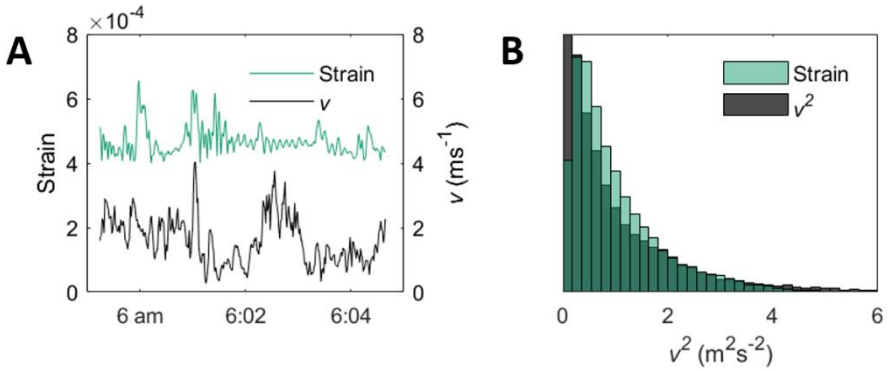


Figure 2 – A: Example five-minute time-series for strain and wind speed. B: Distributions of strain and squared wind speed.

We used two methods to calculate the per tree wind-strain gradient.

1. We split the data for each tree and fitted a least squares regression through the data. This gives an estimate of the wind-strain gradient for each tree.
2. We pooled the data and fitted a random effects model of the form $strain \sim v^2 + (v^2 - 1|tree)$. This allows the slope of the wind-strain relationship to vary for each tree but keeps the intercept fixed for all trees.

We also tested 1 and 10-minute aggregation window lengths and calculated the gradient of the wind-strain relationship using wind speeds measured on trees 1 and 6 separately, which are separated by 63 m horizontally and 25 m vertically. Finally, we then regressed these gradients against tree height.

Green wood material properties

The material properties most relevant to mechanical stability are the green wood density, ρ_{gw}, and modulus of elasticity, E_{gw}. Unfortunately, green wood properties, and especially elasticities, are not often measured. Niklas and Spatz, (2010), collated measurements of green wood properties and we preferentially use measurements from this data set. Species-specific material properties data were available for 6 of our 19 trees. Where no species-specific material properties information was available, we used a genus level average. This covered a further six trees, but for five identified trees there was no species or genus level information available in (K. J. Niklas & Spatz, 2010). In these cases, we used the Global Wood Density data base (Chave et al., 2009) to look up the dry wood density, ρ_{dw}, taking an average where there are a multiple samples of the same species or a genus average where no species specific information was available. We then used the data set compiled by Lavers (1983) to relate dry

wood density to green wood density and elasticity (equations 1-2). The Lavers (1983) data set is a subset of the Niklas and Spatz (2010) data set, except that it also gives dry wood density for each species as well as uncertainty estimates. We found the following relationships for N=178 hardwoods:

$$\rho_{gw} = 1.2 \times \rho_{dw} + 27.3 \ \ (R^2 = 0.97, RMSE = 36) \quad (1)$$

$$E_{gw} = 14.6 \times \rho_{dw} + 157.6 \ \ (R^2 = 0.72, RMSE = 1588) \quad (2)$$

Two trees could not be identified to genus level and were assigned the mean material properties of the other trees. Full details of the material properties used are given in table 1.

Tree tag #	Genus	Species	ρ_{gw} kgm^{-3}	E_{gw} MNm^{-2}	MOR_{gw} MNm^{-2}	DBH cm	Height m
30343	*Parashorea*	*malaanonan*	641	9100	61	110.0	51
30296	*Chisocheton*		626	7443	53	29.8	23
30281	*Pometia*	*pinnata*	787	9399	69	32.2	28
30313	*Shorea*	*parvifolia*	513	6700	48	55.0	39
30476	*Aporusa*	*benthamiana*	781	9326	68	23.3	24
10498	*Shorea*	*parvifolia*	513	6700	48	73.0	46
10542	*Terminalia*	*citrina*	961	13000	94	49.2	42
20447	*Parashorea*	*malaanonan*	641	9100	61	100.0	56
20445	*Orophea*	*myriantha*	747	9680	70	20.6	17
20419			747	9680	70	39.4	31
30409	*Caryodaphnopsis*	*tonkinensis*	747	9680	70	43.5	39
10676	*Shorea*	*pauciflora*	689	9700	68	24.1	34
20523	*Syzygium*	*panzeri*	798	9531	70	40.2	33
10612	*Diospyros*	*tuberculata*	567	6728	47	35.3	34
20557	*Canarium*	*pilosum*	593	6200	41	29.9	32
20596			747	9680	70	21.1	27
20593	*Eusideroxylon*	*zwageri*	1282	17700	143	73.3	43
10643	*Orophea*	*myriantha*	747	9680	70	18.6	18
20649	*Eusideroxylon*	*zwageri*	1282	17700	143	35.4	22
	Shorea	*faguetiana*	673	9700	66	2.13	100.8

Table 1 – Overview of the trees in this study. ρ_{gw} is the green wood density, E_{gw} is the green wood elasticity and MOR_{gw} is the green wood modulus of elasticity.

Terrestrial laser scanning and QSM fitting

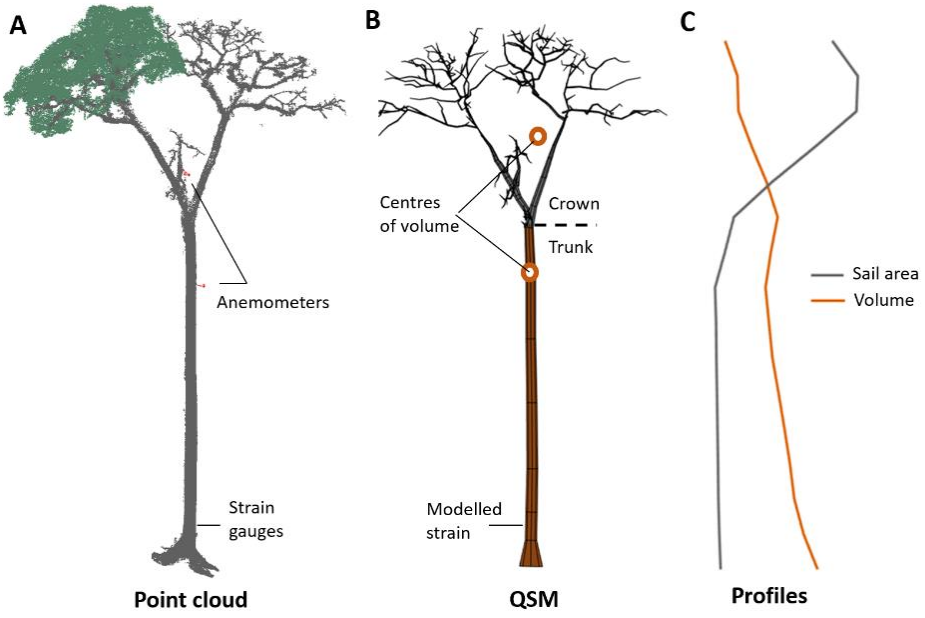


Figure 3 – A: point cloud of tree 1, showing the position of the anemometers and strain gauges. This image also gives an example of the manual leaf filtering, with points assumed to be leaves shown in green on part of the crown. B: Simplified QSM for tree A1n, showing manual definition of the crown and the centre of volume for the whole tree (lower) and the crown (upper). C: Vertical profiles of sail area and volume derived from the QSM and used for the analytical wind model and the mass taper calculation respectively.

TLS data were collected for 1 ha in Danum Valley in April 2017. In order to identify the 19 monitored trees in the 1 ha of TLS data, three circular reflectors were tacked onto each tree in an approximately triangular pattern. We extracted a plot level point cloud including only high reflectance returns and noted the coordinates of the 19 trees. Due to the height of the emergent trees, the dense canopy and the presence of lianas, the point density is low compared to that collected in shorter forests (Burt, 2017; Phil Wilkes et al., 2017). Automatic tree segmentation algorithms did not sufficiently separate individual trees in this point cloud. We therefore manually extracted 15 of the 19 trees, omitting those with very poor data quality and focussing on the taller trees. We then manually separated the stem and branches from the leaves and noise (Fig 3A). This was a long process which involved trimming one branch at a time and then re-connecting them to form a single, clean tree-level point cloud. This process is

subjective and the resulting tree level point clouds are all available online. Buttresses were removed from the tree-level point cloud prior to cylinder fitting, and the height of the buttress noted. TLS scanning and data processing for the tall *Shorea faguetiana* followed a similar protocol, except that drone imagery was used to supplement the crown coverage.

We used a specifically designed cylinder fitting algorithm (*TreeQSM*; Åkerblom, 2017) to fit 360 QSMs to each tree level point cloud. Each of these QSMs is different due to the input parameters and the stochastic nature of the QSM fitting process. The *TreeQSM* optimum QSM selection method proved unreliable, sometimes selecting models with multiple small cylinders at different angles, instead of a single straight cylinder. Therefore, a well fit QSM was selected manually. In order to prepare for finite element analysis we simplified the chosen QSM by averaging together neighbouring cylinders and removing all cylinders with a radius under a given threshold. This threshold was changed based on the QSM, since taller trees had a lower point density in their crowns. For the trees whose buttresses had previously been trimmed from the point cloud, we attached a cylinder at the bottom with the same height as the buttress (Fig 3B). Both the QSM selection and simplification were subjective and the all of the QSMs produced as well as the simplified QSMs are available online.

Tree architecture

We found a good agreement between manual and QSM measurements of dbh, but a systematic underestimation of tree height from the QSMs relative to the point clouds, due to the beam divergence causing increasing noise at the tops of the trees (see S1). The manually measured tree heights show no systematic deviation from those measured on the point clouds. We therefore used height measurements from the point clouds wherever possible and manual measurements elsewhere. We measured tree diameter at multiple heights directly from the point clouds. We used these data to calculate the radius taper, α, defined in equation 3.

$$r(z) = r_0(\frac{H-z}{H})^{\alpha} \qquad (3)$$

where r is the radius, r_0 is the radius at the base of the trunk, H is the height and z is the vertical coordinate. In order to calculate the mass taper, β, we split the QSM into vertical segments and summed the volume of the cylinders within each segment (Fig 3C). We assume uniform density and fit a relationship of the same form as equation 3. These tapers are used in gravitational maximum height estimate iii below.

We could find no generalizable definition of branching order (Osunkoya et al., 2007) and so manually defined the point at which the crown started (Figure 3B). Using this we calculated the ratio of crown mass to stem mass, *K,* and the positions of the centres of mass for the crown and for the whole tree (Fig 3B). Previous work in similar forests found that variation in crown architecture was primarily intraspecific, with only a small proportion of the total variance explained by species (Osunkoya et al., 2007; Iida et al., 2011). These studies also reported a decrease in relative crown size with tree height, which was fit with a power law function (Osunkoya et al., 2007). Therefore, In order to generalize the risk factor calculation, we assumed a power law relationship $K = 0.3H^{-0.5}$, where the parameters were chosen to fit the curve roughly to the data (Fig 6).

We calculated the vertical profile of sail area, $A_{sail}(\mathrm{z})$, for each tree based on the QSM in two ways. First, we calculated the total area of the cylinders projected into the X-Z plane. Second, we calculated the total width of the tree at each height. We calculated these widths from eight points of the compass and took used the mean sail profile (Fig 3C).

Gravitational stability

We calculated the theoretical maximum height each tree could reach before collapsing under gravity, H_{max}, using three different models.

i – The 'classical' model of a beam with uniform circular cross-section. This is the simplest and most commonly used model (K. K. J. Niklas & Spatz, 2012), with C=1.26.

$$H_{max} = C\left(E_{gw}r_0^2/\rho_{gw}\right)^{1/3} \qquad (4)$$

ii – A beam with a fixed taper exponent, $\alpha = 0.5$, and a top weight to represent the crown centred at $0.9H$ (D. King & Loucks, 1978). This model takes the same form as equation 4, but with *C* now dependent *K,* as per equation 5.

$$C = \left(\frac{0.334K^2 + 0.08655K + 0.007601}{0.6125K^3 + 0.1695K^2 + 0.02907K + 0.001427}\right)^{1/3} \qquad (5)$$

iii – A beam with measured radius taper, mass taper and total mass. This model was adapted from Greenhill (1881) by Jaouen et al., (2007) .

$$H_{max} = \sqrt{\frac{\pi E_{gw}}{16M_{tot}g}} \cdot r_0^2 \cdot b \cdot (|\beta - 4\alpha + 2|) \qquad (6)$$

Where M_{tot}, is the total mass of the tree and b is the first root of the Bessel function J_x with

$$x = (4\alpha - 1)/\,(\beta - 4\alpha + 2) \quad (7)$$

Analytical wind model

Since the field data demonstrated that a static approach would be sufficient (Fig 2) we did not attempt to model the dynamic interaction between wind and trees. Instead we used simple analytical model of the bending strain at the base of the trunk in response to wind loading. We assumed quadratic increase in wind speed with height (see S3) and so calculated the vertical profile of force on tree and the resultant moment at the base of the tree, M_{wind}, using equation 8.

$$M_{wind} = \frac{1}{2}\rho_{air} C_d \int_0^z A_{sail}(z) \cdot v(z)^2 \; z \, dz \quad (8)$$

Where ρ_{air} is the density of air and $\mathrm{C_d}$ is the drag coefficient, which is assumed to be fixed at 1. The strain at the base of the tree, ε, was calculated using equation 9 (K. K. J. Niklas & Spatz, 2012).

$$\varepsilon = (4\pi / E_{gw} r^3) \; M_{wind} \quad (9)$$

Finite element models

Each simplified QSM was imported into Abaqus (Simulia Software Company, 2017) via the input file scripting language, using freely available software (Tobias Jackson, 2017). Each cylinder was modelled as a Euler-Bernoulli beam (B31) and assigned either the mean material properties or the species-specific properties given in table 1.

In the field, a tree's resting position is the equilibrium position between gravitational forces and stresses in the wood. In engineering terms, trees are pre-stressed structures. In order to model the effect of gravity accurately, we therefore first apply a reversed gravitational force to each tree, causing the branches to bend upwards. We then extracted the deformed position of each branch and imported these into a new Abaqus session. A gravitational force was then applied downwards, causing the branches to return to their initial position but now with stresses and strains from the trees self-weight. This gravitational force was maintained throughout the analysis, so that if the tree bends in the wind, the additional force of the overhanging crown is modelled. In some cases where the tree was leaning or the crown highly asymmetric the tree passed its original position and continued to deflect unrealistically, see Results.

Risk factor calculations

We calculated multiple risk factors in order to compare the roles of wind and gravity in maximum height limitation. The gravitational risk factors were defined as the ratio of the measured height to the estimated maximum height $R_{grav} = H/H_{max}$. There are three gravitational risk factors, one for each of the maximum height models. We also generalized risk factors i and ii using the regional height-diameter allometry (Feldpausch et al., 2011) and the power law relationship between *K* and *H.*

In order to calculate wind risk factors we first estimate what the bending strain would be at a chosen threshold wind speed by extrapolating from field data e.g. 20 ms^{-1}, ε_{20}. We then calculate the breaking strain for each species ε_{break} (Table 1). The risk factor is then $R_{wind} = \varepsilon_{20}/\varepsilon_{break}$.

Results

Gravitational stability

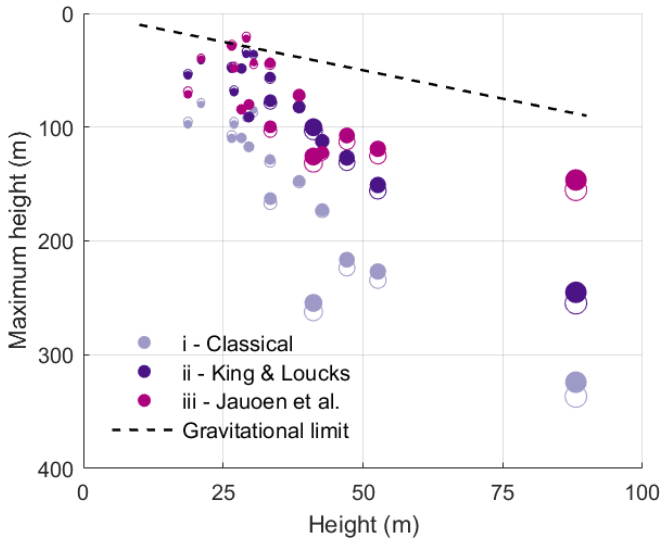


Figure 4 – Maximum height of trees against measured height. The filled and hollow markers represent plot-level-mean and species-specific material properties respectively.

Figure 4 clearly shows that the shorter trees are closer to their gravitational limits than the taller trees. The maximum height estimates based on models ii, and iii predicted a similar pattern to the classical model i (R^2=0.83 and 0.70, respectively). Overall, material properties had surprisingly little effect on gravitational stability estimates. However, this small effect was consistently positive for taller trees, i.e. their species-specific material properties make them stronger than the plot average, and negative for the shorter trees.

The magnitude of the predicted maximum heights diverged significantly between models. Using the classical model, we estimated risk factors ranging from 0.16-0.36, demonstrating that our trees did not approach the maximum height for a cylindrical beam of the same diameter. Model ii, the tapering beam with a top weight, estimated risk factors from 0.33-0.86. This shows that the weight of the crown significantly reduces gravitational stability, and that some of the short trees in this sample do approach the maximum height for their given crown size. Model iii estimated risk factors ranging from 0.25-1.24, with one of the shorter trees actually exceeding its predicted maximum height. This maximum height calculation shows that many of the trees in this sample could not safely grow much taller with their current mass and radius taper. We found model iii to be sensitive to the mass taper exponent, which was strongly dependent on the QSM quality. We therefore focus on model ii in the remainder of this paper.

Change in the wind-strain relationship with height

The 10-minute maximum wind speed and bending strain relationship was characterized by an increased dispersion at high wind speeds (Fig 5A, B). This was due to the distance between anemometer and the focal tree and the small-scale spatial variability of wind flow. The gradient between wind speed and bending strain maxima was steeper for taller trees (Fig 5C), meaning that an equal wind speed will cause larger bending strains in the trunks of taller trees. This shows that the larger diameters or possible higher elasticities of tall trees did not counterbalance the effect of higher wind speeds and increased sail area. We excluded three trees from this analysis due to lack of field data. This result was robust to different aggregation window lengths (1 minute or 10 minute) and different statistical techniques (splitting data by tree and fitting separately or combining data in a random slope model) see Fig S2C. Also, this result was similar whether we used wind speed measurements from a sonic anemometer or from a cup anemometer 63 m away (Fig S2C). Excluding all trees logged with the CR23X data loggers increased the strength of this relationship. Taller trees did not have systematically higher modulus of rupture (Table 1), so the risk of wind damage was not counterbalanced by the strength properties of the wood.

Modelling the wind-strain relationship

Our models predicted an increase in slope of the wind-strain gradient with tree height, but did not perform well against field data. Using wind data measured at the sonic anemometer, a 10-

minute aggregation period and splitting the data by tree to calculate the gradients, the analytical model predicted the wind-strain gradient with R^2=0.04 and the FE model had a negative R^2 value. Model performance varied with input parameters and the choices in field data processing, see S2. This poor model performance is likely due to sheltering effects that are not accounted for.

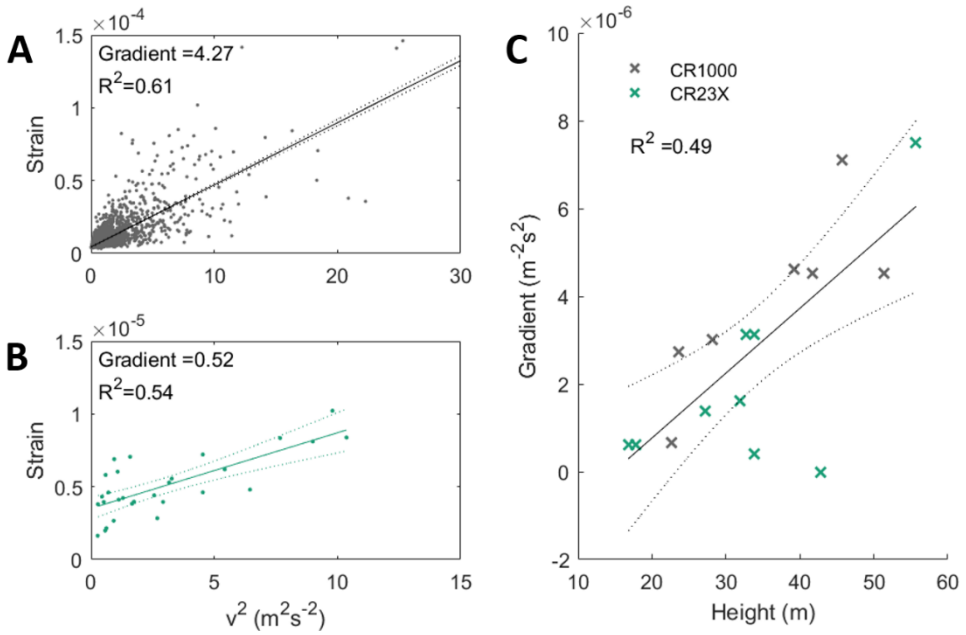


Figure 5 – 10-minute maximum bending strain against maximum squared wind speed measured with the sonic anemometer for (A) 51 m tall Parashorea malaanonan logged with a CR1000 and (B) 17 m tall Orophea myriantha logged with a CR23X. Note the difference in scales and data availability. C: Gradients of the wind-strain relationship against tree height using data from the sonic anemometer, the random effects model and a 10-minute aggregation period.

Wind and gravity risk factors and their variation with height

We found no correlation between the wind and gravitational risk factors for the 11 trees where field and TLS data overlap (p=0.17, 0.08, 0.33 for models i, ii and iii respectively). As demonstrated in the previous sections, wind risk factors tended to increase with tree height while the gravitational risk factors decreased (Fig 6). We also found a similar decrease in gravitational risk with tree height using region-specific allometric equation. The trend of this relationship is not sensitive to the exact parameters used to estimate how crown size varies with tree height, although the intercept is. The wind and gravitational risk factors are not

simply additive, since the gravitational risk factor is derived from a model whereas the wind risk factors are extrapolated from field data collected in the presence of gravity.

Despite the poor performance against field data, we used FE analysis to simulate the combined effect of wind and gravity for the 100 m *Shorea faguetiana* (Fig 7). This demonstrated that the effect of wind dominates the bending response of the tree and that the effect of gravity is secondary (Fig 7). The contribution of gravity increases with wind speed, since the tree deflection is higher and so the overhanging weight of the crown causes a greater moment. For the other trees in our sample, we found that 4 of 15 failed under the simulated gravitational force. These trees were either leaning or had highly asymmetric crowns. This is clearly unrealistic and is likely due to the fact that trees with asymmetric architecture support themselves with asymmetric material properties. While our finite element models are based on detailed information on tree architecture, we do not have data on the variation of material properties within each tree and so cannot include this in the model.

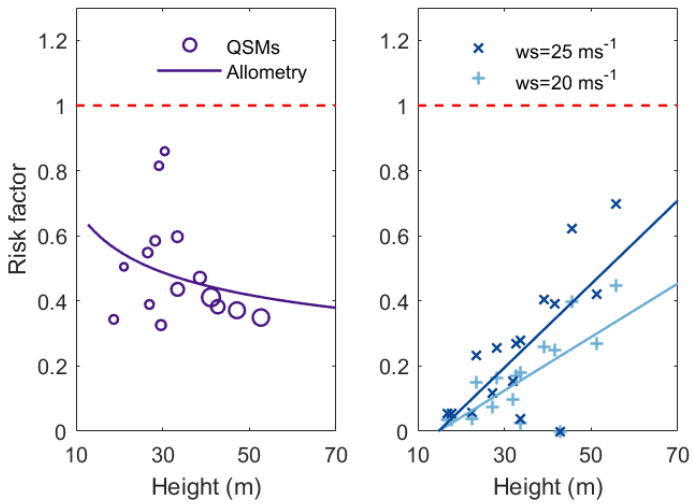


Figure 6 – Left: gravitational risk factors for the trees in this study (points) and general allometry (lines) under two assumptions. Right: wind damage risk factors for a maximum wind speed of 20 and 25 m/s, point indicating specific trees derived from field data and the lines being best fit lines.

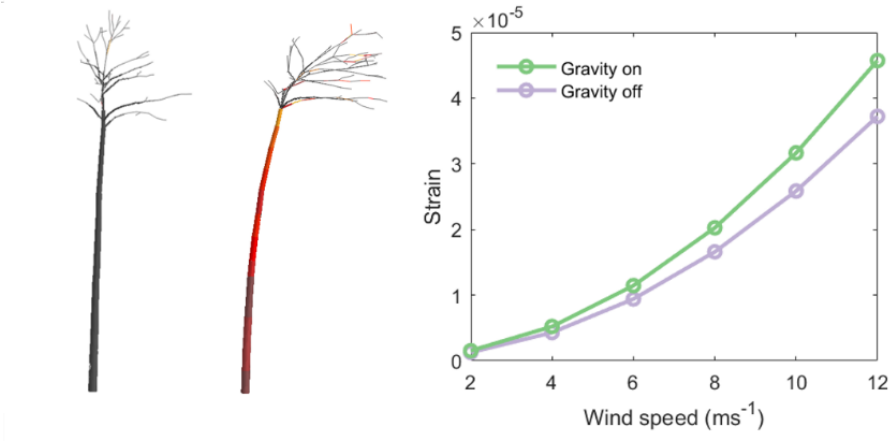


Figure 7 – Left: QSM of the tallest tree in the tropics (a 100 m Shorea faguetiana) in its rest position. Middle: Finite element simulation of same tree under gravity and 12 ms^{-1} wind loading. Right: Strain produced at the base of the stem of the same tree under simulated wind loading with and without gravity.

Discussion

Gravitational risk factor decreases with tree height

All the models of gravitational stability predicted a decrease in risk factor with tree height (Fig 4). In all models the sub-canopy trees were close to their predicted gravitational limit. This is consistent with King et al., (2009) who used height-diameter allometries to show that understory trees are close to their gravitational limits as estimated from model i. Competition for light is strongest in dense forests (MacFarlane & Kane, 2017) and understory trees invest in height growth at the cost of stability. This strategy clearly works because understory trees are sheltered from the wind (D. A. King et al., 2009), but changes in the local wind regime, perhaps due to the death or logging of a nearby large tree, can allow wind to penetrate the understory and destroy many of these unstable pioneers (Silvério et al., 2018). Niklas, (1995) showed that as trees reach the canopy their height-diameter allometry shifts from elastic self-similarity ($H \sim D^{2/3}$) to the more conservative constant stress model ($H \sim D^{1/2}$). This accounts for the observation that many record sized trees, selected based on diameter and height and often found in semi-open conditions, are well below their gravitational limits (McMahon, 1975).

Crown size drives gravitational stability

A novel aspect of this work was the inclusion of detailed 3D tree architecture based on TLS data. This allowed us to measure the woody volume in different parts of the tree and so estimate the weight of the stem and the crown separately. Gravitational maximum height

model ii, which incorporated this information, estimated much higher risk factors than the 'classical' model of a cylindrical beam. This makes intuitive sense and demonstrates the importance of tree architecture in mechanical stability. We also found a similar relationship based on the local height-diameter allometry and a simple relationship between crown size and tree height. Gravitational stability model iii incorporated the stem and mass taper for each tree. This model estimated even higher risk factors than ii with one tree actually exceeding its theoretical maximum height. However, this model proved highly sensitive to the quality of the QSMs was considered less generalizable.

Compared to changes in crown size, material properties had surprisingly little effect on gravitational stability (Fig 4). This is because it is the ratio of wood elasticity and density that appears in equations 4 and 6, and this ratio is relatively constant (K. J. Niklas & Spatz, 2010). However, species-specific material properties decreased the risk factor of tall trees and increased the risk for short trees, suggesting that the trees that make it to the canopy are those with the highest elasticity for a given density (Givnish *et al.* 2014). Previous authors also found that material properties variation made little difference to overall stability (Osunkoya et al., 2007; Sellier & Fourcaud, 2009).

In additional to the separate effects of tree architecture and material properties, our analysis also emphasises their interdependence. FE simulations of asymmetric trees produced unrealistic results, such as predicting that the tree would collapse under gravity although it was observed and scanned in a stable position. We could not test the reasons for this in the FE analysis, but other studies have shown that asymmetric trees will compensate for this asymmetry with reaction wood (Scurfield, 1973), which was not included in the model. It is therefore likely that the failure of these simulations was due to the inclusion of architectural asymmetry while ignoring the asymmetric material properties.

Wind risk increases with tree height

Danum Valley is not a particularly windy site and the maximum recorded wind speed in almost 2000 hours of data was a 10 s average wind speed of 7.17 ms^{-1}. This is perhaps one of the reasons why trees grow so tall here. Our field data showed that the gradient of the wind-strain relationship increased with tree height (Fig 5) i.e. that tall trees are at higher risk of wind damage. This is the opposite trend to the gravitational risk, and the combination of gravity and wind results in a U-shaped profile of mechanical risk through a trees life (Fig 6). This result is consistent with post damage surveys, which found that tall trees were more likely to be damaged by wind (Rifai et al., 2016; Silvério et al., 2018). Although this seems intuitive, since

taller trees are exposed to higher wind speeds, trees are also known to adapt to their local wind environment (Bonnesoeur et al., 2016; Coomes et al., 2018). However, our field data demonstrates that the larger diameters of tall trees are not sufficient to compensate for the increased wind loading. This is likely because the support costs scale with surface area and so increase disproportionately with tree height (Givnish *et al.* 2014). We also emphasise that material property variations, such as the increased stiffness for a given density, do not compensate for the increased wind loading. This suggests that wind plays a role in limiting tree height, which has far ranging implications including forest carbon stocks and biodiversity. One hypothesis generated by this work is that tree height in the Amazon is generally so much lower than in Borneo (Feldpausch et al., 2011) may be the result of the higher wind speeds in this region. It would be interesting to test whether this relationship holds over multiple sites and perform a global analysis on the limitation of canopy height due to wind damage risk.

Is the 100 m *Shorea faguetiana* close to its mechanical limits?

The world's tallest angiosperm provides an important focal point for questions about mechanical stability. Our analysis shows that the strongest mechanical limitation on this tree's height is likely due to wind loading. Extrapolating the best fit line from our field data to the height of this tree we estimate that it would break at 24.1 ms^{-1}. However, this tree, like the previous record holders from Malaysia, is situated in a steep valley and will therefore be sheltered from the wind to a some degree (Jucker et al., 2017). This means that a 24.1 ms^{-1} at our field site may be equivalent to a lower wind speed at the location of this tree.

As well as being exceptionally tall, this tree is but it is also extremely slender having a dbh of just 1.96 m. This means it is much closer to its gravitational limits than a 100 m tall tree with the diameter predicted from the regional allometry (Feldpausch et al., 2011). It has an estimated crown mass of 9,863 kg and a stem mass of 80,124 kg. The stem is extremely straight and the centre of mass is situated at 28 m height with only 60 cm horizontal displacement. We simulated the combined effect of wind and gravity for this tree and found that gravity is clearly a second order effect, although its magnitude increases with crown displacement.

Limitations

Equipment limitations led to the loss of data for 12 of 19 trees. Nine of these trees retained some usable data and appear in Fig 5, but the reduced data availability led to lower confidence in the derived wind-strain gradients and hampered uncertainty analysis. This meant that, while

the broad trend was clear, the field data was error prone. This had knock on effects for model validation, since we had fewer trees than anticipated and increased uncertainty (see S2). Neither the analytical nor the FE model predicted the wind-strain gradients. This was surprising, since the field data demonstrated that a static treatment of wind loading should be sufficient and a similar approach predicted tree response well in a temperate forest (Jackson et al., 2019). This poor model performance could be due to the presence of leaves, which were not considered in (Toby Jackson et al., 2019), and the complex canopy structure and resulting sheltering effects, which were not taken into account in this study.

Another limitation of this study was the lack of an above canopy tower from which to measure wind speed. Instead, we attached anemometers to tall trees and measured the wind speed above the dense canopy but below the canopy of the emergent trees (see S3). This means that the wind measurements are site-specific and if this experiment was repeated in another site they would not be directly comparable.

Conclusion

We studied the mechanical stability of tall trees in the lowland forests of Danum Valley, Malaysia. To the best of our knowledge, this is the first time strain gauges have been used to monitor the motion of tall tropical trees in the wind. We found that wind risk increases with tree height, meaning that neither increased diameter nor material properties counterbalanced this risk. This suggests that wind risk may play a role in limiting tree height, and the lower heights of forests Amazonia may be due to the higher wind speeds in this region.

We used TLS data to map the 3D architecture of these trees and so compared three models of gravitational maximum height. We found that including the crown dimensions significantly reduced the maximum predicted height while material properties had surprisingly little effect. Gravitational risk factors decreased with tree height while wind risk increased. This results in a U-shaped mechanical risk curve with the limiting factor in mechanical stability changing through ontogeny. Therefore, the tallest angiosperm in the world, a 100 m *Shorea faguetiana*, may have only reached its impressive stature due to sheltering either from neighbouring trees or the steep topography in which it was found.

Supplementary information

S1. Testing QSM dimensions against field data

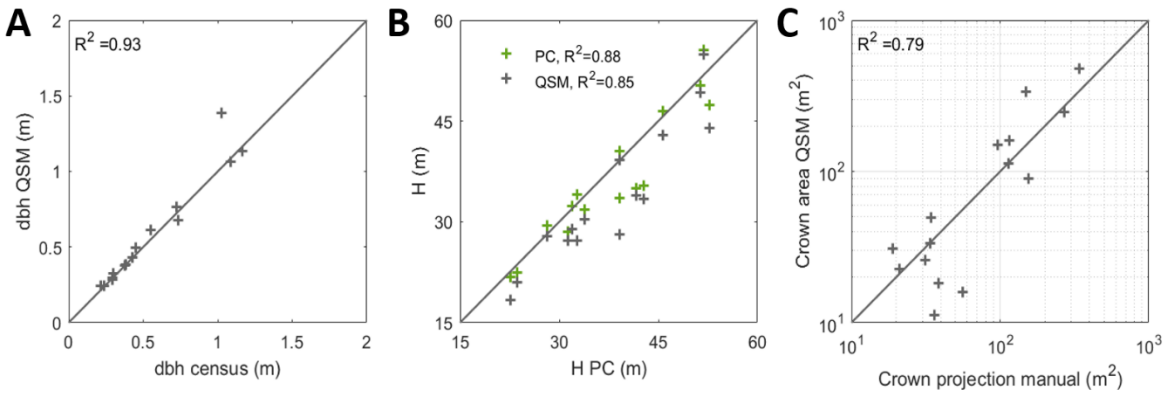


Figure S1 – Field data against QSM measurements for (A) dbh (B) height and (C) crown dimensions. Note that the two crown dimensions variables are not identical and this plot is presented on a log-log scale.

The dbh measurements from the QSMs matched those measured in the field closely. However, the QSMs systematically underestimated tree height. We noted that tree height measurements from point clouds matched the field data more accurately and with normally distributed errors. This shows that the underestimation was due to the cylinder fitting process, which is limited by the resolution of the point cloud and so the laser beam divergence. The overall size of the crown estimated from the QSMs followed a similar pattern to those estimated from the ground. There were large errors, which is unsurprising given that these measurements were not defined in the same way, but these errors were normally distributed.

S2. Wind-strain model validation

We tested two models of the response of trees to wind loading, a simple analytical model and a finite element model. Both were based on the QSMs, and so included detailed structural information for each tree, but neither model predicted the field data accurately. However, there were a number of choices in both the field data processing and in the model constructions which complicated validation. Fig S2 compares the gradients derived from field data using the sonic anemometer and that the difference in aggregating window length only resulted in a change in magnitude, not rank order. These permutations are discussed below.

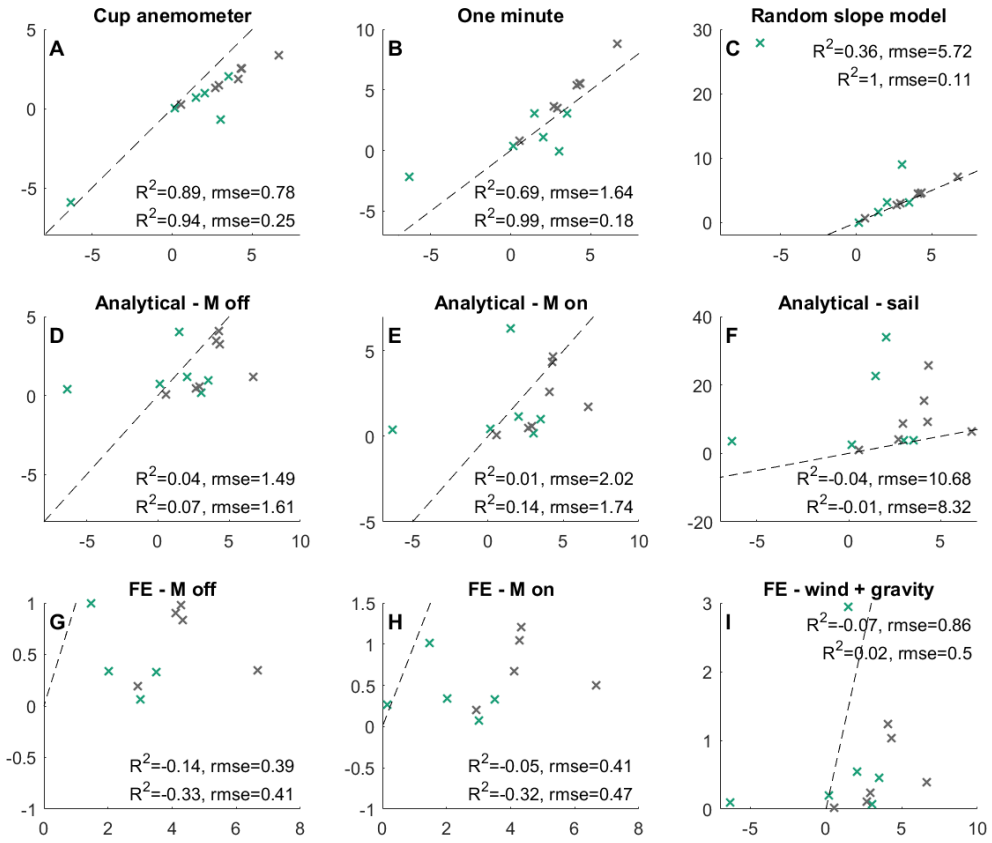


Figure S2 – All of the graphs show wind-strain gradients with units $\mu m^{-2} s^2$. The first R^2 and rmse values refer to all of the trees in the graph while the second refers to only those trees logged with the CR1000s, there is some difference in data availability. All of the graphs have identical x-axes, the estimated wind-strain gradient derived from field data by for each tree separately using the sonic anemometer wind speed data and a ten-minute aggregation period. The y-axes are other estimates of the wind speed gradient. The top row are estimates from field data using (A) wind speed data from a cup anemometer 63 m away from the sonic anemometer (B) a one-minute aggregation period and (C) by pooling the data and fitting a random slope model. The second row are analytical models of the wind-strain gradient (D) with mean material properties (E) with species-specific material properties and (F) with total width of the tree as the sail area, instead of just the branches. The third row are finite element model estimates of the wind-strain gradient with (G) mean material properties (H) species-specific material properties and (I) the effects of gravity included.

The analytical model predicted realistic magnitudes of the wind-strain gradient, but failed to predict the rank order. The FE model predicted the rank order very weakly when the field data was split and each tree treated separately, but otherwise not. The FE model also significantly underestimated the magnitude of the wind-strain gradient. We argue that the magnitudes are less important than the rank order, since they depend on the position and resolution of the wind measurement as well as the aggregation period.

S3. Attaching anemometers to trees

Our method of attaching anemometers to emergent trees is unusual and best practice is to measure measured wind speeds above the canopy. However, this requires a tower which greatly limits the choice of study site. A professional tree climber attached the anemometers to steel poles, which were boomed out from the tree by 1.5 m and supported above and below. The anemometers were attached pointing in different directions so that any directional bias would be evened out. Four anemometers were mounted in this way, at two different heights on two trees which were 63 m apart. This setup was successful insofar as the wind-strain relationships did not vary significantly depending on which anemometer was used. However, this unusual method of measuring wind speed means that our results would not be comparable with other sites.

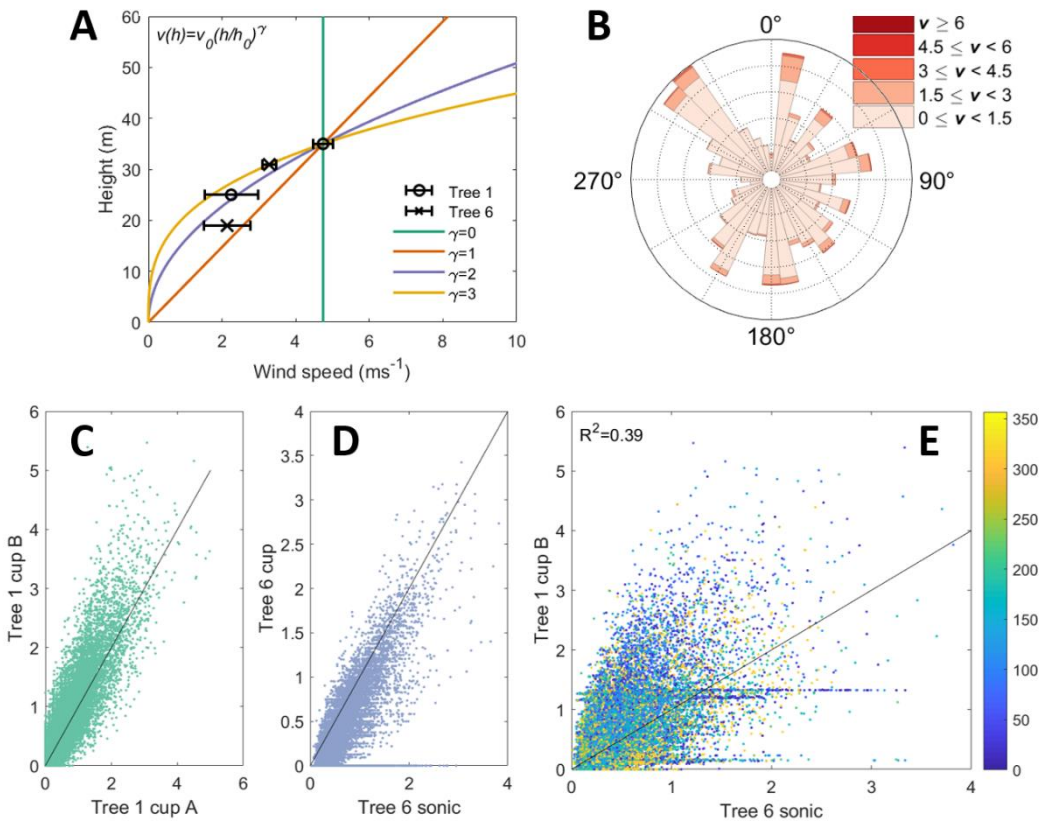


Figure S3 – A: vertical profile of wind speed measurements with possible power law fits overlaid. B: wind rose for 10-minute maximum wind speeds from the sonic anemometer. C and D: 10-minute maximum wind speeds measured at two heights in the tree 1 and 6, respectively. E: Correlation between 10-minute maximum wind speeds measured at tree 6 and that at tree 1, 63 m away, coloured by wind direction.

Discussion

This thesis emphasised the importance of wind as a key environmental factor in forest ecology. Wind influences canopy height and sculpts tree size and shape with implications for forest structure, function and carbon storage. However, wind is often overlooked in ecology, presumably due to the difficulty of measuring and modelling its effects and the difficulty of obtaining reliable tree architecture data. Specialist knowledge and techniques that help us understand the interaction between wind and trees have been developed primarily for research on conifer plantations. This thesis applied some of these techniques to natural forests in order to demonstrate the central role of wind. In addition, techniques such as terrestrial and airborne laser scanning are providing new lenses through which the effects of wind can be studied with the necessary detail. This thesis exploits these technological advances to overcome limitations of previous work, in particular the lack of detailed information on tree architecture for large trees.

This discussion section does not repeat the results of each paper. Rather I bring together themes which are common to all four papers and place them in a wider context. I begin with a comparison of the two field sites Wytham Woods and Danum Valley. I then discuss the link between tree architecture and mechanical stability, which is the central theme of this thesis. Next I discuss the limitations of the current study and conclude by outlining potential future research on this topic.

Comparing Wytham Woods and Danum Valley



Figure 26 – Left: Wytham Woods in Autumn from above, showing the canopy walkway (photo from Yadvinder Malhi). Right: Danum Valley from above (photo from Alexander Shenkin).

Wytham Woods is a semi-natural deciduous woodland in Oxfordshire, UK, dominated by three species and with an almost uniform canopy height of 21-23 m. Danum Valley is a tall, lowland tropical forest with, a dense understory and emergent trees reaching beyond 60 m in height. Wytham Woods is in an early successional stage, with most of the canopy trees dating back to the 1950's, while Danum Valley is an old-growth forest. Many of the trees in Danum Valley have not been identified to species or even genus level.

In practical terms, the environmental conditions hindered field work in Danum Valley. TLS data collected in rainy conditions are unreliable and the changes in temperature and humidity led to large variations in the resistance of the strain gauge balancing circuits. Danum Valley is much less windy, which is perhaps the reason trees grow so much taller there, but also yielded a lower range of wind speeds from which to calculate the wind-strain gradients in paper 4. Also, the height of the canopy in Danum Valley led to a lower resolution in the TLS data. This meant that automatic tree extraction algorithms had trouble with the Danum Valley data and trees had to be manually extracted from the point cloud. Danum Valley also has more complex terrain and canopy structure, so the effect of sheltering is likely to be more heterogeneous, which I believe is the main reason the models couldn't predict wind risk in this site.

In ecological terms, Danum Valley was considered more likely to be affected by mechanical limitations than Wytham Woods. The favourable environmental conditions for tree growth and extreme competition for light may be expected to drive trees to less stable architectures (MacFarlane & Kane, 2017). Also, Wytham Woods is in a comparatively early successional stage, so the canopy may not yet have reached its optimum height. In paper 4 I found that understory trees approached their gravitational limits for height, especially when the size of their crowns and material properties were taken into account. I also found that wind damage risk increased with tree height, meaning that tall trees were unable to compensate for their increased sail area with diameter growth. However, the limitations mentioned above hindered a direct comparison between the two sites.

Wytham Woods is a deciduous forest and the interaction between wind and trees fundamentally change with the presence or absence of leaves. Paper 3 showed that leaves alter the trees susceptibility to wind damage by adding a significant top-weight to the tree, which lowers the fundamental sway frequency. Leaves also increase aerodynamic drag which increases the energy transferred to the tree from the wind, but also helps to dissipate that energy through more efficient damping (Paper 2). The autumn leaf senescence in Wytham Woods coincides with the onset of winter storms and total wind damage risk is a combination

of tree susceptibility to wind damage and the likelihood of strong winds. Additionally, the penetration of wind into the forest is increased in winter due to the lack of leaves, so the vertical wind profile is altered. Overall, this builds a complex picture of the seasonal changes in wind risk in a deciduous forest, and emphasises the value of further study using the data collected in Wytham Woods.

Tree architecture and mechanical stability

One of the key premises of this thesis was that tree architecture is important to understand the response of trees to wind loading, and that this has been understudied due to the difficulty of obtaining detailed 3D maps of trees. TLS overcomes this difficulty and provides QSMs for hundreds of trees from a range of sites. Sellier & Fourcaud (2009) found that variation in tree architecture outweighs material properties in determining tree-wind dynamics. They used a sensitivity analysis, increasing each variable such as branch length and wood density by 20 % to reach this result. This thesis quantifies the range of tree architectures and uses realistic tree architecture as input to finite element simulations.

Paper 3 contains the widest variety of tree architectures based on > 1000 QSMs. The principal component analysis in this paper shows that many of the architectural measures I extracted covary. The first axis in this PCA corresponds to tree size, with *dbh* and total tree volume closely aligned, while the second axis corresponds to crown dimensions. Different types of trees, for instance open-grown trees and temperate forest trees, are grouped together, demonstrating that they have similar architectures.

Paper 3 shows that the fundamental frequencies of broadleaf trees are not well approximated by the cantilever beam approximation. This means that broadleaves, unlike conifers, do not move in a simple manner. Paper 3 goes on, using a modelling approach, to show that architectural information increases the predictability of the fundamental frequency of broadleaf trees. This paper emphasises that, although crown volume ratio, asymmetry and aspect ratio are the most significant architectural measures I tested, all architectural measures explain some of the residual variance in fundamental frequencies.

Paper 2 also finds that architectural information helps predict the response of trees to the wind for one ha in Wytham Woods. In this case the variable of interest is the critical wind speed. I found that sail area and crown volume ratio explained 17 % more variation in critical

wind speed than height, diameter and species alone. Again, the covariance of the architectural measures means that the specific architectural measures are not unique. Any and all architectural information is useful in explaining additional variance in the critical wind speeds.

The tall, emergent trees in paper 4 are the winners of an intense competition for light, reaching their dominant position thanks to a range of beneficial traits as well as good fortune. It is notable that very tall angiosperms all tend to have similar, relatively simple architecture. The above discussion emphasises that complex tree architecture leads to a complex response to wind loading, it is likely that these pole-like tall trees behave like conifers, or cantilever beams, in the wind. This suggests that it may be possible to use a simple model, similar to Pivato, Dupont & Brunet (2014), to model their response to wind loading and so estimate wind damage risk of emergent trees across a tropical forest landscape. These trees must have a single long, straight trunk to reach above the canopy. The finite element analysis in paper 4 demonstrates the negative implications of a leaning trunk, which horizontally displaces the centre of mass. Paper 4 also shows that it is gravitationally more stable to have a small relative crown size. The principal component analysis in paper 3 shows a close alignment between tree height and CVR, demonstrating that this is in fact the case. A simple model of the wind damage risk of tall trees would be highly valuable since these trees dominate the forest carbon stocks (Slik et al., 2013).

Limitations



Figure 27 – Forest research vehicle being crushed by a tree (photo courtesy of Barry Gardiner).

One key limitation of this study was a lack of high quality wind measurements. Studies on wind flow generally use multiple 3D sonic anemometers mounted on above canopy towers and logging at 10 Hz. My equipment consisted of three cup anemometers, which cannot effectively operate faster than 0.1 Hz, and one 2D sonic anemometer which operates at 1 Hz. The result of this limitation is a high uncertainty around vertical profile of wind in the canopy, and no information about vertical wind speeds. However, even if I had multiple 3D anemometers, neither of my plots had an above canopy tower, so the wind measurements are influenced by the local surroundings.

A related uncertainty is a lack of reliable long-term maximum wind speed data, especially for Danum Valley. Wind storms are extreme events and their intensity follows a long-tailed distribution, with the strongest storms being few and far between. It is both important and extremely difficult to estimate accurate return times for the strongest wind storms expected in a given site. This is an essential parameter in site comparisons, e.g. comparing the wind limitation of tree height in Borneo and in the Amazon requires information on the frequency and intensity of wind storms in each site. This is a fundamental limitation of all studies on extreme events and can be attempted to be overcome using a combination of wind speed measurements and simulations. This is, however, beyond the scope of the current thesis.

Another equipment-related limitation was the limited storage capacity of CR23x data loggers. These data loggers have an internal memory of 4 Mb, which fills in approximately 20 minutes with my setup. I therefore streamed data to a raspberry pi and stored it on an SD card. This arrangement worked well in Wytham Woods, where 24 Ah car batteries could be carried to the field site, but the power consumption of the Raspberry Pi proved too high for the 7 Ah motorcycle batteries used in Danum Valley. This ultimately led to data loss.

Literature values on material properties were used throughout this study to maintain generality. However, a number of species of interest in Danum Valley had no material properties information for the species or even at the genus level. Furthermore, elasticity measurements from small samples of wood are not always representative of the whole tree (Ruel et al., 2010). The scale of these variations has not been quantified for many trees.

A limitation of the finite element analysis is that it cannot accurately represent the aerodynamic drag of leaves. Models for tree response to wind loading in Wytham Woods focussed on winter, leaf-off, conditions, because these were considered more important for wind damage. However, Danum Valley is an evergreen tropical forest and the omission of leaves in this context may have contributed to the poor model performance.

Further research

The role of resonance

The role of resonance in wind damage remains unresolved. Numerous studies have monitored trees in the wind, but no published study has observed a tree breaking (J. Moore et al., 2018). However, in June 2018 field campaign in Japan monitored conifers which snapped due to very high wind speeds, results from this study are expected in 2019. Spectral techniques can be used to explore the potential role of resonance in wind damage. Schindler & Mohr (2018) showed that the oscillatory component of tree response to wind loading decreases with increasing wind speed, for four Sitka Spruce trees. I plan to replicate this analysis with the field data collected for this thesis and all available field data on tree sway, including the data from Japan, in order to confidently address the role of resonance. I also intend to collate data from a number of studies which have simultaneously monitored the motion of the branches and that of the trunk. This data can be used to investigate the energy transfer throughout the tree and whether dynamic amplification or damping occurs in the crown.

Finite volume elements

In this thesis I applied finite element analysis using cylindrical beam elements, which is computationally efficient. However, using finite volume elements instead of beams would allow a more detailed representation of the shape of the tree allowing me to test hypothesis about the strength of buttresses. Also, this would enable a more complex treatment of material properties so that I could model the additional support due to reaction wood. The accuracy to which the finite volume method could represent tree architecture would be limited by the quality of the TLS data. One possibility would be an iterative model that calculates the weak points in the tree and so assigns increased wood density and elasticity. This model would converge upon an estimate of the locations distribution of material properties throughout the tree. Currently, the only data set with both TLS data and detailed measurements on destructively harvested trees is the Harvard forest experiment (Orwig et al., 2018).

Open-grown trees

In paper 3 I found some interesting patterns emerging from the architecture and dynamics of open-grown trees. It would be useful to extend this work to additional open-grown trees and collect field data on the same, so that we can test the validity of the method. If it proves accurate, this method could be a valuable tool for tree risk assessments. In order encourage

uptake of this method I also intend to transfer the analysis from Abaqus to an open-source finite element package, Calculix.

Tree architecture

In this thesis, I used tree architectural parameters as explanatory variables to predict tree dynamics. However, it would be interesting to study tree architecture in its own right. Specifically, the TLS-QSM approach provides a unique data set on tree architecture with which to test long standing ecological theories, such as those on the fractal nature of trees. Also, it is likely that much of the residual variation not explained by simple tree height-diameter allometry is due to variable tree architectures, and exploring this further would be highly valuable research. The key challenge to this work is validation, since tree architecture is notoriously difficult and arduous to measure in the field. Preliminary work has found a relatively weak relationship between tree architecture measured in the field and derived from TLS data (Lau et al., 2018), although there are some methodological difficulties with the definition of branching order and even branch length.

Additional tropical forest sites

I would like to explore the role of wind in other tropical forests outside of Malaysia. Specifically, a comparison between tropical forests that experience a range of wind regimes would be highly useful. The key to this study would be reliable wind measurements i.e. taken from towers using an array of 3D sonic anemometers. This would allow a robust multi-site comparison and also be directly comparable to previous work. In addition, an array of anemometers within each forest plot may allow an estimation of the local sheltering effects between trees. However, I believe this may be highly costly and time consuming to perform as well as difficult to translate to other forest types.

Global analysis

Moles *et al.* (2009) and Klein, Randin & Körner (2015)showed that water availability is the best predictor of global canopy height. These studies tested numerous environmental variables as possible drivers but neither tested wind speed. This was partly due to the lack of a comprehensive global wind speed product which is reliable over forested areas. However, products such as the global wind atlas (http://globalwindatlas.net/) are becoming widely available and such an analysis would be highly valuable. Also, the new Global Ecosystem Dynamics Investigation lidar (GEDI) is expected to map canopy height more accurately and with a finer resolution than previously available products. This work would depend on the accuracy and resolution of the wind speed product and its ability to account for topography

and canopy structure. Additionally, the frequency and intensity of extreme events are notoriously difficult to predict accurately, and long-term data is not generally available.

Conclusion

This thesis combined data from strain gauges and terrestrial laser scanning to explore the role of wind damage risk in natural forests. I focussed on two field sites: Wytham Woods, Oxford, and Danum Valley, Malaysia but also collated data on the fundamental sway frequencies of trees from a range of sites. I found that the architecture of a tree influences its response to wind loading and that combining 3D tree models with finite element analysis allows me to model this interaction. These models performed well against field data in Wytham Woods but not in Danum Valley, presumably due to the more complex topography and canopy structure leading to sheltering. In Wytham Woods, the risk of wind damage had a seasonal signal, since the presence of leaves in summer increases the sail area of the trees and also changes the wind environment. In Danum Valley, tree height was positively correlated with the wind-strain gradient, meaning that tall trees are at a higher risk of wind damage and their larger diameters do not sufficiently compensate.

These results emphasise the ecological role of wind damage risk in shaping forest structure and function. Wind is a key environmental factor and wind risk is linked to tree growth rates, species turnover, height-diameter allometries and possibly even the timing of autumn leaf fall in deciduous forests. My work suggests that wind damage risk may limit tree height and forest carbon storage. One key challenge in this field is that wind storms are stochastic and extreme events, which hinders data collection. However, the recent launch of the Global Ecosystem Dynamics Investigation lidar (GEDI) represents a key opportunity to collect large-scale data on wind damage in forests globally. This is an important topic since forests, and particularly the large trees, are an essential store of carbon and the wind regimes they must endure are shifting with climate change.

Data availability and online resources

All of the data and codes developed for this thesis are available online.

- Wytham Woods strain gauge data: https://doi.org/10.5285/533d87d3-48c1-4c6e-9f2f-fda273ab45bc

- Danum Valley strain gauge data: https://doi.org/10.5285/657f420e-f956-4c33-b7d6-98c7a18aa07a

- Scripts used to process strain gauge data: https://github.com/TobyDJackson/WindAndTrees_Wytham

- Point clouds, QSMs and Matlab package to convert a QSM to an Abaqus input file: https://github.com/TobyDJackson/WindAndTrees_FEM

- Matlab package to extract architectural information from QSMs: https://github.com/TobyDJackson/TreeArchitectureQSM

- Matlab scripts to perform analysis for paper 2: https://github.com/TobyDJackson/WindAndTrees_Wytham

- Matlab scripts to perform analysis for paper 3: https://github.com/TobyDJackson/WindAndTrees_Resonance

- Point clouds, QSMs and Matlab scripts to perform analysis for paper 4: https://github.com/TobyDJackson/WindAndTrees_Danum

Data contributed by co-authors is available in the original publications, which are cited in the appropriate papers.

References

Agafonova, O., Koivuniemi, A., Chaudhari, A. & Hämäläinen, J. (2014). Limits of Wasp Modelling in Comparison With Cfd for Wind Flow Over Two-Dimensional Hills. *In Proceedings of the European Wind Energy Association Conference (EWEA '14), Barcelona, Spain, 2014.*

Åkerblom, M. (2017). Inversetampere/Treeqsm: Initial Release. DOI: 10.5281/zenodo.844626

Åkerblom, M., Raumonen, P., Mäkipää, R. & Kaasalainen, M. (2017). Automatic tree species recognition with quantitative structure models. *Remote Sensing of Environment,* 191, 1–12.

Asner, G.P. & Goldstein, G. (1997). Correlating Stem Biomechanical Properties of Hawaiian Canopy Trees with Hurricane Wind Damage1. *Biotropica*, 29, 145–150.

Asner, G.P. & Mascaro, J. (2014). Mapping tropical forest carbon: Calibrating plot estimates to a simple LiDAR metric. *Remote Sensing of Environment*, 140.

Baker, C.J. (1997). Measurements of the natural frequencies of trees. *Journal of Experimental Botany*, 48, 1125–1132.

Baldocchi, D., Falge, E., Gu, L., Olson, R., Hollinger, D., Running, S., Anthoni, P., Bernhofer, C., Davis, K., Evans, R., Fuentes, J., Goldstein, A., Katul, G., Law, B., Lee, X., Malhi, Y., Meyers, T., Munger, W., Oechel, W., Paw, K.T., Pilegaard, K., Schmid, H.P., Valentini, R., Verma, S., Vesala, T., Wilson, K. & Wofsy, S. (2001). FLUXNET: A New Tool to Study the Temporal and Spatial Variability of Ecosystem–Scale Carbon Dioxide, Water Vapor, and Energy Flux Densities. *Bulletin of the American Meteorological Society*, 82, 2415–2434.

Barnett, J.R. & Bonham, V.A. (2004). Cellulose microfibril angle in the cell wall of wood fibres. *Biological Reviews*, 79, 461–472.

Bastin, J.F., Barbier, N., Réjou-Méchain, M., Fayolle, A., Gourlet-Fleury, S., Maniatis, D., De Haulleville, T., Baya, F., Beeckman, H., Beina, D., Couteron, P., Chuyong, G., Dauby, G., Doucet, J.L., Droissart, V., Dufrêne, M., Ewango, C., Gillet, J.F., Gonmadje, C.H., Hart, T., Kavali, T., Kenfack, D., Libalah, M., Malhi, Y., Makana, J.R., Pélissier, R., Ploton, P., Serckx, A., Sonké, B., Stevart, T., Thomas, D.W., De Cannière, C. & Bogaert, J. (2015). Seeing Central African forests through their largest trees. *Scientific Reports*, 5.

Belcher, S.E., Harman, I.N. & Finnigan, J.J. (2012). The Wind in the Willows: Flows in Forest Canopies in Complex Terrain. *Annual Review of Fluid Mechanics*, 44, 479–504.

Bentley, L.P., Stegen, J.C., Savage, V.M., Smith, D.D., von Allmen, E.I., Sperry, J.S., Reich, P.B. & Enquist, B.J. (2013). An empirical assessment of tree branching networks and implications for plant allometric scaling models. *Ecology Letters,* 16, 1069–1078.

Blackburn, G. (1997). The growth and mechanical response of trees to wind loading. PhD Thesis. University of Manchester.

Van Bloem, S.J., Murphy, P.G., Lugo, A.E., Ostertag, R., Costa, M.R., Bernard, I.R., Colon, S.M. & Mora, M.C. (2005). The Influence of Hurricane Winds on Caribbean Dry Forest Structure and Nutrient Pools1. *Biotropica*, 37, 571–583.

Bonnesoeur, V., Constant, T., Moulia, B. & Fournier, M. (2016). Forest trees filter chronic wind-signals to acclimate to high winds. *New Phytologist*, 210, 850–860.

de Borst, K., Bader, T.K. & Wikete, C. (2012). Microstructure-stiffness relationships of ten European and tropical hardwood species. *Journal of Structural Biology*, 177, 532–542.

Boudreault, L.É., Bechmann, A., Tarvainen, L., Klemedtsson, L., Shendryk, I. & Dellwik, E. (2015). A LiDAR method of canopy structure retrieval for wind modeling of heterogeneous forests. *Agricultural and Forest Meteorology*, 201, 86–97.

Brudi, E. & Wassenaer, P. Van. (2001). Trees and Statics: Non-Destructive Failure Analysis. 1–17. *Tree Structure and Mechanics Conference Proceedings: How Trees Stand Up and Fall Down, International Society of Arboriculture,* Champaign, E.T. Smiley, K.D. Coder (Eds.), pp. 53-69

Bunce, A. (2017). Determinants of Tree Sway Frequency in Temperate Deciduous Forests of the Northeast United States. Master's Theses, 74.

Burt, A.P. (2017). New 3D measurements of forest structure. PhD Thesis. University College London.

Butt, N. (2009). Initial Results from Establishment of a Long-term Broadleaf Monitoring Plot at Wytham Woods, Oxford, UK. 1–86.

Calders, K., Burt, A., Origo, N., Disney, M., Nightingale, J., Raumonen, P. & Lewis, P. (2016). Large-area virtual forests from terrestrial laser scanning data. *International Geoscience and Remote Sensing Symposium* (IGARSS), pp. 1765–1767.

Calders, K., Newnham, G., Burt, A., Murphy, S., Raumonen, P., Herold, M., Culvenor, D., Avitabile, V., Disney, M., Armston, J. & Kaasalainen, M. (2015). Nondestructive estimates of above-ground biomass using terrestrial laser scanning. *Methods in Ecology and Evolution*, 6, 198–208.

Calders, K., Origo, N., Burt, A., Disney, M., Nightingale, J., Raumonen, P., Åkerblom, M., Malhi, Y. & Lewis, P. (2018). Realistic Forest Stand Reconstruction from Terrestrial LiDAR for Radiative Transfer Modelling. *Remote Sensing*, 10, 933.

Carrera, E., Giunta, G. & Petrolo, M. (2011). The Euler–Bernoulli and Timoshenko Theories. Beam Structures, pp. 9–22. *John Wiley & Sons*, *Ltd.*

Chao, K.J., Phillips, O.L., Monteagudo, A., Torres-Lezama, A. & Vásquez Martínez, R. (2009). How do trees die? Mode of death in northern Amazonia. *Journal of Vegetation Science*, 20, 260–268.

Chapotin, S.M., Razanameharizaka, J.H. & Holbrook, N.M. (2006). A biomechanical perspective on the role of large stem volume and high water content in baobab trees (*Adansonia spp.; Bombacaceae*). *American Journal of Botany*, 93, 1251–1264.

Chave, J., Coomes, D., Jansen, S., Lewis, S.L., Swenson, N.G. & Zanne, A.E. (2009). Towards a worldwide wood economics spectrum. *Ecology Letters*, 12, 351–366.

Ciftci, C., Brena, S., Kane, B. & Arwade, S. (2012). Effects of crown architecture on dynamic behavior of trees: Understanding the relationship between branches and stem. *International Society of Arboriculture Annual Conference & Trade Show*,

Ciftci, C., Brena, S.F., Kane, B. & Arwade, S.R. (2013). The effect of crown architecture on dynamic amplification factor of an open-grown sugar maple (*Acer saccharum* L.). *Trees - Structure and Function*, 27, 1175–1189.

Coomes, D.A., Šafka, D., Shepherd, J., Dalponte, M. & Holdaway, R. (2018). Airborne laser scanning of natural forests in New Zealand reveals the influences of wind on forest carbon. *Forest Ecosystems*, 5, 10.

Dale, V.H., Joyce, L.A., McNulty, S., Neilson, R.P., Ayres, M., Flannigan, M.D., Hanson, P.J., Irland, L.C., Lugo, A.E., Peterson, C.J., Simberloff, D., Swanson, F.J., Stocks, B.J. & Wotton, M. (2011). Climate Change and Forest Disturbances. *BioScience*, 51, 723–734.

Dean, T.J. & Long, J.N. (1986). Validity of Constant-stress and Elastic-instability Principles of Stem Formation in *Pinus contorta* and *Trifolium pratense*. *Ann. Bot.,* 58, 833–840.

Disney, M.I., Boni Vicari, M., Burt, A., Calders, K., Lewis, S.L., Raumonen, P. & Wilkes, P. (2018). Weighing trees with lasers: Advances, challenges and opportunities. *Interface Focus*, 8.

Dupont, S., Pivato, D. & Brunet, Y. (2015). Wind damage propagation in forests. *Agricultural and Forest Meteorology*, 214–215, 243–251.

Van Emmerik, T., Steele-Dunne, S., Hut, R., Gentine, P., Guerin, M., Oliveira, R.S., Wagner, J., Selker, J. & Van De Giesen, N. (2017). Measuring tree properties and responses using low-cost accelerometers.

Sensors (Switzerland), 17.

Espírito-Santo, F.D.B., Gloor, M., Keller, M., Malhi, Y., Saatchi, S., Nelson, B., Junior, R.C.O., Pereira, C., Lloyd, J., Frolking, S., Palace, M., Shimabukuro, Y.E., Duarte, V., Mendoza, A.M., López-González, G., Baker, T.R., Feldpausch, T.R., Brienen, R.J.W., Asner, G.P., Boyd, D.S. & Phillips, O.L. (2014). Size and frequency of natural forest disturbances and the Amazon forest carbon balance. *Nature Communications*, 5.

Everham, E.M. & Brokaw, N.V.L. (1996). Forest damage and recovery from catastrophic wind. *The Botanical Review*, 62, 113–185.

Feldpausch, T.R., Banin, L., Phillips, O.L., Baker, T.R., Lewis, S.L., Quesada, C.A., Affum-Baffoe, K., Arets, E.J.M.M., Berry, N.J., Bird, M., Brondizio, E.S., De Camargo, P., Chave, J., Djagbletey, G., Domingues, T.F., Drescher, M., Fearnside, P.M., França, M.B., Fyllas, N.M., Lopez-Gonzalez, G., Hladik, A., Higuchi, N., Hunter, M.O., Iida, Y., Salim, K.A., Kassim, A.R., Keller, M., Kemp, J., King, D.A., Lovett, J.C., Marimon, B.S., Marimon-Junior, B.H., Lenza, E., Marshall, A.R., Metcalfe, D.J., Mitchard, E.T.A., Moran, E.F., Nelson, B.W., Nilus, R., Nogueira, E.M., Palace, M., Patiño, S., Peh, K.S.H., Raventos, M.T., Reitsma, J.M., Saiz, G., Schrodt, F., Sonké, B., Taedoumg, H.E., Tan, S., White, L., Wöll, H. & Lloyd, J. (2011). Height-diameter allometry of tropical forest trees. *Biogeosciences*, 8, 1081–1106.

Finnigan, J. (2000). Turbulence in Plant Canopies. *Annual Review of Fluid Mechanics*, 32, 519–571.

Finnigan, J.J. & Brunet, Y. (1995). Turbulent airflow in forests on flat and hilly terrain. *Wind and Trees (eds P.M. Coutts & J. Grace)*, pp. 3–40. Cambridge University Press

Gale, N. & Barfod, A.S. (1999). Canopy tree mode of death in a western Ecuadorian rain forest. *Journal of Tropical Ecology,* 15, 415–436.

Gale, N. & Hall, P. (2001). Factors determining the modes of tree death in three Bornean rain forests. *Journal of Vegetation Science*, 12, 337–346.

Gardiner, B.A. (1992). Mathematical modelling of the static and dynamic characteristics of plantation trees. *Mathematical modelling of Forest Ecosystems*, 40–61.

Gardiner, B.A. (1995). The interactions of wind and tree movement in forest canopies. *Wind and Trees (eds P.M. Coutts & J. Grace*), pp. 41–59. Cambridge University Press.

Gardiner, B., Byrne, K., Hale, S., Kamimura, K., Mitchell, S.J., Peltola, H. & Ruel, J.C. (2008). A review of mechanistic modelling of wind damage risk to forests. *Forestry*, 81, 447–463.

Gardiner, B., Peltola, H. & Kellomäki, S. (2000). Comparison of two models for predicting the critical wind speeds required to damage coniferous trees. *Ecological Modelling*, 129, 1–23.

Givnish, T.J., Wong, S.C., Stuart-Williams, H., Holloway-Phillips, M. & Farquhar, G.D. (2014). Determinants of maximum tree height in Eucalyptus species along a rainfall gradient in Victoria, Australia. *Ecology,* 95, 2991–3007.

Gonzalez de Tanago Menaca, J., Lau, A., Bartholomeusm, H., Herold, M., Avitabile, V., Raumonen, P., Martius, C., Goodman, R., Disney, M., Manuri, S., Burt, A. & Calders, K. (2017). Estimation of above-ground biomass of large tropical trees with Terrestrial LiDAR. *Methods in Ecology and Evolutio*n.

Greenhill. (1881). Determination of the greatest height consistent with stability that a vertical pole or mast can be made, and of the greatest height to which a tree of given proportions can grow. *Proceedings of the Cambridge philosophical society,* pp. 65–73.

Guillemette, F., Gauthier, M.M. & Ouimet, R. (2017). Partitioning risks of tree mortality by modes of death in managed and unmanaged northern hardwoods and mixedwoods. *Forestry Chronicle*, 93, 246–258.

Hale, S.A., Gardiner, B., Peace, A., Nicoll, B., Taylor, P. & Pizzirani, S. (2015). Comparison and validation of three versions of a forest wind risk model. *Environmental Modelling and Software*, 68, 27–41.

Hale, S.E., Gardiner, B.A., Wellpott, A., Nicoll, B.C. & Achim, A. (2012). Wind loading of trees: Influence of

tree size and competition. *European Journal of Forest Research*, 131, 203–217.

Hemp, A., Zimmermann, R., Remmele, S., Pommer, U., Berauer, B., Hemp, C. & Fischer, M. (2017). Africa's highest mountain harbours Africa's tallest trees. *Biodiversity and Conservation,* 26, 103–113.

Hepworth, D.G., Vincent, J.F. V, Stringer, G. & Jeronimidis, G. (2002). Variations in the morphology of wood structure can explain why hardwood species of similar density have very different resistances to impact and compressive loading. *Philosophical transactions. A,* 360, 255–72.

Holzwarth, F., Kahl, A., Bauhus, J. & Wirth, C. (2013). Many ways to die - partitioning tree mortality dynamics in a near-natural mixed deciduous forest (P. Zuidema, Ed.). *Journal of Ecology,* 101, 220–230.

Ibanez, T., Keppel, G., Menkes, C., Gillespie, T.W., Lengaigne, M., Mangeas, M., Rivas, G. & Birnbaum, P. (2018). Globally consistent impact of tropical cyclones on the structure of tropical and subtropical forests. *Journal of Ecology*.

Iida, Y., Kohyama, T.S., Kubo, T., Kassim, A.R., Poorter, L., Sterck, F. & Potts, M.D. (2011). Tree architecture and life-history strategies across 200 co-occurring tropical tree species. *Functional Ecology*, 25, 1260–1268.

Ishii, H.R., Azuma, W., Kuroda, K. & Sillett, S.C. (2014). Pushing the limits to tree height: could foliar water storage compensate for hydraulic constraints in Sequoia sempervirens? *Functional ecology*, *28*(5), 1087-1093

Jackson, T. (2017). Convert QSM to Abaqus Input. http://doi.org/10.5281/zenodo.894543

Jackson, T. (2018). Strain measurements on 21 trees in Wytham Woods, UK. https://doi.org/10.5285/533d87d3-48c1-4c6e-9f2f-fda273ab45bc

Jackson, T., Shenkin, A., Wellpott, A., Calders, K., Origo, N., Disney, M., Burt, A., Raumonen, P., Gardiner, B.A., Herold, M., Fourcaud, T. & Malhi, Y. (2019). Finite element models of trees in the wind based on terrestrial laser scanning data. *Agricultural and Forest Meteorology*.

James, K.R., Dahle, G.A., Grabosky, J., Kane, B. & Detter, A. (2014). Tree biomechanics literature review: Dynamics. *Arboriculture and Urban Forestry*, 40, 1–15.

James, K.R., Haritos, N. & Ades, P.K. (2006). Mechanical stability of trees under dynamics loads. *American Journal of Botany*. *93*(10), 1522-1530

Jaouen, G., Almeras, T., Coutand, C. & Fournier, M. (2007). How to determine sapling buckling risk with only a few measurements. *American Journal of Botany*, 94, 1583–1593.

Jönsson, M.T., Fraver, S., Jonsson, B.G., Dynesius, M., Rydgård, M. & Esseen, P.A. (2007). Eighteen years of tree mortality and structural change in an experimentally fragmented Norway spruce forest. *Forest Ecology and Management*, 242, 306–313.

Jucker, T., Asner, G.P., Dalponte, M., Brodrick, P., Philipson, C.D., Vaughn, N., Brelsford, C., Burslem, D.F.R.P., Deere, N.J., Ewers, R.M., Kvasnica, J., Lewis, S.L., Malhi, Y., Milne, S., Nilus, R., Pfeifer, M., Phillips, O., Qie, L., Renneboog, N., Reynolds, G., Riutta, T., Struebig, M.J., Svátek, M., Teh, Y.A., Turner, E.C. & Coomes, D.A. (2017). A regional model for estimating the aboveground carbon density of Borneo's tropical forests from airborne laser scanning. *arXiv preprint arXiv:1705.09242*

Kane, B. (2014). Determining parameters related to the likelihood of failure of red oak (Quercus rubra L.) from winching tests. *Trees - Structure and Function,* 28, 1667–1677.

Kane, B. & James, K.R. (2011). Dynamic properties of open-grown deciduous trees. *Canadian Journal of Forest Research*, 41, 321–330.

Kane, B., Modarres-Sadeghi, Y., James, K.R. & Reiland, M. (2014). Effects of crown structure on the sway characteristics of large decurrent trees. *Trees - Structure and Function*, 28, 151–159.

Kerzenmacher, T. & Gardiner, B. (1998). A mathematical model to describe the dynamic response of a spruce tree to the wind. *Trees - Structure and Function*, 12, 385–394.

Kheraj, S. (2007). Restoring Nature: Ecology, Memory, and the Storm History of Vancouver's Stanley Park. *Canadian Historical Review*, 88, 577–612.

King, D.A., Davies, S.J., Tan, S. & Nur Supardi, M.N. (2009). Trees approach gravitational limits to height in tall lowland forests of Malaysia. *Functional Ecology*, 23, 284–291.

King, D. & Loucks, O.L. (1978). The theory of tree bole and branch form. *Radiation and Environmental Biophysics*, 15, 141–165.

Klein, T., Randin, C. & Körner, C. (2015). Water availability predicts forest canopy height at the global scale. *Ecology Letters*, 18, 1311–1320.

Koch, G.W., Stillet, S.C., Jennings, G.M. & Davis, S.D. (2004). The limits to tree height. *Nature,* 428, 851–854.

Krauss, T., Shure, L. & Little, J. (1994). Signal processing toolbox for use with MATLAB®: user's guide.

de Langre, E. (2008). Effects of Wind on Plants. *Annual Review of Fluid Mechanics*, 40, 141–168.

Larjavaara, M. (2014). The world's tallest trees grow in thermally similar climates. *New Phytologist*, 202, 344–349.

Lau, A., Patrick Bentley, L., Martius, C., Bartholomeusm, H., Shenkin, A., Raumonen, P., Malhi, Y., Jackson, T. & Herold, M. (2018). Quantifying branch architecture of tropical trees using terrestrial LiDAR and 3D modelling. *Trees.* 1-13

Lavers, G.M. (1983). The strength properties of timbers. *Forest Products Research Laboratory Bulletin* 50.

Ligot, G., Gourlet-Fleury, S., Ouédraogo, D.-Y., Morin, X., Bauwens, S., Baya, F., Brostaux, Y., Doucet, J.-L. & Fayolle, A. (2018). The limited contribution of large trees to annual biomass production in an old-growth tropical forest. *Ecological Applications*, 28, 1273–1281.

Loehle, C. (2016). Biomechanical constraints on tree architecture. *Trees* 30, no. 6 (2016): 2061-2070.

Lopez, D., Michelin, S. & De Langre, E. (2011). Flow-induced pruning of branched systems and brittle reconfiguration. *Journal of Theoretical Biology*, 284, 117–124.

Lutz, J.A., Furniss, T.J., Johnson, D.J., Davies, S.J., Allen, D., Alonso, A., Anderson-Teixeira, K.J., Andrade, A., Baltzer, J., Becker, K.M.L., Blomdahl, E.M., Bourg, N.A., Bunyavejchewin, S., Burslem, D.F.R.P., Cansler, C.A., Cao, K., Cao, M., Cárdenas, D., Chang, L.W., Chao, K.J., Chao, W.C., Chiang, J.M., Chu, C., Chuyong, G.B., Clay, K., Condit, R., Cordell, S., Dattaraja, H.S., Duque, A., Ewango, C.E.N., Fischer, G.A., Fletcher, C., Freund, J.A., Giardina, C., Germain, S.J., Gilbert, G.S., Hao, Z., Hart, T., Hau, B.C.H., He, F., Hector, A., Howe, R.W., Hsieh, C.F., Hu, Y.H., Hubbell, S.P., Inman-Narahari, F.M., Itoh, A., Janík, D., Kassim, A.R., Kenfack, D., Korte, L., Král, K., Larson, A.J., Li, Y. De, Lin, Y., Liu, S., Lum, S., Ma, K., Makana, J.R., Malhi, Y., McMahon, S.M., McShea, W.J., Memiaghe, H.R., Mi, X., Morecroft, M., Musili, P.M., Myers, J.A., Novotny, V., de Oliveira, A., Ong, P., Orwig, D.A., Ostertag, R., Parker, G.G., Patankar, R., Phillips, R.P., Reynolds, G., Sack, L., Song, G.Z.M., Su, S.H., Sukumar, R., Sun, I.F., Suresh, H.S., Swanson, M.E., Tan, S., Thomas, D.W., Thompson, J., Uriarte, M., Valencia, R., Vicentini, A., Vrška, T., Wang, X., Weiblen, G.D., Wolf, A., Wu, S.H., Xu, H., Yamakura, T., Yap, S. & Zimmerman, J.K. (2018). Global importance of large-diameter trees. *Global Ecology and Biogeograph*y, 27.

MacFarlane, D.W. & Kane, B. (2017). Neighbour effects on tree architecture: functional trade-offs balancing crown competitiveness with wind resistance. *Functional Ecology*, 31, 1624–1636.

Mackerle, J. (2005). Finite element analyses in wood research: a bibliography. *Wood Science and Technology*, 39, 579–600.

Magnabosco Marra, D., Trumbore, S.E., Higuchi, N., Ribeiro, G.H.P.M., Negrón-Juárez, R.I., Holzwarth, F., Rifai, S.W., dos Santos, J., Lima, A.J.N., Kinupp, V.F., Chambers, J.Q. & Wirth, C. (2018). Windthrows control biomass patterns and functional composition of Amazon forests. *Global Change Biology*. *24*(12), 5867-5881

Malhi, Y., Baldocchi, D.D. & Jarvis, P.G. (1999). The carbon balance of tropical, temperate and boreal forests. *Environmen*t, 22, 715–740.

Malhi, Y., Jackson, T., Patrick Bentley, L., Lau, A., Shenkin, A., Herold, M., Calders, K., Bartholomeus, H. & Disney, M.I. (2018). New perspectives on the ecology of tree structure and tree communities through terrestrial laser scanning. *Interface Focus,* 8, 20170052.

Marks, C.O., Muller-Landau, H.C. & Tilman, D. (2017). Tree diversity in relation to maximum tree height: evidence for the harshness hypothesis of species diversity gradients. *Ecology Letters*, 20, 398–399.

Martini, A.M.Z., Lima, R.A.F., Franco, G.A.D.C. & Rodrigues, R.R. (2008). The need for full inventories of tree modes of disturbance to improve forest dynamics comprehension: An example from a semideciduous forest in Brazil. *Forest Ecology and Management,* 255, 1479–1488.

Mathworks, M. (2017). MATLAB and Statistics Toolbox Release 2017b, The MathWorks, Inc., Natick, Massachusetts, United States.

Mayer, H. (1987). Wind-induced tree sways. *Trees*, 1, 195–206.

Mayhead, G.J. (1973). Some drag coefficients for british forest trees derived from wind tunnel studies. *Agricultural Meteorology*, 12, 123–130.

McDowell, N., Barnard, H., Bond, B., Hinckley, T., Hubbard, R., Ishii, H., Köstner, B., Magnani, F., Marshall, J., Meinzer, F., Phillips, N., Ryan, M. & Whitehead, D. (2002). The relationship between tree height and leaf area: sapwood area ratio. *Oecologia*, 132, 12–20.

McMahon, T. (1975). The mechanical design of trees. *Scientific American*, 233, 93–132.

van der Meer, P.J. & Bongers, F. (1996). Patterns of Tree-Fall and Branch-Fall in a Tropical Rain Forest in French Guiana. *The Journal of Ecology*, 84, 19.

Moles, A.T., Warton, D.I., Warman, L., Swenson, N.G., Laffan, S.W., Zanne, A.E., Pitman, A., Hemmings, F.A. & Leishman, M.R. (2009). Global patterns in plant height. *Journal of Ecology*, 97, 923–932.

Moore, J.R., Gardiner, B.A., Blackburn, G.R.A., Brickman, A. & Maguire, D.A. (2005). An inexpensive instrument to measure the dynamic response of standing trees to wind loading. *Agricultural and Forest Meteorology*, 132, 78–83.

Moore, J., Gardiner, B. & Sellier, D. (2018). Tree Mechanics and Wind Loading. Plant Biomechanics, pp. 79–106. (Ed. Anja Geitmann and Joseph Gril) *Springer International Publishing*, Cham, Switzerland

Moore, J.R. & Maguire, D.A. (2004). Natural sway frequencies and damping ratios of trees: concepts, review and synthesis of previous studies. *Trees - Structure and Function*, 18, 195–203.

Moore, J.R. & Maguire, D.A. (2008). Simulating the dynamic behavior of Douglas-fir trees under applied loads by the finite element method. *Tree Physiology*, 28, 75–83.

Mortensen, N. G., Landberg, L., Rathmann, O., Frank, H. P., Troen, I., & Petersen, E. L. (2001). Wind atlas analysis and application program (WAsP). In *Wind Energy Department: Scientific and technical progress 1999-2000*.

Nicoll, B.C., Gardiner, B.A., Rayner, B. & Peace, A.J. (2006). Anchorage of coniferous trees in relation to species, soil type, and rooting depth. *Canadian Journal of Forest Research*, 36, 1871–1883.

Niklas, K.J. (2007). Maximum plant height and the biophysical factors that limit it. *Tree Physiology*, 27, 433–440.

Niklas, K.J. (1995). Size-dependent allometry of tree height, diameter and trunk-taper. *Annals of Botany*, 75, 217–227.

Niklas, K.J. & Spatz, H.-C. (2004). Growth and hydraulic (not mechanical) constraints govern the scaling

of tree height and mass. *Proceedings of the National Academy of Sciences of the United States of America*, 101, 15661–15663.

Niklas, K.K.J. & Spatz, H.H.-C. (2012). Plant physics. University of Chicago Press, Chicago.

Niklas, K.J. & Spatz, H.C. (2010). Worldwide correlations of mechanical properties and green wood density. *American Journal of Botany,* 97, 1587–1594.

Nishimura, T.B. (2005). Tree characteristics related to stem breakage of *Picea glehnii* and *Abies sachalinensis*. *Forest Ecology and Management*, 215, 295–306.

Orwig, D.A., Boucher, P., Paynter, I., Saenz, E., Li, Z. & Schaaf, C. (2018). The potential to characterize ecological data with terrestrial laser scanning in Harvard Forest, MA. *Interface Focus*, 8.

Osunkoya, O.O., Omar-Ali, K., Amit, N., Dayan, J., Daud, D.S. & Sheng, T.K. (2007). Comparative height-crown allometry and mechanical design in 22 tree species of Kuala Belalong rainforest, Brunei, Borneo. *American Journal of Botany*, 94, 1951–1962.

Pan, Y., Birdsey, R.A., Fang, J., Houghton, R., Kauppi, P.E., Kurz, W.A., Phillips, O.L., Shvidenko, A., Lewis, S.L., Canadell, J.G., Ciais, P., Jackson, R.B., Pacala, S.W., McGuire, A.D., Piao, S., Rautiainen, A., Sitch, S. & Hayes, D. (2011). A large and persistent carbon sink in the world's forests. *Science*, 333, 988–993.

Patton, E.G., Horst, T.W., Sullivan, P.P., Lenschow, D.H., Oncley, S.P., Brown, W.O.J., Burns, S.P., Guenther, A.B., Held, A., Karl, T., Mayor, S.D., Rizzo, L. V., Spuler, S.M., Sun, J., Turnipseed, A.A., Allwine, E.J., Edburg, S.L., Lamb, B.K., Avissar, R., Calhoun, R.J., Kleissl, J., Massman, W.J., Paw U, K.T. & Weil, J.C. (2011). The Canopy Horizontal Array Turbulence Study. *Bulletin of the American Meteorological Society*, 92, 593–611.

Peltola, H., Gardiner, B.A. & Nicoll, C.B. (2013). Mechanics of wind damage. in Living with Storm Damage to Forests, (Ed. Barry Gardiner, Andreas Schuck, Mart-Jan Schelhaas, Christophe Orazio, Kristina Blennow and Bruce Nicoll) *European Forest Institute.* Joensuu, Finland. Pages 31-38

Pepper, D. & Heinrich, J. (2017). The Finite Element Method: Basic Concepts and Applications with MATLAB, MAPLE, and COMSOL. CRC Press.

Pivato, D., Dupont, S. & Brunet, Y. (2014). A simple tree swaying model for forest motion in windstorm conditions. *Trees - Structure and Function*, 28, 281–293.

Poëtte, C., Gardiner, B., Dupont, S., Harman, I., Böhm, M., Finnigan, J., Hughes, D. & Brunet, Y. (2017). The Impact of Landscape Fragmentation on Atmospheric Flow: A Wind-Tunnel Study. *Boundary-Layer Meteorology*, 163, 393–421.

Rao, S. (2017). The finite element method in engineering. Butterworth-heinemann, 2017.

Raumonen, P., Casella, E., Calders, K., Murphy, S., Åkerbloma, M. & Kaasalainen, M. (2015). Massive-Scale Tree Modelling From TLS Data. ISPRS Annals of Photogrammetry, *Remote Sensing and Spatial Information Sciences*, II-3/W4, 189–196.

Raupach, M.R. & Thom, A.S. (1981). Turbulence in and above Plant Canopies. *Annual Review of Fluid Mechanics*, 13, 97–129.

Rayleigh, R. (1877). On progressive waves. *Proceedings of the London Mathematical Society*, s1-9, 21–26.

Reiland, M., Kane, B., Modarres-Sadeghi, Y. & Ryan, H.D.P. (2015). The effect of cables and leaves on the dynamic properties of red oak (Quercus rubra) with co-dominant stems. *Urban Forestry and Urban Greening*, 14, 844–850.

Ricklefs, R.E. & He, F. (2016). Region effects influence local tree species diversity. *Proceedings of the National Academy of Sciences,* 113, 674–679.

Rifai, S.W., Urquiza Muñoz, J.D., Negrón-Juárez, R.I., Ramírez Arévalo, F.R., Tello-Espinoza, R.,

Vanderwel, M.C., Lichstein, J.W., Chambers, J.Q. & Bohlman, S.A. (2016). Landscape-scale consequences of differential tree mortality from catastrophic wind disturbance in the Amazon. *Ecological Applications*, 26, 2225–2237.

Riutta, T., Malhi, Y., Kho, L.K., Marthews, T.R., Huaraca Huasco, W., Khoo, M., Tan, S., Turner, E., Reynolds, G., Both, S., Burslem, D.F.R.P., Teh, Y.A., Vairappan, C.S., Majalap, N. & Ewers, R.M. (2018). Logging disturbance shifts net primary productivity and its allocation in Bornean tropical forests. *Global Change Biology*, 24, 2913–2928.

Rodriguez, M., De Langre, E. & Moulia, B. (2008). A scaling law for the effects of architecture and allometry on tree vibration modes suggests a biological tuning to modal compartmentalization. *American Journal of Botany*, 95, 1523–1537.

Rodriguez, M., Ploquin, S., Moulia, B. & de Langre, E. (2012). The Multimodal Dynamics of a Walnut Tree: Experiments and Models. *Journal of Applied Mechanics*, 79, 044505.

Roodbaraky, H.J., Baker, C.J., Dawson, A.R. & Wright, C.J. (1994). Experimental observations of the aerodynamic characteristics of urban trees. *Journal of Wind Engineering and Industrial Aerodynamics*, 52, 171–184.

Rudnicki, M., Lieffers, V.J. & Silins, U. (2003). Stand structure governs the crown collisions of lodgepole pine. *Canadian Journal of Forest Research*, 33, 1238–1244.

Rudnicki, M., Silins, U., Lieffers, V.J. & Josi, G. (2001). Measure of simultaneous tree sways and estimation of crown interactions among a group of trees. *Trees,* 15, 83–90.

Ruel, J.C., Achim, A., Herrera, R.E. & Cloutier, A. (2010). Relating mechanical strength at the stem level to values obtained from defect-free wood samples. *Trees - Structure and Function*, 24, 1127–1135.

Savage, V.M., Bentley, L.P., Enquist, B.J., Sperry, J.S., Smith, D.D., Reich, P.B. & von Allmen, E.I. (2010). Hydraulic trade-offs and space filling enable better predictions of vascular structure and function in plants*. Proceedings of the National Academy of Sciences*, 107, 22722–7.

Schelhaas, M.-J.J., Nabuurs, G.-J.J. & Schuck, A. (2003). Natural disturbances in the European forests in the 19th and 20th centuries. *Global Change Biology*, 9, 1620–1633.

Schindler, D. & Mohr, M. (2018). Non-oscillatory response to wind loading dominates movement of Scots pine trees. *Agricultural and Forest Meteorology*, 250–251, 209–216.

Schindler, D., Schönborn, J., Fugmann, H. & Mayer, H. (2013). Responses of an individual deciduous broadleaved tree to wind excitation. *Agricultural and Forest Meteorology*, 177, 69–82.

Schütz, J.P., Götz, M., Schmid, W. & Mandallaz, D. (2006). Vulnerability of spruce (Picea abies) and beech (Fagus sylvatica) forest stands to storms and consequences for silviculture. DOI: 10.1007/s10342-006-0111-0

Scurfield, G. (1973). Reaction wood: its structure and function. *Science*, 179, 647–655.

Seidl, R., Fernandes, P.M., Fonseca, T.F., Gillet, F., Jönsson, A.M., Merganičová, K., Netherer, S., Arpaci, A., Bontemps, J.-D., Bugmann, H., González-Olabarria, J.R., Lasch, P., Meredieu, C., Moreira, F., Schelhaas, M.-J. & Mohren, F. (2011). Modelling natural disturbances in forest ecosystems: a review. *Ecological Modelling*, 222, 903–924.

Sellier, D., Brunet, Y. & Fourcaud, T. (2008). A numerical model of tree aerodynamic response to a turbulent airflow. *Forestry,* 81, 279–297.

Sellier, D. & Fourcaud, T. (2005). A mechanical analysis of the relationship between free oscillations of Pinus pinaster Ait. saplings and their aerial architecture. *Journal of Experimental Botany*, 56, 1563–1573.

Sellier, D. & Fourcaud, T. (2009). Crown structure and wood properties:Influence on tree sway and response to high winds. *American Journal of Botany*, 96, 885–896.

Sellier, D., Fourcaud, T. & Lac, P. (2006). A finite element model for investigating effects of aerial

architecture on tree oscillations. *Tree Physiology*, 26, 799–806.

Silvério, D. V., Brando, P.M., Bustamante, M.M.C., Putz, F.E., Marra, D.M., Levick, S.R. & Trumbore, S.E. (2018). Fire, fragmentation, and windstorms: A recipe for tropical forest degradation (D. Edwards, Ed.). *Journal of Ecolog*y.

Simulia Software Company. (2017). Abaqus Theory Guide Abacus 6.41. 2014. URL http://50.16.225.63/v6.14/books/stm/default.htm

Slik, J.W.F., Paoli, G., Mcguire, K., Amaral, I., Barroso, J., Bastian, M., Blanc, L., Bongers, F., Boundja, P., Clark, C., Collins, M., Dauby, G., Ding, Y., Doucet, J.L., Eler, E., Ferreira, L., Forshed, O., Fredriksson, G., Gillet, J.F., Harris, D., Leal, M., Laumonier, Y., Malhi, Y., Mansor, A., Martin, E., Miyamoto, K., Araujo-Murakami, A., Nagamasu, H., Nilus, R., Nurtjahya, E., Oliveira, Á., Onrizal, O., Parada-Gutierrez, A., Permana, A., Poorter, L., Poulsen, J., Ramirez-Angulo, H., Reitsma, J., Rovero, F., Rozak, A., Sheil, D., Silva-Espejo, J., Silveira, M., Spironelo, W., ter Steege, H., Stevart, T., Navarro-Aguilar, G.E., Sunderland, T., Suzuki, E., Tang, J., Theilade, I., van der Heijden, G., van Valkenburg, J., Van Do, T., Vilanova, E., Vos, V., Wich, S., Wöll, H., Yoneda, T., Zang, R., Zhang, M.G. & Zweifel, N. (2013). Large trees drive forest aboveground biomass variation in moist lowland forests across the tropics. *Global Ecology and Biogeography*, 22, 1261–1271.

Spatz, H.C., Brüchert, F. & Pfisterer, J. (2007). Multiple resonance damping or how do trees escape dangerously large oscillations? *American Journal of Botany*, 94, 1603–1611.

Spatz, H.C. & Jochen, P. (2013). Mechanical properties of green wood and their relevence for tree risk assessment. *Arboriculture & Urban Forestry*, 39, 219–225.

Spatz, H. & Theckes, B. (2013). Plant Science Oscillation damping in trees. *Plant Science*, 207, 66–71.

Sullivan, M.J.P., Lewis, S.L., Hubau, W., Qie, L., Baker, T.R., Banin, L.F., Chave, J., Cuni-Sanchez, A., Feldpausch, T.R., Lopez-Gonzalez, G., Arets, E., Ashton, P., Bastin, J.-F., Berry, N.J., Bogaert, J., Boot, R., Brearley, F.Q., Brienen, R., Burslem, D.F.R.P., de Canniere, C., Chudomelová, M., Dančák, M., Ewango, C., Hédl, R., Lloyd, J., Makana, J.-R., Malhi, Y., Marimon, B.S., Junior, B.H.M., Metali, F., Moore, S., Nagy, L., Vargas, P.N., Pendry, C.A., Ramírez-Angulo, H., Reitsma, J., Rutishauser, E., Salim, K.A., Sonké, B., Sukri, R.S., Sunderland, T., Svátek, M., Umunay, P.M., Martinez, R.V., Vernimmen, R.R.E., Torre, E.V., Vleminckx, J., Vos, V. & Phillips, O.L. (2018). Field methods for sampling tree height for tropical forest biomass estimation. *Methods in Ecology and Evolution*, 9, 1179–1189.

Sunden, B. (2016). Tubes, Crossflow over. A-to-Z Guide to Thermodynamics, Heat and Mass Transfer, and Fluids Engineering, 2016.

Telewski, F.W. (2006). A unified hypothesis of mechanorperception in plants. *American Journal of Botany*, 93, 1466–1476.

Telewski, F.W. (1995). Wind-induced physiological and developmental responses in trees. Wind and Trees,*(eds P.M. Coutts & J. Grace)*, pp. 237–263. Cambridge University Press

Théckès, B., Boutillon, X. & De Langre, E. (2015). On the efficiency and robustness of damping by branching. *Journal of Sound and Vibration*, 357, 35–50.

Thomas, S.C., Martin, A.R. & Mycroft, E.E. (2015). Tropical trees in a wind-exposed island ecosystem: Height-diameter allometry and size at onset of maturity. *Journal of Ecology,* 103, 594–605.

de Toledo, J.J., Magnusson, W.E., Castilho, C. V. & Nascimento, H.E.M. (2012). Tree mode of death in Central Amazonia: Effects of soil and topography on tree mortality associated with storm disturbances. *Forest Ecology and Management*, 263, 253–261.

Viberg, M. (1995). Subspace-based methods for the identification of linear time-invariant systems. *Automatica*, 31, 1835–1851.

Vicari, M.B. (2017). Leaf separation in TLS data. DOI: 10.5281/ZENODO.802233

Vitasse, Y., Delzon, S., Dufrêne, E., Pontailler, J.-Y., Louvet, J.-M., Kremer, A. & Michalet, R. (2009a). Leaf

phenology sensitivity to temperature in European trees: Do within-species populations exhibit similar responses? *Agricultural and Forest Meteorology,* 149, 735–744.

Vitasse, Y., Porté, A.J., Kremer, A., Michalet, R. & Delzon, S. (2009b). Responses of canopy duration to temperature changes in four temperate tree species: relative contributions of spring and autumn leaf phenology. *Oecologia*, 161, 187–198.

Wellpott, A. (2008). The stability of continuous cover forests. University of Edinburgh, PhD, 160.

Wessolly, L. & Erb, M. (2016). Manual of Tree Statics and Tree Inspection (K. Faust, Tran.). Patzer Verlag. Berlin

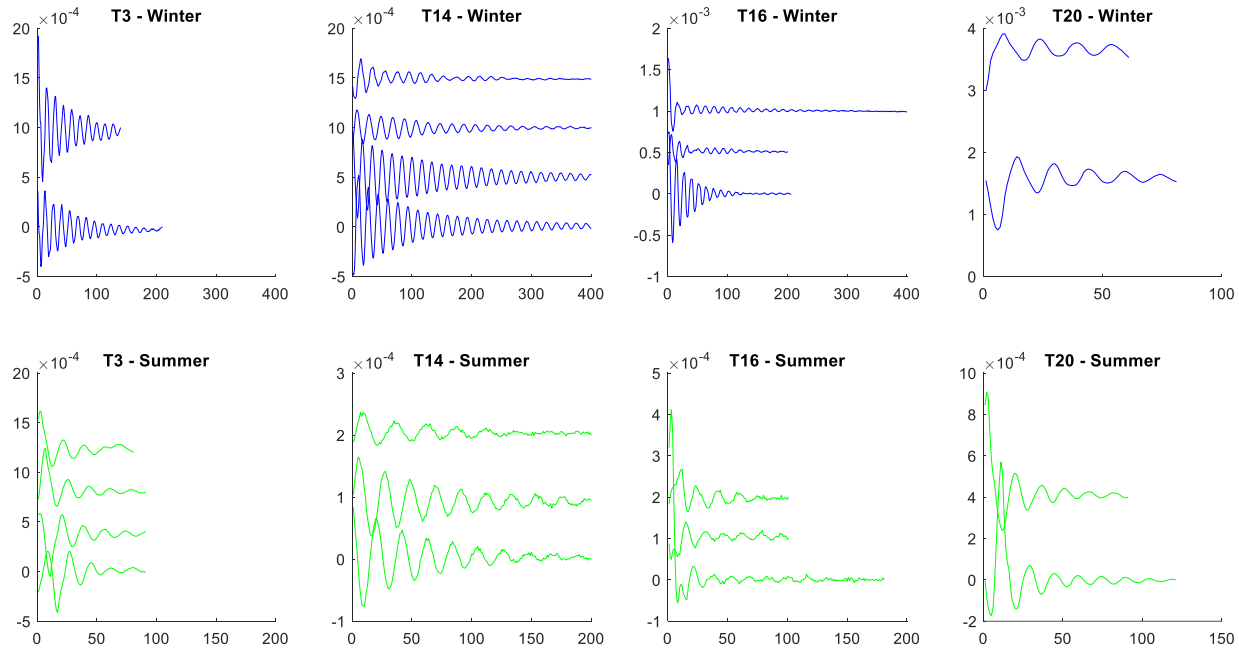
Wilkes, P.;, Disney, M., Boni Vicari, M., Calders, K. & Burt, A. (2018). Estimating urban Above Ground Biomass with multi-scale LiDAR. *Carbon Balance and Management*.

Wilkes, P., Lau, A., Disney, M., Calders, K., Burt, A., Gonzalez de Tanago, J., Bartholomeus, H., Brede, B. & Herold, M. (2017). Data acquisition considerations for Terrestrial Laser Scanning of forest plots. *Remote Sensing of Environment,* 196, 140–153.

Woodland Trust, (2014). Nature's Calendar. URL https://naturescalendar.woodlandtrust.org.uk/

Yang, M., Défossez, P., Danjon, F. & Fourcaud, T. (2014). Tree stability under wind: Simulating uprooting with root breakage using a finite element method. *Annals of Botany,* 114, 695–709.

Appendix 1 – Pull and release data



These strain data were recorded in Wytham Woods by attaching a rope to the top of the trunk and having three or four people pull and then suddenly release the rope. I chose calm conditions so that the trees would not be swaying due to wind and so complicate the signals. This data was used in paper 3 to calculate the change in fundamental frequency and damping ratio induced by leaves. This data could also be used to calibrate a leaf parameterization in the finite element model.

Appendix 2 – Example Abaqus input file

```
** This Abaqus input file gives an example of the format used to simulate trees in the wind.
** A single * signifies a function, and the following lines are the parameters
**
**
*Heading
Example QSM in Abaqus simulation
** PARTS
*Part, name=QSM_TREE
**
** THE NODES ARE THE START COORDINATES OF THE CYLINDERS
**
*Node
1,0,0,0
2,3.7331e-05,0.0087833,2.4
3,-0.056442,0.066452,4.9802
4,-0.14089,0.1559,8.9497
5,-0.28472,0.14264,15.0023
6,-0.43699,0.076978,20.8512
7,-0.58216,0.10625,26.4839
8,-0.87891,-0.031148,31.0896
9,-1.1551,0.42332,33.0547
10,-1.6558,1.3646,35.6721
**
** THE ELEMENTS CONNECT THE NODES TOGETHER
**
*Element, type=B31
2,1,2
2,1,2
3,2,3
4,3,4
5,4,5
6,5,6
7,6,7
8,7,8
9,8,9
10,9,10
11,10,11
**
** EACH ELEMENT IS DEFINED AS BELONGING TO ITS OWN SET
**
*Elset, elset=set2
2,
*Elset, elset=set3
3,
*Elset, elset=set4
4,
*Elset, elset=set5
5,
*Elset, elset=set6
6,
*Elset, elset=set7
7,
```

```
*Elset, elset=set8
8,
*Elset, elset=set9
9,
*Elset, elset=set10
10,
*Elset, elset=output_set
2,3,4,5,6
**
** THE OUTPUT SET IS THE ELEMENTS FOR WHICH STRAIN DATA IS WRITTEN TO A DAT FILE
** EACH ELEMENET IS DEFINED AS A BEAM (B31), USING THE RADIUS AND VECTOR COMPONENTS
**
*Beam Section, elset=set2,material=wood,section=circ
1.0652
0.99958,-0.022171,0.018627
*Beam Section, elset=set3,material=wood,section=circ
0.53258
0.99958,-0.022171,0.018627
*Beam Section, elset=set4,material=wood,section=circ
0.53258
0.99965,-0.02559,-0.0065006
*Beam Section, elset=set5,material=wood,section=circ
0.50575
0.99945,-0.02894,-0.016111
*Beam Section, elset=set6,material=wood,section=circ
0.48396
0.99956,-0.02973,-0.00032158
*Beam Section, elset=set7,material=wood,section=circ
0.45308
0.99697,-0.069088,-0.035873
*Beam Section, elset=set8,material=wood,section=circ
0.45329
0.96579,-0.14119,0.21752
*Beam Section, elset=set9,material=wood,section=circ
0.30678
0.92628,-0.18418,0.32876
*Beam Section, elset=set10,material=wood,section=circ
0.2617
0.93717,-0.16124,0.30937
**
** THE LOWEST CYLINDER IS ATTACHED TO THE GROUND VIA A U-JOINT AND DASHPOT SPRING SYSTEM
**
*Dashpot, elset=Springs/Dashpots-1-dashpot
4
10
*Element, type=Dashpot1, elset=Springs/Dashpots-1-dashpot
512, 1
*End part
**
** THIS DEFINES THE ASSEMBLY. A MODEL IN ABAQUS
** CONSISTS OF INSTANCES OF A PART WITHIN AN ASSEMBLY
**
*Assembly, name=Assembly1
**
*Instance, name=Instance1, part=QSM_TREE
*End Instance
**
```

```
** THE ROOT CAN BEND IN TWO DIRECTIONS USING A U-JOINT ELEMENT
**
*Element, type=CONN3D2
1, Instance1.1,
*Connector Section, elset=Wire-1-Set-1, behavior=ConnSect-1
UJoint,
"Datum csys-2",
*Nset, nset=Wire-1-Set-1, instance=Instance1
 1,
*Elset, elset=Wire-1-Set-1
 1,
*Nset, nset=_M6, internal, instance=Instance1
 1,
*Orientation, name="Datum csys-2"
        1.,         0.,         0.,         0.,         1.,         0.
3, 0.
*End Assembly
**
** THE BEHAVIOUR OF THE ELEMENTS IS DEFINED BELOW
**
*Connector Behavior, name=ConnSect-1
*Connector Elasticity, component=4
5000000.,
*Connector Elasticity, component=6
5000000.,
**
** MATERIAL PROPERTIES DEFINED BELOW
**
*Material, name=wood
*Damping, alpha=0.2, beta=0.001, composite=0, structural=0
*Density
641,
*Elastic
9100000000, 0.38
*Surface Interaction, name=Contact1
1.,
*Contact
*Contact Inclusions, ALL EXTERIOR
*Contact Property Assignment
 ,  , Contact1
**
** THE VARIATION IN FORCING IS DEFINED VIA AMPLITUDES BELOW
**
*Amplitude, name=CWS_Amp
0,0
0.1,0.1
0.2,0.2
0.3,0.3
0.4,0.4
0.5,0.5
0.6,0.6
0.7,0.7
0.8,0.8
0.9,0.9
1,1
**
** THE AQUA MODULE IS INITIATED BELOW, BUT WE USE 0 DEPTH OF WATER
```

```
** INSTEAD WE USE WIND FORCING
**
*AQUA
0.0, 0.0, 9.81, 0.0
*WIND
1.27,35, 1,1, 1, 0,0
**
** THE FIRST STEP IS A GRAVITY FORCE, WITH NO OUTPUT REQUESTS
**
*STEP,name=Gravity,NLGEOM=YES,UNSYMM=YES
*STATIC
1., 100., 5e-11, 1.
**
** THE SECOND STEP IS AN EIGENVALUE / FREQUENCY EXTRACTION
**
** STEP: Frequency
*Step, name=Frequency, nlgeom=YES, perturbation
*Frequency, eigensolver=subspace, normalization=displacement, sim=no
100, , , 38, 500
** OUTPUT REQUESTS
*Restart, write, frequency=0
** FIELD OUTPUT: F-Output-1
*Output, field, variable=PRESELECT
*End Step
**
** THE THIRD STEP IS THE ACTUAL WIND LOADING
**
** STEP: CWS_Wind
*Step, name=CWS_Wind, NLGEOM=YES, UNSYMM=YES, INC=50000
**DRAG LOADS
*DYNAMIC
0.1,120, 1e-11, 0.25
*DLOAD
Assembly1.Instance1.set2, WDD, 1,2.1303,0.82,1,CWS_Amp
Assembly1.Instance1.set3, WDD, 1,1.0652,0.82,1,CWS_Amp
Assembly1.Instance1.set4, WDD, 1,1.0652,0.82,1,CWS_Amp
Assembly1.Instance1.set5, WDD, 1,1.0115,0.82,1,CWS_Amp
Assembly1.Instance1.set6, WDD, 1,0.96792,0.82,1,CWS_Amp
Assembly1.Instance1.set7, WDD, 1,0.90616,0.82,1,CWS_Amp
Assembly1.Instance1.set8, WDD, 1,0.90658,0.82,1,CWS_Amp
Assembly1.Instance1.set9, WDD, 1,0.61356,0.82,1,CWS_Amp
Assembly1.Instance1.set10, WDD, 1,0.5234,0.82,1,CWS_Amp
*EL PRINT, ELSET=Assembly1.Instance1.output_set, FREQUENCY=1
7,11
E11,
*End Step
```